UNIVERSITÀ DEGLI STUDI DI NAPOLI FEDERICO II

Scuola Politecnica e delle Scienze di Base
Dipartimento di Ingegneria Elettrica e Tecnologie dell'Informazione

DOCTORAL THESIS

Modeling, analysis, and control of complex networks in the presence of temporality and coevolution

Author:
Anna Di Meglio

Tutor:
Prof. Franco Garofalo

Submitted in fulfilment of the requirements for the degree of Doctor of Philosophy in Information Technology and Electrical Engineering, XXXII Ciclo. Coordinator: Prof. Daniele Riccio.

1 October 2020

A Electra

Abstract

In the last decades, complex dynamical networks have attracted the attention of a highly heterogeneous community. Indeed, they are a suitable tool to study the emergence of collective behaviors in ensembles of coupled dynamical systems. Under simplifying and standard assumptions on the individual dynamics and on the static interaction topology, the control of such collective behaviors is now quite assessed. However, a deeper understanding is required when the structures of the interconnections change with time. Spurred by the belief that achieving insights on the interplay between the node dynamics and the time-varying topology could be beneficial from a control perspective, in this thesis, we focus on modeling and control of what we called evolving networks. In the first part of the thesis, we deal with the so-called temporal networks, i.e., networks whose structure changes in time, and show how their optimal control can be challenging in a realistic scenario in which only a probabilistic, instead of deterministic, knowledge of the topology is available. Indeed, controlling a large static network, while keeping the control energy limited, has always been a chimera. Recent results suggested that deterministic knowledge of network temporality can be exploited to substantially reduce the energy required to control the network. In a more realistic scenario, we illustrate that the temporality can be exploited to our advantage only provided that the variability of the network structure matches the intrinsic time scales of the nodes we aim to control. Considering a time-varying law is not the only way to account for the evolution of network structure. In the second part of the thesis, we introduce the more general concept of coevolving networks, in which both the nodes and the structure dynamically evolve in an interdependent fashion. We exploit the potential of this modeling framework in a socio-economic context and then show how the laws governing the coevolution of the network topology and of the node dynamics can be properly tuned to achieve specific control goals. In line with the idea of relaxing standard assumptions, and verifying if we can still gain advantage from the networked nature of complex networks, in the third part of the thesis, we focus on special static networks (networks endowed with symmetries and networks whose structures can be negatively weighted) that can provide further challenges and opportunities for control design.

Acknowledgements

I wish to thank Professor Franco Garofalo, who greatly contributed to all the works and the experiences I did during my PhD, and most importantly, motivated me during this journey to catch all the inherent nuances that dominate the human being. I need to thank Francesco Lo Iudice to have donated me time for reading and revise this work together with Pietro De Lellis that I also thank for has been my young *maestro*. His technical skills were as valuable as his empathy, which is a rare talent. I would also like to thank the people I had the pleasure to collaborate with when preparing all the papers I worked on, Mario di Bernardo, Fabio Dercole, Francesco Sorrentino and Fabio Della Rossa. All of them contributed to my scientific awareness. I am profoundly grateful to all the loving people that supported me during these beautiful years in Napoli and in Albuquerque not only for the natural scientific debates we had but especially for being part of my life. Last but not least, I am indebted to the Italiano's family as they have unconsciously helped me always in sailing towards the right buoy.

Contents

1 Introduction

1.1 Control of complex networks

A great variety of real-world phenomena and applications ranging from engineering to socio-economics science can be modeled as ensembles of dynamical systems in mutual interaction, commonly denoted *complex dynamical networks*. More specifically, a complex dynamical network is constituted by a graph whose nodes are associated to dynamical systems interconnected and mutually influenced by a set of edges. For their descriptive power, complex networks have been extensively employed in diverse domains of application, including power grids [1], socio-economic dynamics [2–4], modeling, and control of spreading processes [5], and opinion formation [6–8]. The cross-fertilization among different disciplines yielded the development of a variety of methodologies and approaches, each of which employed to uncover a specific aspect of complex networks. For instance, tools from statistical mechanics have been employed to identify the mechanism underlying the formation of the topology interconnecting the dynamical systems. Algorithms were developed to synthetically generate network topologies whose properties resembled those observed in real networks, e.g., the small-world effect [9] or the preferential attachment in the scale-free networks formation [10]. Dynamical systems theory is instead, interested in elucidating how the interplay between the individual dynamics of the nodes and the topology of interactions yields to a wide range of emerging collective behaviors. Due to its numerous applications, spanning from distributed sensing to cooperative unmanned aerial vehicles [11], synchronization [12] deserves a place of honor among such collective behaviors that take place in complex networks. In formal terms, synchronization occurs when the trajectories of all individuals converge towards each other. Researchers investigated under which conditions synchronization spontaneously emerges in complex networks. However, from the perspective of control theory, the problem arises of i) inducing synchronization when it is not self-induced, and ii) assigning a desired reference trajectory to the network. In the last decades, designed *ad hoc* algorithms and control protocols have been extensively proposed to impose a desired collective behavior to the networks, that is, to synchronize onto the desired trajectory or to converge toward a point in the state space.

However, the strong interplay between the two constituent elements of a network, that is, its topology and the individual nodes' dynamics, make its control particularly challenging [13]. Even the standard Kalman condition of controllability for linear systems

needs to be adapted to properly take into account the specific nature of a complex network. Indeed, starting from the pioneering work of Liu et al. [13], a research line has successfully tried to relate the *controllability* properties of complex networks with their topological features, identifying the minimum number of nodes to enforce controllability of all nodes. Later works observed that, even if a network is in principle controllable, may not be practically controllable, in the sense that the required control *energy* exponentially grows with the dimension of the network [14, 15]. Then, several works have proposed strategies to reduce the energy required to control linear networks while keeping contained the number of control inputs, as [16], in which the targeted optimal control aims to scale the required control energy. Whichever the network dynamics are, a powerful strategy to face with the control of complex networks is what we can define a *dimensionality reduction* approach. Indeed, provided that the entire network cannot be controlled, or that a *complete* network state cannot be achieved, it is possible to employ distinctive features of the network to extract the portion that effectively determines its controllability properties and so affects the control design. This is the case of cluster consensus and synchronization where distributed protocols are designed to steer the states of different parts (i.e., the clusters) of the network towards different desired states, or of the partial pinning control [17] in which the nodes to be controlled are selected to maximize the fraction of nodes of the whole network that asymptotically synchronize to a reference trajectory, or of the targeted optimal control [18] where a sized number of nodes are selected to be controlled through a small number of control inputs and a small amount of control energy.

Therefore, outlining, the general goal of control networks theory is that of exploring the controllability properties of a network, providing the “space" of the controllable network’s states, and designing suitable protocols by taking advantage of the structured nature of the network. As in real life, it is not rare that one has to accept the inability to control a complex network and fall back on the understanding of the intriguing nature of the system. A byproduct of such awareness, as in real life, is the happiness of controlling even partially the network or of achieving by chance the desired network state without dreaming the impossible mission of controlling the entire network. Such awareness will be useful in reading this work in which we propose a daring step forward in controlling complex networks.

1.2 Key research questions

Most of the results of control networks theory have been achieved by means of a fundamental assumption on the interactions among the nodes of the network independently on what they represent:

“The edges of the network do not change in time.”

This assumption is, of course, a good approximation when the *variability* of the interactions can be neglected respect to those of the nodes, or, in other words, when there exists a sufficient time-scale separation between them. Relaxing this assumption means considering that the edge sets is a time-varying set and eventually can be associated with a specific dynamics describing the evolution of the interactions. The class of complex

networks whose structure changes in time has been labeled differently during the last 20 years, here and in the rest of the thesis we denote them *evolving* complex dynamical networks, or for brevity, evolving networks. The class includes *temporal* networks [19], *adaptive* networks [20], and what we will formally define in Part , Chapter 1 as *coevolving* networks. Different from [21], these concepts are framed within complex networks of *dynamical systems*, where the evolution of the network topology affects the dynamics at the nodes. A network can exhibit temporality in several ways, and indeed each type of evolving network model serves different purposes. For instance, temporal networks are employed to model cases in which the interactions among the nodes can be active or inactive for a nonnegligible time. The adaptive networks, instead, model the virtuous feedback loop existing, in some scenarios, between network state and the topology, that is, the topology changes depending on the network state and vice-versa. Finally, coevolving networks face with an extra dimension of temporality and introduce a different concept of the network state. Indeed, the edges' time behaviors are described by dynamical systems. Consequently, both the switching behavior of the temporal networks and the feedback loop of the adaptive networks are considered in the coevolving networks. In all the cases where these features are nonnegligible, static networks do not fit.

The analysis of such kind of networks offers a higher descriptive power especially of some phenomena as social systems [22], opinion formation [23, 24], biological systems as neural networks [25], economic systems [2, 3, 26], technological networks [27] or in epidemics spreading [28]. The price of this finer-grained modeling is in introducing undesired complications that limit the applicability of the standard analysis techniques. Their control is challenging as well. Indeed, on one side we generally prefer to work with time-invariant systems for which several results are well assessed and a plethora of proprieties can be employed. On the other the cost associated with a control that has to chase a so tangled dynamics risks to be prohibitive. However, the daily experience of continuously diving in temporality and the fact that history has already taught us how complex networks can be a useful tool in modeling and control real-world systems spur us to invest in a refurbishment of our understanding of complex networks.

Therefore, in this work, we present both modeling and control instances as a possible way to face evolving networks. Specifically, following the footsteps of classical complex networks scientists, with this work we attempt to give a reply as complete as possible to the following big vision questions:

1. When is it possible to extend the obtained results for the traditional complex dynamical networks to the aforementioned evolving networks?
2. What is the gain of considering evolving rather than static networks worth from a modeling and control perspective?

1.3 Contribution of the thesis

In this thesis, we answer to the above research questions with contributions in different areas.

- In part I, we show how the control of temporal networks can be challenging in real scenarios. Indeed, the authors of [29] show the possibility to take advantages from controlling a temporal network respect with a static one. This no intuitive result is claimed by means of standard control measures, as the size of the controllability space, the control energy and the locality of the controlled trajectory. In this work, we investigate if such advantages hold in a realistic scenario in which at the beginning of the control horizon, rather than having a deterministic knowledge of the temporal network, we can only face with its probabilistic description (we will name this kind of networks *stochastic temporal networks*, see Definition 4.1).
- In part II, we give a formal definition of *coevolving networks* (see Definition 7.1). Then, we offer an instance of how to use this framework as a modeling tool for describing socio-economic phenomena [2, 3] (Part II, Chapter 8). Moreover, we state and solve two control problems concerning the pinning synchronization of coevolving networks (Part II, Chapters 9). Specifically, we address the problem of selecting edge dynamics for pinning synchronizing a network while minimizing the control energy required to reject local perturbations. Then, in the same context of pinning control, we show how to dynamically evolve the edges weights to maximize the class of systems that can be synchronized.
- In part III, we present two types of networks whose topology peculiarities give rise some difficulties in control design. In Chapter 12, we present networks whose topologies endows with *symmetries* [30]. In [31, 32], is pointed out that networks where the interactions couplings among the nodes is diffusive and that endow symmetries are not controllable. In Chapter 12 we reformulate the problem of controlling networks with symmetries when the interactions are coded by the adjacency matrix and give an example of how symmetries can be used to identify the *effective* size of the network to control and then taking advantage even from networks that apparently prevent from controlling their collective behaviors [33]. In Chapter 13, we present *signed* graphs as a useful tool for modeling interactions among the nodes when they can be both cooperative and antagonistic. Then, we propose a strategy for solving a containment control problem in presence of large networks [34]. Indeed, provided that contain the entire network state within a given region could be unfeasible or undesired, we provide an algorithm to maximize the portion of the network that can be contained with a limited number of control inputs. This part is focused on topics that are of great interest per se, and therefore we studied them in the simpler context of static graphs, leaving the implications for the analysis of temporal and coevolving networks for future works.

1.4 Notation

In this section, we give the general notation we will use throughout the thesis.

Notation concerning sets is as follows, Q being a generic set:

- $\mathbb{N}$ is the set of natural numbers including zero, and $\mathbb{N}_{>0}$ is the set of natural numbers excluding zero,
- $\mathbb{R}$ is the set of real numbers, $\mathbb{R}_{\geq 0}$ excludes negative numbers, and $\mathbb{R}_{>0}$ excludes non-positive numbers,
- $\varnothing$ is the empty set,
- if Q is finite, $|Q|$ is its cardinality.
- If $Q \subset \mathbb{R}$, the notation $Q \leq 0$ means that $\forall s \in Q$, $s \leq 0$ (analogously for $\geq$, $=$, etc.),

Notation concerning operators is as follows:

- the dot diacritic $\dot{}$ represents total derivative with respect to time,
- $\frac{\partial a}{\partial b}$ is the partial derivative of a with respect to b,
- ∇ is the gradient and is a row vector,
- $\otimes$ denotes the Kronecker product,
- $\times$ is the Cartesian product,
- $^{\mathsf{T}}$ is the transpose,
- $:=$ means "is defined as",
- the right vertical bar with a subscript means "evaluated with the subscript as a constraint". For example, "$f(x, y)|_{x=1}$" is the same as "$f(1, y)$".

Notation concerning scalars is as follows, $s \in \mathbb{R}$ being a generic scalar:

- $|s|$ is the absolute value of s (although if $s \in \mathbb{C}$, then $|s|$ is the module of s),
- $\operatorname{sign}(s)$ is its sign (with $\operatorname{sign}(0) = 0$),
- $\lfloor s \rfloor$ is the largest integer r such that $r \leq s$,
- $\lceil s \rceil$ is the smallest integer r such that $r \geq s$.
- e is Euler's number.

Notation concerning vectors is as follows, $\mathbf{v} \in \mathbb{R}^n$ being a generic vector:

- normally we will denote a vector by a lower-case bold letter; if not specified differently, we assume it is a column vector,
- $|\mathbf{v}| = [|v_1| \;\; |v_2| \;\; \cdots \;\; |v_n|]^{\mathsf{T}}$,
- $\operatorname{sign}(\mathbf{v}) = [\operatorname{sign}(v_1) \;\; \operatorname{sign}(v_2) \;\; \cdots \;\; \operatorname{sign}(v_n)]^{\mathsf{T}}$,
- $\mathbf{1}_n$ the n-column vector of 1 and $\mathbf{0}_n$ is the null column vector with n entries; we will omit the subscripts when not necessary,
- $\operatorname{diag}(\mathbf{v}) \in \mathbb{R}^{n \times n}$ is the diagonal matrix having the elements of vector $\mathbf{v}$ on its diagonal,
- $\|\mathbf{v}\|_p$ is the p-norm of $\mathbf{v}$, with p being equal to 2 if it is omitted.

Notation concerning matrices is as follows, $A \in \mathbb{R}^{n \times m}$ being a generic matrix:

- A_{ij} is the (i, j)-th element of A,

- $\lambda_i(A)$ is its i-th eigenvalue, with the eigenvalues being sorted in an increasing order if they are all real ($\lambda_{\min}(A) := \lambda_1(A)$ is the smallest one),
- $\|A\|_p$ is the p-norm of A, with p being equal to 2 if it is omitted,
- The notation $A > 0 (A \geq 0)$ indicates that A is positive (semi-) definite (analogously for negative definiteness),
- I_n is the $n \times n$ identity matrix; we will omit the subscript when not necessary,
- $0_{n \times m}$ is the $n \times m$ null matrixwe will omit the subscript when not necessary,
- $\mathcal{R}(A) = \{A\mathbf{v} \mid \mathbf{v} \in \mathbb{R}^m\}$ denotes the column space of A.

Part I

Control of temporal networks

2 Controlling linear networks

In this background chapter, we focus on a topic that has been extensively studied in the literature on complex networks, that is, the problem of controlling a linear dynamical network, see e.g., [13, 15, 35, 36] . Specifically, we consider a set of N scalar linear dynamical systems coupled on a graph $\mathcal{G} = \{\mathcal{V}, \mathcal{E}\}$, whose dynamics are described by

$$\begin{aligned} \dot{\mathbf{x}}(t) &= A\mathbf{x}(t) + B\mathbf{u}(t) \\ \mathbf{x}(0) &= \mathbf{x}_0 \end{aligned} \tag{2.1}$$

where:

- $\mathbf{x} = [x_1(t), \dots, x_N(t)]^T \in \mathbb{R}^N$ is the network *state* vector, which is the stack of the states of the N network nodes,
- $\mathbf{x}_0 \in \mathbb{R}^N$ is the initial network state,
- $t \in \mathbb{R}_{\geq 0}$ is time,
- $A \in \mathbb{R}^{N \times N}$ is the adjacency matrix associated to graph $\mathcal{G}$,
- $B \in \mathbb{R}^{N \times p}$ is the input matrix,
- $\mathbf{u} \in \mathbb{R}^p$ is the control input vector.

In particular, we focus on the minimum energy control of a complex network. Indeed, it has been shown that, even though a network is theoretically controllable, our ability to actually control it is limited, since an excessive amount of energy might be required. Therefore, in what follows, we start by stating the minimum energy control problem for static networks and then report some useful results for the case of temporal networks, which is the goal of Part I.

2.1 Minimum energy control of complex networks

The classic control-theoretic questions, e.g., "is the system controllable (reachable)?", "what is the minimum control energy to drive a system toward a target state?", also apply to complex networks. In the last decade, researchers have tried to leverage the network structure of (2.1) to relate the properties of the graph describing the interactions among the network nodes to these classic control-theoretic questions. To start with, we report the following definitions of reachability and controllability for network (2.1).

Definition 2.1 (Reachability). *A network state* $\mathbf{x}_f = \mathbf{x}(t_f)$ *is reachable at time* t_f *if for some* $t_0 < t_f$, $\exists \mathbf{u}(t)$, *with* $t \in [t_0, t_f]$ *that transfers the network state from the origin at* t_0 *to* $\mathbf{x}_f$ *at* t_f.

All the reachable network states $\mathbf{x}_f$ constitutes a linear subspace of the state space, the reachability space, Ω_r.

Definition 2.2 (Controllability). *A network state* $\mathbf{x}_0$ *is controllable at* t_0 *if for some* $t > t_f$ *there exists* $\mathbf{u}(t)$ *that transfers the network state from* $\mathbf{x}_0$ *at* t_0 *to the origin in* t_f.

As for Ω_r, all the controllable network states $\mathbf{x}_0$ define the controllable subspace of the state space, Ω_c. In what follows, in virtue of the Reduction Theorem (Theorem 5, page 266 of [37]) stating the equivalence, for linear systems, and so for linear networks, between the controllability on $[t_0, t_f]$ and the reachability on $[t_0, t_f]$, without loss of generality, we will refer to the reachability problem.

From Definition 2.1 if $\mathbf{x}_f$ is reachable at t_f, there exists an input $\mathbf{u}(t)$ such that

$$\mathbf{x}_f = \int_{t_0}^{t_f} \mathrm{e}^{A(t_f-\tau)} B\mathbf{u}(t)\mathrm{d}\tau$$

then, the range of the integral map

$$L_r(\mathbf{u}, t_0, t_f) := \int_{t_0}^{t_f} \mathrm{e}^{A(t_f-\tau)} B\mathbf{u}(\tau)\mathrm{d}\tau$$

coincides with the reachability subspace, Ω_r for system (2.1). Moreover, it can be shown that

$$\mathcal{R}(L_r) \equiv \mathcal{R}(W_r)$$

where W_r is defined as follows

Definition 2.3 (Reachability gramian). *The reachability gramian of network* (2.1) *is the symmetric positive semidefinite matrix*

$$W_r(t_0, t_f) := \int_{t_0}^{t_f} \mathrm{e}^{A(t_f-\tau)} BB^T \mathrm{e}^{A^T(t_f-\tau)}\mathrm{d}\tau. \tag{2.2}$$

Therefore, an input $\mathbf{u}(t)$ that attempts to the desired transfer state exists if and only if

$$\bar{\mathbf{x}}_f := \mathbf{x}_f - \mathrm{e}^{A(t_f-t_0)}\mathbf{x}_0 \in \Omega_r = \mathcal{R}(W_r)$$

and is of the form

$$\mathbf{u}(t) = B^T \mathrm{e}^{A^T(t_f-t)}\boldsymbol{\eta} \tag{2.3}$$

where $\boldsymbol{\eta}$ is the solution of $W_r\boldsymbol{\eta} = \bar{\mathbf{x}}_f$.

It is worth to be noted that the control input resulting from (2.3), that is,

$$\mathbf{u}(t) = B^T \mathrm{e}^{A^T (t_f - t)} W_r^{-1} \bar{\mathbf{x}}_f \tag{2.4}$$

is also the input that minimizes the control effort, that is, it is the exact solution of the following optimal control problem

$$\begin{aligned} \min_{\mathbf{u}} \mathrm{J}(\mathbf{u}(t)) := \frac{1}{2} \int_{t_0}^{t_f} & \mathbf{u}(t)^T \mathbf{u}(t) \mathrm{d}t \\ & s.t. \\ & \dot{\mathbf{x}}(t) = A\mathbf{x}(t) + B\mathbf{u}(t) \\ & \mathbf{x}(t_0) = \mathbf{x}_0 \\ & \mathbf{x}(t_f) = \mathbf{x}_f \end{aligned} \tag{2.5}$$

Therefore, for the Minimum Cost Control Theorem [37], if a network pair (A, B) is controllable on $[t_0, t_f]$, then $\forall\ \mathbf{x}_0, \mathbf{x}_f \in \mathbb{R}^N$, the control input (2.4) steers the network from $\mathbf{x}_0$ to $\mathbf{x}_f$, in finite time, and with the minimum possible control energy $\int_{t_0}^{t_f} \mathbf{u}(t)^T \mathbf{u}(t) \mathrm{d}t$. For its role in the control of linear networks, we report here some properties of the reachability gramian (2.2)[1] that will turn useful in reading the next chapters. Indeed, it concurrently concerns

1. **The reachability of the network.**
   As $\mathcal{R}(L_r) = \mathcal{R}(W_r)$, all the states that can be reached at time t_f are in the range of W_r. Verifying that $\det(W_r) \neq 0$ is equivalent to: i) the traditional Kalman rank condition [38] and, ii) $\mathcal{R}(L_r) = \mathbb{R}^N$.
2. **The control energy of the network.**
   If in (2.4) $\mathbf{x}_0 = 0$, the minimum energy of problem 2.5 is $\mathrm{J}^\star(\mathbf{u}(t)) = \mathbf{x}_f^T W_r^{-1} \mathbf{x}_f$. This implies that, denoting $\lambda_i(W_r), \mathbf{v}_i(W_r)$ the eigenvalues and the corresponding orthonormal eigenvectors of the nonsingular reachability gramian, network (2.1) can reach, for a unit cost, any point of the energy-ellipsoid whose semiaxes are $\mathbf{v}_i(W_r)/\sqrt{\lambda_i(W_r)}$ (see Figure 2.1 for the simplest case of two nodes). Therefore, if we sort the eigenvalues in ascending order $\lambda_1 \geq \ldots \geq \lambda_N$, then $\mathbf{v}_N$ identifies the most energetically demanding direction to reach.

From the above discussion, the required energy to control a network is strongly related to the singularity of the reachability gramian W_r, then a proxy of the efficiency of reaching a specific network state is the reciprocal condition number γ of W_r, defined as

$$\gamma := \frac{\lambda_{\min}(W_r)}{\lambda_{\max}(W_r)}.$$

This is the main issue in considering (2.1) as it is, a network. Indeed, in [14], it is shown that, even for a chain topology, that is $A_{ij} = \delta_{i,j+1}$ and $B_i = \delta_{1i}$ for which $rank(\Omega_r) = N$,

[1] We refer to the reachability gramian but similar results hold for the controllability gramian.

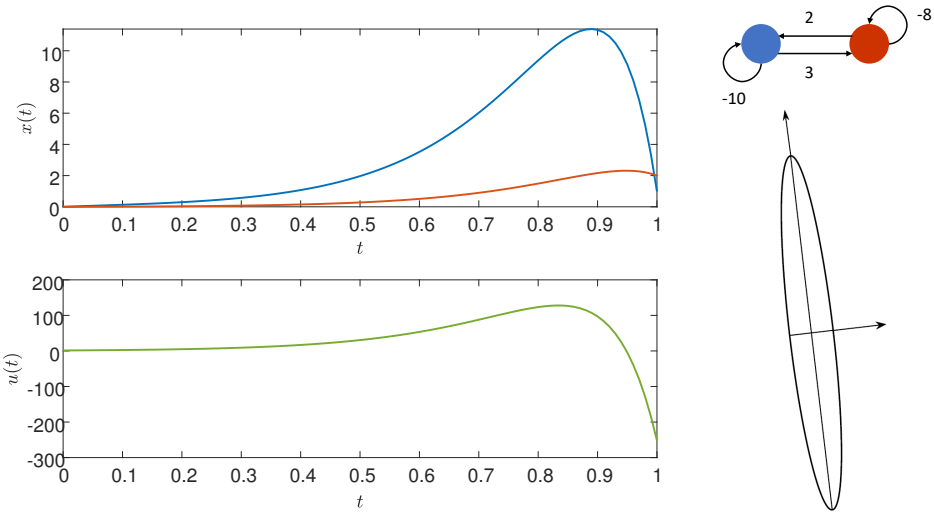

(a) (b)

Figure 2.1: In the top-left panel the controlled nodes states' trajectories of the toy network depicted in the top-right panel with initial conditions $\mathbf{x}_0 = [0\ 0]^T$, forced by the control signal plotted in green in the bottom-left panel to be steered towards $\mathbf{x}_f = [1\ 2]^T$ in one unit time. In the bottom-right panel the energy ellipse whose semi-axes are $\mathbf{v}_i/\sqrt{\lambda_i}$ with $i = 1, 2$.

as the size of the network chain increases, the gramian becomes nearly singular. Moreover, as the number of driver nodes decreases, γ exponentially decreases towards zero.

Unfortunately, network topologies are not designed, in general, to be efficiently controlled, thus a trivial workaround to be sure to control the network by spending the minimum possible control energy is that of having $p = N$ drivers nodes. The advantage of having $B \in \mathbb{R}^{N\times N}$ is that it allows keeping the controlled trajectories *local* [14], that is, traveling directly towards the target state, $\mathbf{x}_f$, instead of wandering around the state space. As this is the exception rather than the rule, most of the issues coming from considering (2.5) in terms of control of networks are related to the fact that the control signals only affect a limited number of inputs ($p < N$) and that there is no guarantee that the topology will be energetically efficient [35, 39]. Summarizing, ensuring the Kalman condition is verified or equivalently the gramian is nonsingular, only theoretically guarantees we are able to control a network, as in practice, unbearable energy costs might limit our ability to control real large networks.

3 Control of temporal networks

In the direction of finding a way to reduce the control energy without increasing the number of drivers, the authors of [29] suggested that exploiting temporality, that is, the network variability over time, could substantially reduce energy requirements. In what follows we give some preliminaries on temporal networks (Section 3.1) and then summarize the results shown in [29] (Sections 3.2–3.4).

3.1 Temporal networks

The first natural extension of static networks, allowing to explicitly account for the time intervals at which the interactions among the agents occur, is represented by temporal networks. In this thesis, we refer to temporal networks whose graphs are denoted *interval graphs* in [19], where the nodes are given, while the edges are active over a set of consecutive time intervals $\mathcal{T} = \{[t_0, t_1), \ldots, [t_{m-1}, t_m)\}$, that is, the interactions are encoded in an ordered sequence of time-invariant adjacency matrices $\mathcal{A} = \{A_0, A_1, \ldots, A_k, \ldots, A_{m-1}\}$. Moreover, we denote the pair $\{A_k, [t_k, t_{k+1})\}$, the k-th time-snapshot or, for brevity, snapshot. A wide range of natural and artificial systems can be modeled as interval graphs. For instance, this is the case of ensembles of mobile agents, where proximity plays a relevant role in determining their interaction patterns: the edge between a pair of agents is only active in the time intervals when they have been sufficiently close. Other notable examples of systems where interval graphs modeling is required include computer networks where continuous network connectivity may lack [40], neuroscience [25], and finance [41], among the others. The unavoidable complication due to an extra dimension, time, is, sometimes, worth the effort in terms of the increased accuracy in understanding the phenomenon the network is describing and therefore in controlling such phenomenon, as we will show next.

The authors of [29] presented a threefold exciting result that would indicate a fundamental advantage in facing with the control of temporal rather than static linear dynamical networks. To allow comparing temporal and static networks, thus allowing to appreciate this advantage, for a given temporal network, they define its static counterpart as the corresponding aggregated network, with adjacency matrix A_s that is the average of each of the adjacency matrices A_k, for $k = 0, \ldots, m-1$(see Figure 3.1 for an example).

They show that for the temporal network described by

$$\begin{aligned} \dot{\mathbf{x}}(t) =& A_k \mathbf{x}(t) + B\mathbf{u}(t) \quad t \in [t_k, t_{k+1}) \;\; k = 0, \ldots, m-1 \\ \mathbf{x}_0 =& 0, \end{aligned} \tag{3.1}$$

1. The controllable subspace of network (3.1) never shrinks respect with that of its static counterpart, that is, network (3.1) with A_s for all $t \in [t_0, t_m)$ instead of A_k in $[t_k, t_{k+1})$ $k = 0, \ldots, m-1$.
   Indeed, even if one or more snapshots[1] are uncontrollable, the entire temporal network can be controllable or, at least more controllable than its static counterpart (see Figure 3.1 for an example). To quantify how much more controllable it is, they define S_t (S_s) as the number of snapshots required to have full controllability of the temporal (static) network. Unfortunately, there is no proof of the existence of an order relation between S_s and S_t (see details in Section 3.2).
2. The minimum energy required to steer the temporal network from $\mathbf{x}_0$ to $\mathbf{x}_f$ is less than the energy required to control its static counterpart from $\mathbf{x}_0$ to $\mathbf{x}_f$ by orders of magnitude (see details in Section 3.3).
3. Some real systems are such that the states of the nodes should not take arbitrary values. For instance, the generator frequencies in the power grid can only vary within a narrow range around their normal operating point, without inducing failures. Therefore, the controlled trajectories cannot arbitrarily wander into the state space but must exhibit a high degree of locality [14]. To test the degree of locality in temporal networks, they compute the length of the network controlled trajectories, as $L = \int_{t_0}^{t_f} \|\dot{\mathbf{x}}(t)\| \mathrm{dt}$ (see details in Section 3.4).

3.2 Controllability of temporal networks

Consider the temporal network in (3.1). The controllable subspace, Ω_c is

$$\Omega_c = \langle A_{m-1} \mid B \rangle + \sum_{k=0}^{m-2} \prod_{j=m-1}^{k} \mathrm{e}^{A_j \delta_j} \langle A_k \mid B \rangle \tag{3.2}$$

where $\langle A_k \mid B \rangle = \sum_{i=0}^{N-1} A_k^i \mathcal{R}(B)$ is the controllable subspace of the k-th snapshot with time interval $\delta_k := t_{k+1} - t_k$. Therefore, network (3.1) is controllable if

$$\Omega_c \equiv \mathbb{R}^N \text{[2]}. \tag{3.3}$$

According to Equation (3.2), the controllable subspace will never shrink as the topology varies. Hence, it is possible to define S_t as the minimum number of snapshots before network (3.1) becomes fully controllable.

[1] Note that as we are dealing with controlled temporal networks with *snapshot* we denote the triplet $\{A_k, B_k, [t_k, t_{k+1})\}$. However, as we will consider $B_k = B$ for all k, we can still identify the snapshot through the pair $\{A_k, [t_k, t_{k+1})\}$.

[2] Note that condition (3.3) for a static network (i.e., with $A_k = A$), corresponds to the traditional Kalman rank condition.

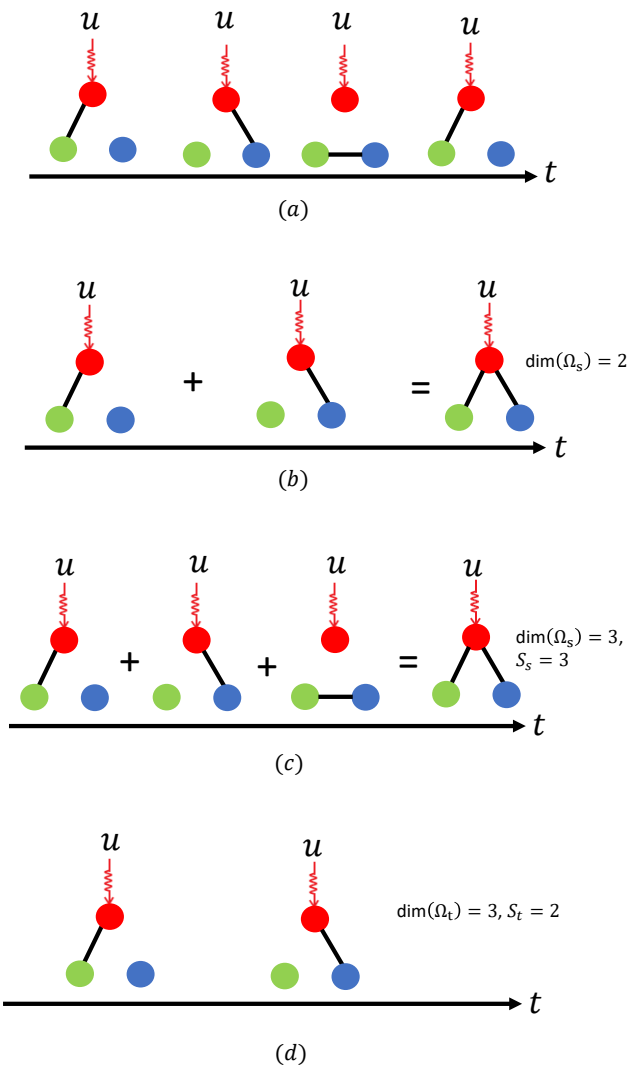

Figure 3.1: Toy example of a linear temporal network [29], as an ordered sequence of static graphs (a). In (b) the static graph obtained by aggregating the first two snapshots of the temporal graph depicted in (a) is uncontrollable as the dimension of its controllability space is less than 3, i.e., $|\Omega_s| < N$. In (c), it is shown that by adding an extra snapshot the corresponding static network is controllable as $\Omega_s \equiv \mathbb{R}^N$, as $S_s = 3$. However, the temporal network becomes fully controllable at the second snapshot as $S_t = 2$ (Panel (d)).

To make the point clear, in Figure 3.1, we report the toy example shown in [29]. Specifically, in Panel (a) of Figure 3.1 a 3-node temporal network with uncontrollable snapshots is considered, and in panels (b)-(d) is shown the meaning of S_t and of S_s. Indeed, while to obtain a corresponding controllable static network $S_s = 3$ snapshots are needed, the temporal network is controllable after $S_t = 2$ snapshots. It has to pointed out that there is no formal proof of the relation between S_t and S_s for a given temporal network.

3.3 Minimum energy control of temporal networks

To quantify how a wider controllable subspace with respect to that of a static network reflects in a more efficient control action, the authors of [29] search for the minimum energy control input $\mathbf{u}(t)$ as the solution of the following *conceptual* optimal control:

$$\begin{aligned} \min_{\mathbf{u}} \frac{1}{2} \int_{t_0}^{t_f} & \mathbf{u}(t)^T \mathbf{u}(t) \mathrm{d}t \\ & s.t. \\ & \dot{\mathbf{x}}(t) = A_k \mathbf{x}(t) + B\mathbf{u}(t) \quad t \in [t_k, t_{k+1}) \;\; k = 0, \dots, m-1 \\ & \mathbf{x}(t_0) = \mathbf{x}_0 \\ & \mathbf{x}(t_f) = \mathbf{x}_f \end{aligned} \tag{3.4}$$

where A_k is the static adjacency matrix at the k-th snapshot, i.e., in $[t_k, t_{k+1})$. Then, they reformulate problem (3.4) by exploiting the Bellman Principle [42] according to which the control energy stockpiled over each snapshot, say up to the k-th snapshot, must also be minimal for the control sub-problems of traveling between the initial and final states of each snapshots, say $(\mathbf{x}_k, \mathbf{x}_{k+1})$ for all $k = 0, \dots, m-1$. Indeed, in each snapshot k, the optimal control input according to (2.4) is

$$\mathbf{u}(t) = B^T \mathrm{e}^{A_k^T (t_{k+1} - t)} \mathbf{c}_k \quad \text{for} \quad t_k \le t \le t_{k+1}, \;\; k = 0, \dots, m-1 \tag{3.5}$$

with $\mathbf{c}_k = W_k^{-1} \left(\mathbf{x}_{k+1} - \mathrm{e}^{A_k (t_{k+1} - t_k)} \mathbf{x}_k \right)$ where the $(k+1)$-th waypoint, $\mathbf{x}_{k+1}$, is the real decision variable in the k-th control subproblem. Therefore, after some algebra, the unfeasible problem in (3.4) can be written in a mathematically treatable form as follows

$$\begin{aligned} \min_{\mathbf{c}} & \frac{1}{2} \mathbf{c}^T W \mathbf{c} \\ & s.t. \\ & H\mathbf{c} = \mathbf{d} \end{aligned} \tag{3.6}$$

where:

- $\mathbf{c} = (\mathbf{c}_0^T, \dots, \mathbf{c}_{m-1}^T)^T \in \mathbb{R}^{mN}$;
- $\mathbf{d} = \mathbf{x}_m - \mathrm{e}^{A_{m-1} \delta_{m-1}} \dots \mathrm{e}^{A_0 \delta_0} \mathbf{x}_0 \in \mathbb{R}^N$;
- $W = \mathrm{diag}(W_0, W_1, \dots, W_{m-1}) \in \mathbb{R}^{mN \times mN}$ with $W_k = \int_{t_k}^{t_{k+1}} \mathrm{e}^{A_k (t_{k+1} - t)} B B^T \mathrm{e}^{A_k^T (t_{k+1} - t)} \mathrm{d}t \in \mathbb{R}^{N \times N}$;

- $H = (e^{A_{m-1}\delta_{m-1}} \dots e^{A_1\delta_1} W_0, \dots, e^{A_{m-1}\delta_{m-1}} \dots e^{A_{k+1}\delta_{k+1}} W_k, \dots, W_m) \in \mathbb{R}^{N\times mN}$

with m the total number of snapshots and $\delta_k := t_{k+1} - t_k$. The optimal solution turns out to be

$$\mathbf{c}^* = S^T \left(SWS^T\right)^{-1} \mathbf{d}, \tag{3.7}$$

with the corresponding minimum control energy being

$$J^*(t_0, t_f) = \frac{1}{2}\mathbf{d}^T W_{\text{eff}}^{-1}\mathbf{d}, \tag{3.8}$$

where

- $t_f \equiv t_m \in \mathbb{R}_{\geq 0}$
- $S = \left(e^{A_{m-1}\delta_{m-1}} \dots e^{A_1\delta_1}, \dots, e^{A_{m-1}\delta_{m-1}} \dots e^{A_{k+1}\delta_{k+1}}, \dots, I_N\right) \in \mathbb{R}^{N\times mN}$;
- $W_{\text{eff}} = SWS^T$ is called *effective* gramian matrix. Note that $W_{\text{eff}} \neq W$ as the effective portion of the network concurring to the increase of the control energy does not correspond to the entire considered temporal network.

As the control energy grows as $\mathbf{x}_0$ and $\mathbf{x}_f$ come further apart, if we set $\mathbf{x}_0 = 0$ and normalize (3.8), that is,

$$\bar{J} = \frac{\mathbf{x}_f^T \left(SWS^T\right)^{-1} \mathbf{x}_f}{2\mathbf{x}_f^T\mathbf{x}_f} \tag{3.9}$$

we can obtain the following bounds

$$\frac{1}{2\lambda_{\max}(W_{\text{eff}})} \leq \bar{J} \leq \frac{1}{2\lambda_{\min}(W_{\text{eff}})}.$$

Besides the scaling behavior of the energy bounds, to make the comparison between the energy required to control a temporal network with respect to its static counterpart, the authors of [29] show by numerical simulations, both on real and synthetic data, that $J^*_{\text{temporal}} << J^*_{\text{static}}$. Practically speaking, this apparently counterintuitive finding can be explained by considering that the temporality of a network allows its state to move along the more efficient directions when it is possible (i.e., when the topology changes in a favorable direction) and eventually to stop when the cost of control is prohibitive. On the contrary, in a static network we have no choice and we must control also in energetically costly directions. However, the orders of magnitude in the energy saving are strongly linked with the choice of the static counterpart as we will show in Section 4.2.

3.4 Locality of the controlled trajectories

The locality of the controlled trajectories is an extra measure of the efficiency in controlling a network. Indeed, as shed out in [14], whenever the control input and the energy required to steer a network from an initial state to a final state in finite time is, by chance,

numerically computable, if the drivers nodes are less than the number of nodes, the controlled trajectories show a high degree of non-locality. Let,

$$L = \int_{t_0}^{t_f} \|\dot{\mathbf{x}}(t)\| \mathrm{d}t \tag{3.10}$$

be the length of the optimally controlled trajectory of a network steered from $\mathbf{x}_0$ to $\mathbf{x}_f$, $\eta := \|\mathbf{x}_f - \mathbf{x}_0\|$ being their distance, and for the sake of simplicity, set $\mathbf{x}_0 = 0$. Then, it easy to see that L, independently on the temporality of the network, increases linearly with $\|\mathbf{x}_f\|$, indeed the controlled trajectory of a static network is

$$\mathbf{x}(t) = W_{t_0,t} W_{t_0,t_f}^{-1} \mathrm{e}^{A(t_f - t_0)} \mathbf{x}_f$$

where $W_{t_0,t} = \int_{t_0}^{t} \mathrm{e}^{A(\tau - t_0)} B B^T \mathrm{e}^{A^T(\tau - t_0)} \mathrm{d}\tau$. The control energy in (3.9) decreases by orders of magnitude with respect to that of its static counterpart as, for a fixed η, the locality degree [14] decreases by orders of magnitude as numerically illustrated in [29]. Indeed, the general non-locality of the controlled trajectories is a natural consequence of the fact that not all the eigen-direction are energetically efficient and that to target the final state the controller could travel zigzag in the state space. On the contrary, the more locality of the temporal networks trajectories, again, is a byproduct of the possibility of the controller to move along more energetically efficient direction and straight to $\mathbf{x}_f$.

4 Control of stochastic temporal networks

In this Chapter we present the problem of controlling temporal networks in the scenario where only a probabilistic description of the network evolution is available [43]. To do so, we first introduce the concept of *stochastic temporal graphs*.

Definition 4.1 (Stochastic temporal networks). *A* stochastic *interval graph defined over a set of consecutive time intervals* $\mathcal{T} = \{[t_0, t_1), \ldots, [t_{m-1}, t_m)\}$ *is an interval graph in which the adjacency matrices are independently drawn from a family* $\mathcal{F} = \{A_i\}_{i \in \mathcal{I}}$ *according to a given probability distribution. We will refer to it also as a* stochastic *temporal graph.*

Hence, the sequence of adjacency matrices regulating the network topology can be viewed as a stationary stochastic process. To simplify the notation, we model this by enforcing that at each time-instant the realization $A_{\sigma(k)} = \left[a_{ij}(\sigma(k))\right]_{i,j=1}^{n}$ depends on the value of the i.i.d. switching signal $\sigma(k)$. Consequently, the stochastic temporal networks we aim to control are described by

$$\dot{\mathbf{x}}(t) = A_{\sigma(k)}\mathbf{x}(t) + B\mathbf{u}(t), \qquad t \in [t_k, t_{k+1}), \quad k = 0, 1, 2, \ldots, m \tag{4.1}$$

where:

- $A_{\sigma(k)} \in \mathbb{R}^{N \times N}$ is the adjacency matrix of the stochastic temporal graph in the k-th snapshot;
- $B \in \mathbb{R}^{N \times p}$ is the time-invariant input matrix that identifies the set of $p \leq N$ driver nodes which we directly influence through the control input $\mathbf{u}(t) \in \mathbb{R}^N$;
- $[t_k, t_{k+1})$ is the k-th snapshot.

The main goal is to uncover when the opportunities offered by temporality (and reported in Chapter 3) prevail over uncertainty.

In this stochastic scenario,
does temporality still represent an advantage for network control?

To answer this question we must first find the signal $\mathbf{u}(t)$ that minimizes the *expected*

energy required to drive the network from an initial state $\mathbf{x}(t_0)$ to a final state $\mathbf{x}(t_m)$, that is,

$$\begin{aligned}\min_{\mathbf{u}(t)} \mathrm{E}\left[J(\mathbf{u}(t))\right] =& \frac{1}{2}\int_{t_0}^{t_m} \mathbf{u}(t)^T \mathbf{u}(t)\mathrm{d}t \\ & s.t. \\ & \dot{\mathbf{x}}(t) = A_{\sigma(k)}\mathbf{x}(t) + B\mathbf{u}(t) \quad t \in [t_k, t_{k+1}) \;\; k = 0, \ldots, m-1 \\ & \mathbf{x}(t_0) = \mathbf{x}_0 \\ & \mathbf{x}(t_f) = \mathbf{x}_f\end{aligned} \tag{4.2}$$

Note that problem in (4.2) is unsolvable as it is, since the N constraints on the network state depend on a stochastic variable $A_{\sigma(k)}$. Therefore, in what follows we reformulate and solve (4.2) by means of tools by Stochastic Optimal Control theory.

4.1 Minimum energy control of stochastic temporal networks

To do so we must first give a condition for controllability that suits this scenario. As the sequence of future snapshots is unknown *a priori*, guaranteeing that a temporal network is controllable, implies selecting a B such that any possible realization of the pair (A_k, B), $k = 0, \ldots, m-1$ is controllable. This ensures that in each snapshot

$$\mathbf{u}^*(t) = B^T \mathrm{e}^{A^T_{\sigma(k)}(t_{k+1}-t_k)} W_k^{-1} (\mathbf{x}_{k+1} - \mathrm{e}^{A^T_{\sigma(k)}(t_{k+1}-t_k)} \mathbf{x}_k) \tag{4.3}$$

where by $\mathbf{x}_j$ we denote $\mathbf{x}(t_j)$, is the well-defined minimum energy control input.

Under this assumption, to investigate whether temporality can mitigate the control effort, in what follows we employ Stochastic Optimal Control. Therefore, we find the signal $\mathbf{u}(t)$ that minimizes the *expected* energy required to drive the network from an initial state $\mathbf{x}_0$ to a final state $\mathbf{x}_m$. It turns out that minimizing (4.2) implies transitioning between any two consecutive waypoints with minimum energy. This can be achieved, in each snapshot, by means of the classic minimum energy control input (4.3). At the onset of the k-th snapshot (i.e., at time t_k), as $\mathbf{u}^*(t)$ is a function of $\mathbf{x}_k$ and $\mathbf{x}_{k+1}$, the actual choice for the decision maker is the next waypoint. Following this observation, also our problem becomes that of finding the optimal sequence of waypoints with the non negligible difference of not knowing, at t_k, the future actual sequence of the adjacency matrices, i.e., $A_{\sigma(k+1)}, \ldots, A_{\sigma(m-1)}$.

Denoting by ς_k the vector $[\sigma(k), \ldots, \sigma(m-1)]^T$, we pose the following optimization problem, which consists in minimizing the expected control energy:

$$\begin{aligned}\min_{\mathbf{u}(t)} J_{\text{temporal}} :=& \mathop{\mathrm{E}}_{\varsigma_1}\left[J(\mathbf{u})\right] \\ & \text{s.t.} \\ & \dot{\mathbf{x}}(t) = A_{\sigma(k)}\mathbf{x}(t) + B\mathbf{u}(t), \quad t \in [t_k, t_{k+1}), \quad k = 0, \ldots, m-1, \\ & \mathbf{x}(t_0) = \mathbf{x}_0, \quad \mathbf{x}(t_m) = \mathbf{x}_m, \quad A_{\sigma(0)} = A_0\end{aligned} \tag{4.4}$$

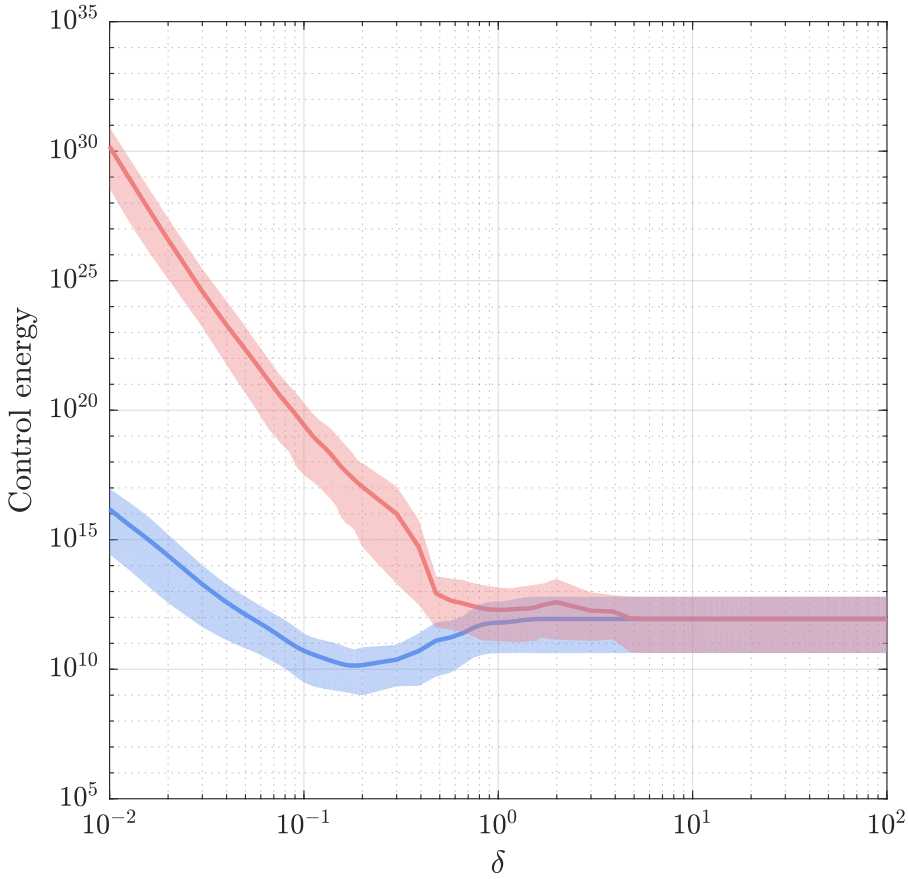

Figure 4.1: **Control energy requirements in the deterministic (blue) and stochastic (red) scenario for the yeast Saccharmoyces Cerevisiae.** The solid lines are the minimum energies averaged over 10^3 final states $\mathbf{x}(t_m)$, selected on the unit hypersphere centered in the origin, as a function of $\delta = (t_m - t_0)/m$. The shaded areas are enclosed by the observed minimum and maximum energies. The minimum energy feedback control strategy is implemented both in the stochastic and in the deterministic scenario (see the numerical settings details in Section 6.2, Appendix 6). The picture shows that in the stochastic scenario the control can be orders of magnitude more energetically demanding with respect to the deterministic scenario. The energy gap tends to vanish when δ increases, that is, when the temporality becomes slower.

where

$$\mathop{\mathrm{E}}_{\varsigma_1}[J(\mathbf{u})] = \int_{-\infty}^{+\infty} \cdots \int_{-\infty}^{+\infty} J(\mathbf{u}) f_{\varsigma_1}(\varsigma_1) \mathrm{d}\sigma(1) \cdots \mathrm{d}\sigma(m-1),$$

with f_{ς_1} being the joint probability distribution of the variables $\sigma(1), \ldots, \sigma(m-1)$. To solve this problem, some preliminary considerations have to be made on the cost function. Indeed, we can write

$$\mathop{\mathrm{E}}_{\varsigma_1}[J(\mathbf{u})] = \mathop{\mathrm{E}}_{\varsigma_1}\left[\sum_{k=0}^{m-1} J_k(\mathbf{u}_k)\right], \tag{4.5}$$

where

$$J_k(\mathbf{u}_k) = \int_{t_k}^{t_{k+1}} \mathbf{u}_k(t)^T \mathbf{u}_k(t) \mathrm{d}t,$$

and $\mathbf{u}_k(t)$ is the restriction of $\mathbf{u}(t)$ to $[t_k, t_{k+1})$, for $k = 0, \ldots, m-1$. As anticipated, notice that for given values of $\mathbf{x}_k$, $\mathbf{x}_{k+1}$, and $\sigma(k)$, the input $\mathbf{u}_k^*$ minimizing J_k is the well-known solution of the following standard minimum energy control problem:

$$\begin{aligned} &\min_{\mathbf{u}_k} J_k(\mathbf{u}_k) \\ &\quad \text{s.t.} \\ &\dot{\mathbf{x}}(t) = A_{\sigma(k)}\mathbf{x}(t) + B\mathbf{u}(t), \quad t \in [t_k, t_{k+1}), \\ &\mathbf{x}(t_k) = \mathbf{x}_k, \\ &\mathbf{x}(t_{k+1}) = \mathbf{x}_{k+1}. \end{aligned} \tag{4.6}$$

Namely, the optimal solution is

$$\mathbf{u}_k^*(\mathbf{x}_k, \mathbf{x}_{k+1}, \sigma(k), t) = B^T \mathrm{e}^{A_{\sigma(k)}^T (t_{k+1}-t)} W_k^{-1} \left(\mathbf{x}_{k+1} - \mathrm{e}^{A_{\sigma(k)}(t_{k+1}-t_k)}\mathbf{x}_k\right), \quad t \in [t_k\ t_{k+1}), \tag{4.7}$$

where

$$W_k = \int_{t_k}^{t_{k+1}} \mathrm{e}^{A_{\sigma(k)}(t_{k+1}-\tau)} B B^T \mathrm{e}^{A_{\sigma(k)}^T (t_{k+1}-\tau)} d\tau$$

is the reachability gramian[1]. Noting that $J_k(\mathbf{u}_k) \geq J_k(\mathbf{u}_k^*)$ for all possible $\mathbf{x}_k$, $\mathbf{x}_{k+1}$, and $\sigma(k)$, we can conclude that the structure of the solution of (4.4) is given by Equation (4.7). This entails that problem (4.4) can be viewed as a concatenation of problems (4.6) in each of which $\mathbf{x}_k$ is given and $\mathbf{x}_{k+1}$ is the actual decision variable. Accordingly, solving (4.4) becomes equivalent to select the optimal waypoints $\mathbf{x}_1^*, \ldots, \mathbf{x}_{m-1}^*$. Therefore, substituting (4.7) in the objective function (4.5), we have

$$J_k(\mathbf{x}_k, \mathbf{x}_{k+1}) = \left(\mathbf{x}_{k+1} - \mathrm{e}^{\delta_k A_{\sigma(k)}}\mathbf{x}_k\right)^T W_k^{-1} \left(\mathbf{x}_{k+1} - \mathrm{e}^{\delta_k A_{\sigma(k)}}\mathbf{x}_k\right). \tag{4.8}$$

Hence, we can rewrite the minimum energy control problem as

$$\min_{\substack{\mathbf{x}_1 \\ \vdots \\ \mathbf{x}_{m-1}}} \mathop{\mathrm{E}}_{\varsigma_1}\left[\sum_{k=0}^{m-1} J_k(\mathbf{x}_k, \mathbf{x}_{k+1})\right], \tag{4.9}$$

[1]We remark that the well-posedness of problem (4.6) requires the pair $(A_{\sigma(k)}, B)$ to be reachable.

where, at each k, $A_{\sigma(k)}$ is known. The following theorem provides a recursive solution for computing the optimal waypoints.

Theorem 4.2. *The solution of the optimal control problem (4.9) is given by*

$$\mathbf{x}_k^* = P_k \mathbf{x}_m + Q_k \mathbf{x}_{k-1}, \quad k = 1, \dots, m-1, \tag{4.10}$$

where

$$\begin{aligned} P_k &= \left(W_{k-1}^{-1} + \sum_{i=k}^{m-1} \mathop{\mathrm{E}}_{\varsigma_k} \left[{R_k^i}^T W_i^{-1} R_k^i \right] \right)^{-1} \sum_{i=k}^{m-1} \mathop{\mathrm{E}}_{\varsigma_k} \left[{R_k^i}^T W_i^{-1} F_k^i \right], \\ Q_k &= \left(W_{k-1}^{-1} + \sum_{i=k}^{m-1} \mathop{\mathrm{E}}_{\varsigma_k} \left[{R_k^i}^T W_i^{-1} R_k^i \right] \right)^{-1} W_{k-1}^{-1} \mathrm{e}^{\delta_{k-1} A_{\sigma(k-1)}}, \end{aligned} \tag{4.11}$$

with

$$\begin{aligned} R_k^i &= \begin{cases} \mathrm{e}^{\delta_k A_{\sigma(k)}} - Q_{k+1}, & i = k, \\ R_{k+1}^i Q_{k+1}, & i > k, \end{cases} \quad k = 0, \dots, m-2, \\ F_k^i &= \begin{cases} P_{k+1}, & i = k, \\ F_{k+1}^i - R_{k+1}^i P_{k+1}, & i > k, \end{cases} \quad k = 0, \dots, m-2, \\ R_{m-1}^{m-1} &= \mathrm{e}^{\delta_{m-1} A_{\sigma(m-1)}}, \qquad F_{m-1}^{m-1} = I. \end{aligned} \tag{4.12}$$

Furthermore, the associated optimal cost is given by

$$J_{\text{temporal}}^* = \mathop{\mathrm{E}}_{\varsigma_1} \left[\sum_{i=0}^{m-1} \left(F_0^i \mathbf{x}_m - R_0^i \mathbf{x}_0 \right)^T W_i^{-1} \left(F_0^i \mathbf{x}_m - R_0^i \mathbf{x}_0 \right) \right]. \tag{4.13}$$

Proof. See Section 6.1 in Appendix 6. □

To shad out that (4.13) is equivalent to (3.8) when the temporal network is not stochastic, i.e., $A_{\sigma(k)} = A_k$, we report here the optimal value of the control energy when $\mathbf{x}_0 = 0$, $\delta_k = \delta \ \forall k$ and $m = 2$. According to (3.8), the optimal control energy is:

$$\begin{aligned} J_2^\star =& \frac{1}{2} \mathbf{x}_2^T \left(S W S^T \right)^{-1} \mathbf{x}_2 = \frac{1}{2} \mathbf{x}_2^T \left(\mathrm{e}^{A_1 \delta} W_0 \mathrm{e}^{A_1^T \delta} + W_1 \right)^{-1} \mathbf{x}_2 = \\ & \frac{1}{2} \left[W_1^{-1} - W_1^{-1} \mathrm{e}^{A_1 \delta} \left(\mathrm{e}^{A_1^T \delta} W_1^{-1} \mathrm{e}^{A_1 \delta} + W_0^{-1} \right)^{-1} \mathrm{e}^{A_1^T \delta} W_1^{-1} \right] \mathbf{x}_2 \end{aligned} \tag{4.14}$$

where the last inequalities comes from applying the Inversion Lemma[2]. Now, (4.13) in the same instance can be rewritten as

$$J_2^* = \frac{1}{2} \mathbf{x}_m^T \mathop{\mathrm{E}}_{\varsigma(1)} \left[\sum_{i=0}^{m-1} {F_0^i}^T W_i^{-1} F_0^i \right] \mathbf{x}_m = \frac{1}{2} \mathbf{x}_m^T W_{\exp} \mathbf{x}_m.$$

[2]For the Inversion Lemma, given matrices A, E, if $E = BCD$, the inversion of their sum is $(A+E)^{-1} = A^{-1} - A^{-1}B(DA^{-1}B + C^{-1})^{-1}DA^{-1}$.

with $W_{\text{exp}} := \mathrm{E}_{\varsigma(1)}\left[\sum_{i=0}^{m-1} F_0^{i\,T}\, W_i^{-1} F_0^i\right]$ being the *expected* gramian in $(0, t_2)$. After some calculations, it can be seen that when $A_{\sigma(k)} = A_k$, that is, when we drop off the expected values, the expression of W_{eff} coincides with that of W_{exp} becoming

$$\left(\mathrm{e}^{A_1 \delta} W_0 \mathrm{e}^{A_1^T \delta} + W_1\right).$$

As a gramian, W_{exp} encodes the energy structure of the stochastic temporal network and thus its trace represents the expected energy required to reach any point on the ellipsoid whose semiaxes are $\mathbf{v}_i(W_{\text{exp}})/\sqrt{\lambda_i(W_{\text{exp}})}$ starting from the origin (see Section 2.1). We leverage the developed machinery to compare the tasks of controlling a temporal network in a deterministic and in a stochastic setting. An exemplary illustration of the effect of uncertainty is reported in Figure 4.1, which depicts the minimum energy required to control a temporal network obtained from the time-varying protein-protein binding interactions [44], condensed over consecutive time windows of equal length δ. Compared with the deterministic case where the sequence of snapshots is known a priori, and thus the waypoints can be computed in advance, the stochastic setting demands orders of magnitude more energy when the network temporality is fast (small δ). This difference reduces and asymptotically vanishes as the duration of each snapshot increases. In what follows we delve into the above points, that is, the relation with the selected static benchmark and the impact of the duration of each snapshot on the amount of energy required.

4.2 Benchmark energy

To support the evidence of Figure 4.1, we introduce an appropriate benchmark for the a priori expected minimum energy (4.13) required to drive the stochastic temporal network (4.1) from $\mathbf{x}_0$ to $\mathbf{x}_m$. Notice that, as we consider a i.i.d. process $\sigma(k)$, the marginal probability distribution $f_{\sigma(k)}(\sigma(k))$ will be the same for all k, that is, we can write

$$f_{\sigma(k)}(\sigma(k)) = f_\sigma(\sigma).$$

Now, for each feasible realization of σ, we can consider the following static optimization problem where matrix $A_{\sigma(k)} = A_\sigma$ for all k:

$$\begin{aligned} \min_{\mathbf{u}} \; & \int_{t_0}^{t_m} \mathbf{u}(t)^T \mathbf{u}(t) \mathrm{d}t \\ & \text{s.t.} \\ \dot{\mathbf{x}}(t) &= A_\sigma \mathbf{x}(t) + B\mathbf{u}(t), \quad t \in [t_0, t_m), \\ \mathbf{x}(t_0) &= \mathbf{x}_0, \\ \mathbf{x}(t_m) &= \mathbf{x}_m, \end{aligned} \tag{4.15}$$

with associated optimal cost

$$J^*_{\text{static}}(\sigma) = \left(\mathbf{x}_m - \mathrm{e}^{(t_m - t_0) A_\sigma} \mathbf{x}_0\right)^T W_\sigma^{-1} \left(\mathbf{x}_m - \mathrm{e}^{(t_m - t_0) A_\sigma} \mathbf{x}_0\right), \tag{4.16}$$

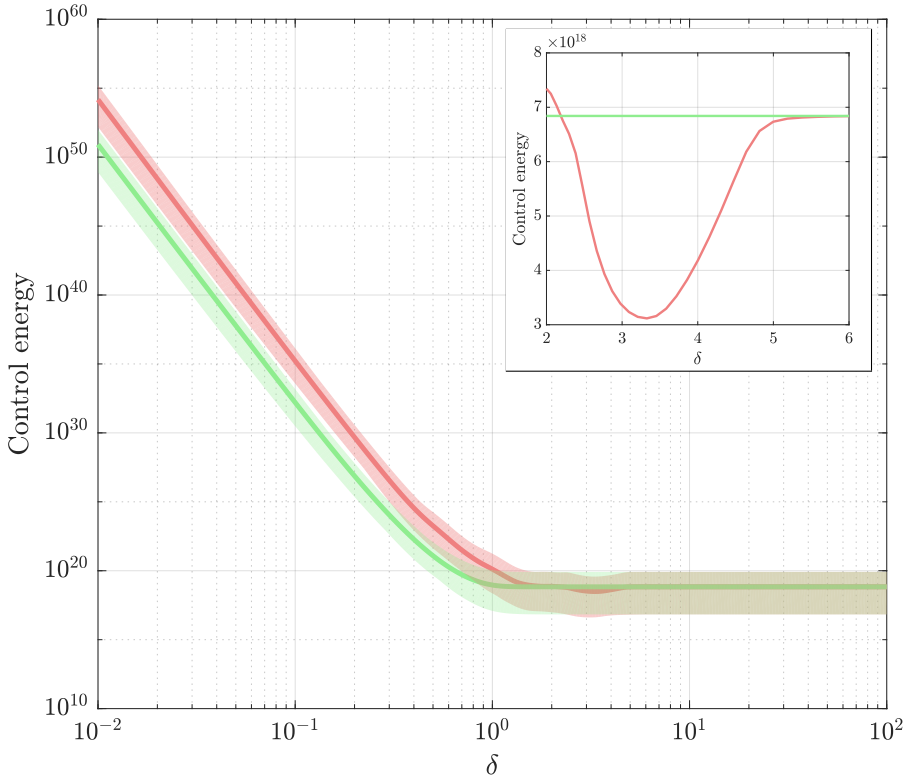

Figure 4.2: **The advantage of temporal networks in the stochastic scenario.** The solid lines represent the minimum expected energy (in red) averaged over all possible final states on the unit hypersphere centered in the origin and the benchmark energy (in green) as a function of $\delta = (t_m - t_0)/m$. The shaded areas are enclosed by the minimum and the maximum energies observed over 10^5 final states on the unit hypersphere (see Section 6.2, Appendix 6). In the fast regime (i.e., for small δ), uncertainty prevails over temporality with the expected energy required to control a temporal network being larger than the benchmark energy. As temporality vanishes (i.e., for large δ), the energy difference becomes negligible. The advantage of temporality appears in the intermediate temporality regime and is shown in the inset.

where

$$W_\sigma = \int_{t_0}^{t_m} \mathrm{e}^{A_\sigma(t_m-\tau)} B B^T \mathrm{e}^{A_\sigma^T(t_m-\tau)} \mathrm{d}\tau. \tag{4.17}$$

Therefore, a natural benchmark in our setting is the expected value of the minimum energy associated to the family of static problems in (4.15), that is,

$$J_\mathrm{b}^* := \mathop{\mathrm{E}}_{\sigma} \left[J_{\mathrm{static}}^*(\sigma) \right]. \tag{4.18}$$

Notice that our choice is different from that made in [29], where the benchmark energy was selected as the energy required to control the aggregate network, an average network, that is, a network described by matrix $\bar{A} = \mathrm{E}_\sigma [A_\sigma]$. This choice would yield the apparent paradox of temporality being beneficial even when so slow to be taken into consideration as it is better explained in the next Section.

4.3 The effect of temporality regime

As shown in Figure 4.2, in the fast temporality regime (with very small δ) the expected energy required to control a temporal network can exceed by orders of magnitude that required by a static network. On the other hand, in the slow temporality regime, we observe that this difference becomes negligible. To support our intuition, as most real systems in their normal mode of operation exhibit stability [45], we focus on the case in which, for all k, all the admissible topologies $A_{\sigma(k)}$ are described by Hurwitz matrices. Under this hypothesis, by using the analytic solution provided by Thorem 4.2, we show that when the network temporality is extremely slow ($\delta \to \infty$), the difference between expected energy J^* associated to the optimal solution and the energy J_b^* associated to the static benchmark tends to be negligible. On the contrary, when the network variability is extremely fast ($\delta \to 0$), temporality becomes detrimental, that is $J^* > J_\mathrm{b}^*$, with the only exception of the two-snapshot case in which $J^* = J_\mathrm{b}^*$.
For the sake of illustration, we derive results first in the two-snapshot case, and $\mathbf{x}_0 = 0$. Then, we extend the derivations to the general case.

4.3.1 The case of two snaphots

In this case, the expected optimal energy for controlling the stochastic temporal network can be written as

$$\begin{aligned} J^* = \mathop{\mathrm{E}}_{\sigma(0)} [J_{\mathrm{temporal}}^*] &= x_2^T \, \mathrm{E}\left[W_1^{-1}\right] x_2 \\ &- x_2^T \, \mathrm{E}\left[W_1^{-1} \mathrm{e}^{\delta A_{\sigma(1)}}\right] \mathrm{E}\left[\left(\mathrm{E}\left[W_{c,1}^{-1}\right] + W_0^{-1}\right)^{-1}\right] \mathrm{E}\left[\mathrm{e}^{\delta A_{\sigma(1)}^T} W_1^{-1}\right] x_2, \end{aligned} \tag{4.19}$$

where $W_{c,1}$ is the controllability gramian, which is by definition related to the reachability gramian as follows:

$$W_{c,1}^{-1} = \mathrm{e}^{\delta A_{\sigma(1)}^T} W_1^{-1} \mathrm{e}^{\delta A_{\sigma(1)}}.$$

Taking the limit for $\delta \to +\infty$, as the spectrum of the matrices $A_{\sigma(k)}$ belongs to the open-left half complex plane for all k, we have

$$\lim_{\delta \to +\infty} \mathrm{e}^{\delta A_{\sigma(1)}} = 0.$$

Now, taking advantage of the following well-known relationship between the finite-time and infinite-time gramians [46]

$$W_1 = W_1^{\infty} - \mathrm{e}^{\delta A_{\sigma(1)}} W_1^{\infty} \mathrm{e}^{\delta A_{\sigma(1)}^T},$$

where

$$W_1^{\infty} = \int_{t_0}^{\infty} \mathrm{e}^{\tau A_{\sigma(1)}} B B^T \mathrm{e}^{\tau A_{\sigma(1)}^T} \mathrm{d}\tau,$$

one obtains

$$\lim_{\delta \to +\infty} W_1 = W_1^{\infty}, \text{ and } \lim_{\delta \to +\infty} W_{c,1}^{-1} = 0,$$

thus finally yielding

$$\lim_{\delta \to +\infty} J^* = x_2^T \, \mathrm{E}\left[(W_1^{\infty})^{-1} \right] x_2 = \lim_{\delta \to +\infty} J_{\mathrm{b}}^*. \tag{4.20}$$

A similar result can be achieved when the network variability is much faster than the fastest time constant of all possible snapshots. Indeed, when $\delta \to 0$, one obtains

$$\mathrm{e}^{\delta A_{\sigma(k)}} = I_N, \tag{4.21}$$

for all $k = 0, \ldots, m-1$, and for all $\sigma(k)$ associated to a positive value of the probability density function $f(\sigma(k))$. This also implies that

$$\lim_{\delta \to 0} W_{c,k} = \lim_{\delta \to 0} W_k = \lim_{\delta \to 0} \delta B B^T \tag{4.22}$$

independently from the realization of $\sigma(k)$. Hence, from (4.19) we get

$$\begin{aligned} \lim_{\delta \to 0} J^* &= \lim_{\delta \to 0} \left(\mathbf{x}_2^T (\delta B B^T)^{\dagger} \mathbf{x}_2 - \mathbf{x}_2^T (\delta B B^T)^{\dagger} \frac{\delta}{2} B B^T (\delta B B^T)^{\dagger} \mathbf{x}_2 \right), \\ &= \lim_{\delta \to 0} \frac{1}{2} \mathbf{x}_2^T (\delta B B^T)^{\dagger} \mathbf{x}_2 \end{aligned} \tag{4.23}$$

which is exactly what we obtain also for the static benchmark, as we indeed have

$$\lim_{\delta \to 0} \mathop{\mathrm{E}}_{\sigma} [W_{\sigma}] = \lim_{\delta \to 0} 2\delta B B^T,$$

implying $\lim_{\delta \to 0} J_{\mathrm{b}}^* = \lim_{\delta \to 0} \mathbf{x}_m^T W_{\sigma}^{-1} \mathbf{x}_m = \lim_{\delta \to 0} \mathbf{x}_m^T (2\delta B B^T)^{-1} \mathbf{x}_m = \lim_{\delta \to 0} J^*$.

4.3.2 Generalization

Case $\delta \to 0$

When $\delta \to 0$, from the recursive equations (4.11) and (4.12), some algebra allows to derive that

$$P_k, Q_k = \frac{I_N}{2}, \qquad k = 1, \dots, m-1, \tag{4.24}$$

and, for all $k = 0, \dots, m-1$, that

$$F_k^i = R_k^i = \alpha_k^i I_N, \qquad 0 \le k \le i \le m-1, \tag{4.25}$$

where

$$\alpha_k^i = \begin{cases} 1, & i = k, i = m-1, \\ 1/2, & i = k, i < m-1, \\ \alpha_k^{i-1}/2, & i > k, i < m-1, \\ \alpha_k^{i-1}, & i > k, i = m-1. \end{cases} \tag{4.26}$$

Notice that as $\sum_{i=k}^{m-1} \alpha_k^i = 1$ and $\alpha_k^i > 0$ for all i, k, then

$$\sum_{i=k}^{m-1} {\alpha_k^i}^2 \ge \frac{1}{m-k}, \qquad k = 0, \dots, m-1. \tag{4.27}$$

From (4.13), we can then write

$$\lim_{\delta \to 0} \mathop{\mathrm{E}}_{\sigma(0)} \left[J^*_{\text{temporal}} \right] = \sum_{i=0}^{m-1} {\alpha_0^i}^2 \lim_{\delta \to 0} (\mathbf{x}_m - \mathbf{x}_0)^T \left(\delta B B^T \right)^{-1} (\mathbf{x}_m - \mathbf{x}_0). \tag{4.28}$$

On the other hand, the static benchmark when δ tends to zero becomes

$$\lim_{\delta \to 0} \mathop{\mathrm{E}}_{\sigma} \left[J^*_{\text{static}}(\sigma) \right] = \frac{1}{m} \lim_{\delta \to 0} (\mathbf{x}_m - \mathbf{x}_0)^T \left(\delta B B^T \right)^{-1} (\mathbf{x}_m - \mathbf{x}_0). \tag{4.29}$$

Now, from (4.27) we have that $\sum_{i=0}^{m-1} {\alpha_0^i}^2 \ge 1/m$. Considering that $\sum_{i=0}^{m-1} {\alpha_0^i}^2 = 1/m$ if and only if $\alpha_0^i = \alpha_0^j$ for all i, j, we can finally conclude that

$$\lim_{\delta \to 0} \mathop{\mathrm{E}}_{\sigma(0)} \left[J^*_{\text{temporal}} \right] \begin{cases} = \lim_{\delta \to 0} \mathop{\mathrm{E}}_{\sigma} \left[J^*_{\text{static}}(\sigma) \right] & \text{if } m = 1, 2, \\ > \lim_{\delta \to 0} \mathop{\mathrm{E}}_{\sigma} \left[J^*_{\text{static}}(\sigma) \right] & \text{if } m \ge 3. \end{cases} \tag{4.30}$$

Moreover, by combining equations (4.10) and (4.24), we obtain

$$\mathbf{x}_k^* = \frac{\mathbf{x}_{k-1} + \mathbf{x}_m}{2}, \tag{4.31}$$

that is, the next optimal waypoint is halfway between the current waypoint and the final state $\mathbf{x}_m$.

Case $\delta \to +\infty$

When $\delta \to +\infty$, we have that $\lim_{\delta\to+\infty} \mathrm{e}^{\delta A_{\sigma(k)}} = 0$ for all possible realization of $\sigma(k)$, and for all k. Furthermore,

$$\lim_{\delta\to+\infty} W_k = W_k^{\infty} := \int_{t_0}^{+\infty} \mathrm{e}^{\tau A_{\sigma(k)}} B B^T \mathrm{e}^{\tau A_{\sigma(k)}^T} \mathrm{d}\tau.$$

Now, notice that from equations (4.11) and (4.12) we can write

$$\begin{aligned} R_k^i &= 0_N, \quad k = 0, \dots, m-1, \ k \le i \le m-1 \\ F_k^i &= \begin{cases} I_N, & \text{if } i = m-1, \\ 0_N, & \text{otherwise,} \end{cases} \end{aligned} \tag{4.32}$$

This yields

$$\lim_{\delta\to+\infty} \mathop{\mathrm{E}}_{\sigma(0)} \left[J^*_{\text{temporal}} \right] = \mathbf{x}_m^T \mathop{\mathrm{E}}_{\sigma(m-1)} \left[(W_{m-1}^{\infty})^{-1} \right] \mathbf{x}_m. \tag{4.33}$$

Now, observing that $\mathop{\mathrm{E}}_{\sigma(m-1)} \left[(W_{m-1}^{\infty})^{-1} \right] = \lim_{\delta\to+\infty} \mathop{\mathrm{E}}_{\sigma} \left[W_{\sigma}^{-1} \right]$, we finally get

$$\lim_{\delta\to+\infty} \mathop{\mathrm{E}}_{\sigma(0)} \left[J^*_{\text{temporal}} \right] = \lim_{\delta\to+\infty} \mathop{\mathrm{E}}_{\sigma} \left[J^*_{\text{static}}(\sigma) \right]. \tag{4.34}$$

Notice that equations (4.11) and (4.12) also implies that

$$P_k = 0_N, \quad Q_k = 0_N, \quad k = 1, \dots, m-1, \tag{4.35}$$

thus yielding $\mathbf{x}_k^* = 0$ for all $k = 1, \dots, m-1$.

Our derivations provide a formal proof of the intuition that when the temporality is so fast ($\delta \to 0$) that we do not have time to exploit it, the effect of uncertainty prevails. When instead the temporality is so slow ($\delta \to +\infty$) that most of the energy fed to the network in order to reach a targeted waypoint is dissipated in the next snapshots, we rather wait for the last snapshot, thus treating a temporal network as if it were static. The above formal analysis clarifies that the apparent paradox reported in [29] that temporality is advantageous even when so slow to be negligible is due to the use of an *ad hoc* static benchmark. Interestingly, we do find that there is a regime where temporality prevails on uncertainty (see the inset of Figure 4.2). To delve into this regime, we should take into account that all real world systems that can be modeled as dynamical networks are characterized by time scales. The digital communication networks [47], for instance, are determined by the time-scale of the dynamical flow of the data packets, while those of epidemic spreading processes [48] depend on the specific infection rate, and can range from few days to months [19]. For a linear network, and thus for each of our snapshots, the time scale is related to the eigenvalues of the matrix A_k. Our numerical results reveal that shifting the spectrum of the snapshots shifts the regime where the advantage of temporality is touchable (see Figure 4.3). In other words, temporality prevails on uncertainty, provided it matches the time scales of the network we are trying to control.

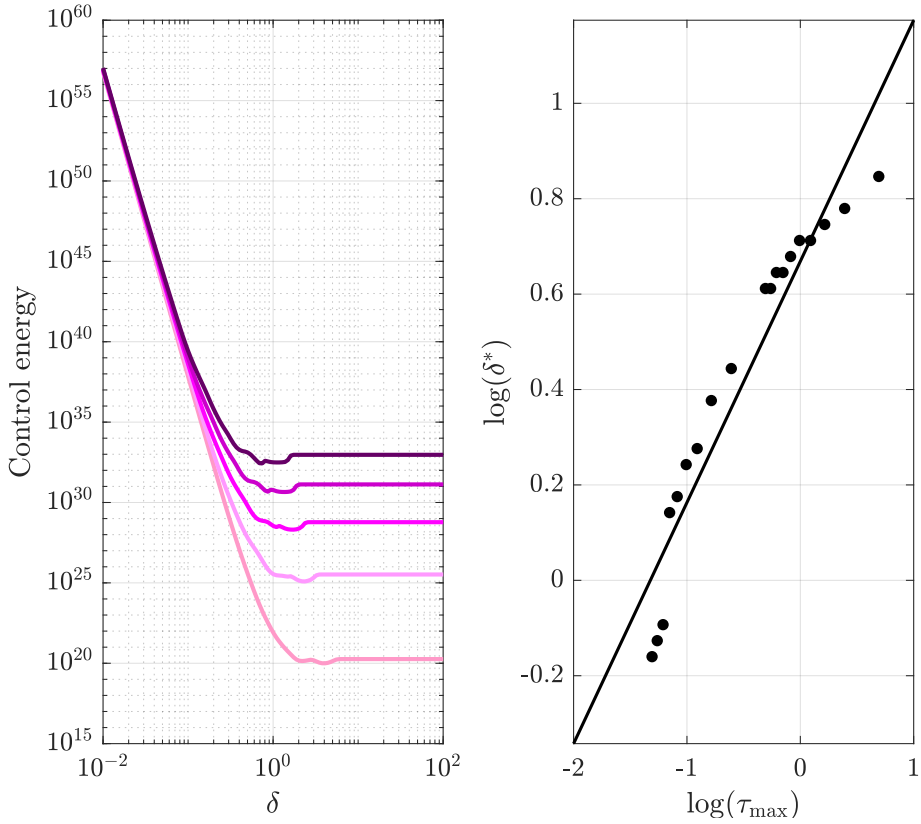

Figure 4.3: **Network temporality and time scales.** We consider 19 temporal networks with $N = 100$ nodes over $m = 3$ snapshots and differing only in the dominant time constant $\tau_{\max}$ that is chosen as a measure of the network time scale. The left panel shows the expected control energy averaged over all possible final states $\mathbf{x}(t_m)$ on the unit hypersphere centered in the origin for 5 of the 19 networks. The Figure displays that the network becomes more energetically demanding and that the minimum point of the energy shifts towards faster temporality regimes as $\tau_{\max}$ becomes smaller (i.e., as the curves become darker). The right panel highlights the relation between temporality and time scales, with the black dots representing $\log(\delta^*)$ as a function of $\log(\tau_{\max})$ for each of the 19 networks. Specifically, the minimum point δ^*, numerically obtained, corresponds to the value of δ associated to the minimum expected control energy.

5 Discussion

One of the historical puzzle of the control network theory is

“ Is it effectively possible to control a complex network?”

We have explained in Chapter 2 the meaning of controlling a linear dynamical network and shaded out why it is important to investigate whenever a provided theoretically control input could be realistically implemented. In Chapter 3, we revised the findings of [29] according to which exploiting the temporality of the networks would improve our ability to control real networks. However, in Chapter 4 we question that in such real world systems temporality comes hand in hand with uncertainty. Indeed, who can determinstically predict the future chemical reactions in a metabolic network, or the time instant at which a mobile device will activate? In this scenario, after reformulating the problem by means of stochastic programming, we proved that exploiting temporality is not a workaround to achieve the chimera we are chasing since 2011 [13], that is, controlling complex networks with a very limited number of driver nodes. More precisely, our findings stress the fact that there is not a unique answer to this question. We never experience that temporality yields orders of magnitude of energy savings in the realistic scenario we faced with in Chapter 4. Rather, we highlight how selecting a misleading static benchmark we could end in the paradox of temporality being beneficial independently on how slowly the topology changes. Not only, our deep understanding of the intricate relation existing between the time-scale of the network and its temporality, allows us find that there exists a regime where temporality still offers energy savings, even in a stochastic scenario. This example witnesses how without dreaming missions impossible, we can end in an exceptional understanding of the complexity of real-world networks. Indeed, both temporality and uncertainty represents one of the assets the research community is mature to invest in to accomplish a new shift of prospective.

6 Appendix

6.1 Proof of Theorem 4.2

In this Section we report the proof of Theorem 4.2.

Proof. For all $k = 0, \dots, m-1$, let us define

$$V_k(x_k) = \underset{\varsigma_{k+1}}{\mathrm{E}} \left[\sum_{i=k}^{m-1} J_i(x_i, x_{i+1}) \right]. \tag{6.1}$$

By applying dynamic programming [42] to problem (4.9), we know that the optimal cost J^*_{temporal} is equal to $V^*_0(x_0)$, obtained as the last step of the recursive algorithm

$$\begin{cases} V^*_{m-1}(\mathbf{x}_{m-1}) = J_{m-1}(\mathbf{x}_{m-1}, \mathbf{x}_m), \\ V^*_k(\mathbf{x}_k) = \min\limits_{\mathbf{x}_{k+1}} \underset{\varsigma_{k+1}}{\mathrm{E}} \left[J_k(\mathbf{x}_k, \mathbf{x}_{k+1}) + V^*_{k+1}(\mathbf{x}_{k+1}) \right], & k = 0, \dots, m-2. \end{cases} \tag{6.2}$$

Now, let us pick any $h \in \{1, \dots, m-1\}$. If we could write

$$V^*_h(\mathbf{x}_h) = \underset{\varsigma_{h+1}}{\mathrm{E}} \left[\sum_{i=h}^{m-1} \left(F^i_h \mathbf{x}_m - R^i_h \mathbf{x}_h \right)^T W_i^{-1} \left(F^i_h \mathbf{x}_m - R^i_h \mathbf{x}_h \right) \right], \tag{6.3}$$

we would then have that

1. *Equation* (4.10) *would hold for* $k = h$. Indeed,

$$\begin{aligned} V^*_{h-1}(\mathbf{x}_{h-1}) &= \min_{\substack{\mathbf{x}_h \\ \mathbf{x}_{m-1}}} \underset{\varsigma_h}{\mathrm{E}} \left[\left(\mathbf{x}_h - \mathrm{e}^{\delta_{h-1} A_{\sigma(h-1)}} \mathbf{x}_{h-1} \right)^T W_{h-1}^{-1} \left(\mathbf{x}_h - \mathrm{e}^{\delta_{h-1} A_{\sigma(h-1)}} \mathbf{x}_{h-1} \right) + \sum_{i=h}^{m-1} J_k(\mathbf{x}_k, \mathbf{x}_{k+1}) \right] \\ &= \min_{\mathbf{x}_h} \underset{\varsigma_h}{\mathrm{E}} \left[\left(\mathbf{x}_h - \mathrm{e}^{\delta_{h-1} A_{\sigma(h-1)}} \mathbf{x}_{h-1} \right)^T W_{h-1}^{-1} \left(\mathbf{x}_h - \mathrm{e}^{\delta_{h-1} A_{\sigma(h-1)}} \mathbf{x}_{h-1} \right) + V^*_h(\mathbf{x}_h) \right] \end{aligned}$$

From (6.3), we get

$$\begin{aligned} V^*_{h-1}(\mathbf{x}_{h-1}) = \min_{\mathbf{x}_h} \Bigg(& \left(\mathbf{x}_h - \mathrm{e}^{\delta_{h-1} A_{\sigma(h-1)}} \mathbf{x}_{h-1} \right)^T W_{h-1}^{-1} \left(\mathbf{x}_h - \mathrm{e}^{\delta_{h-1} A_{\sigma(h-1)}} \mathbf{x}_{h-1} \right) \\ & + \underset{\varsigma_h}{\mathrm{E}} \left[\sum_{i=h}^{m-1} \left(F^i_h \mathbf{x}_m - R^i_h \mathbf{x}_h \right)^T W_i^{-1} \left(F^i_h \mathbf{x}_m - R^i_h \mathbf{x}_h \right) \right] \Bigg). \end{aligned} \tag{6.4}$$

As the cost function (6.4) is convex with respect to $\mathbf{x}_h$, to find its minimum we can compute the gradient and set it to zero, thus obtaining

$$2\mathbf{x}_h^T W_{h-1}^{-1} - 2\mathbf{x}_{h-1}^T \mathrm{e}^{\delta_{h-1} A_{\sigma(h-1)}^T} W_{h-1}^{-1} + 2\mathbf{x}_h^T \sum_{i=h}^{m-1} \mathop{\mathrm{E}}_{\varsigma_h} \left[{R_h^i}^T W_i^{-1} R_h^i \right]$$
$$- 2\mathbf{x}_m^T \sum_{i=h}^{m-1} \mathop{\mathrm{E}}_{\varsigma_h} \left[{F_h^i}^T W_i^{-1} R_h^i \right] = 0,$$

which implies

$$\left(W_{h-1}^{-1} + \sum_{i=h}^{m-1} \mathop{\mathrm{E}}_{\varsigma_h} \left[{R_h^i}^T W_i^{-1} R_h^i \right] \right) \mathbf{x}_h = \sum_{i=h}^{m-1} \mathop{\mathrm{E}}_{\varsigma_h} \left[{R_h^i}^T W_i^{-1} F_h^i \right] \mathbf{x}_m$$
$$+ W_{h-1}^{-1} \mathrm{e}^{\delta_{h-1} A_{\sigma(h-1)}} \mathbf{x}_{h-1}.$$

As matrix $\left(W_{h-1}^{-1} + \sum_{i=h}^{m-1} \mathop{\mathrm{E}}_{\varsigma_h} \left[{R_h^i}^T W_i^{-1} R_h^i \right] \right)$ is positive definite, we finally get

$$\begin{aligned} \mathbf{x}_h^* &= \left(W_{h-1}^{-1} + \sum_{i=h}^{m-1} \mathop{\mathrm{E}}_{\varsigma_h} \left[{R_h^i}^T W_i^{-1} R_h^i \right] \right)^{-1} \sum_{i=h}^{m-1} \mathop{\mathrm{E}}_{\varsigma_h} \left[{R_h^i}^T W_i^{-1} F_h^i \right] \mathbf{x}_m \\ &+ \left(W_{h-1}^{-1} + \sum_{i=h}^{m-1} \mathop{\mathrm{E}}_{\varsigma_h} \left[{R_h^i}^T W_i^{-1} R_h^i \right] \right)^{-1} W_{h-1}^{-1} \mathrm{e}^{\delta_{h-1} A_{\sigma(h-1)}} \mathbf{x}_{h-1} \\ &= P_h \mathbf{x}_m + Q_h \mathbf{x}_{h-1}. \end{aligned} \tag{6.5}$$

2. *Equation* (6.3) *also holds for* $k = h - 1$. Indeed, combining (6.4) and (6.5), we get

$$V_{h-1}^*(\mathbf{x}_{h-1}) = \left(P_h \mathbf{x}_m + \left(Q_h - \mathrm{e}^{\delta_{h-1} A_{\sigma(h-1)}} \right) \mathbf{x}_{h-1} \right)^T W_{h-1}^{-1} \left(P_h \mathbf{x}_m + \left(Q_h - \mathrm{e}^{\delta_{h-1} A_{\sigma(h-1)}} \right) \mathbf{x}_{h-1} \right)$$
$$+ \mathop{\mathrm{E}}_{\varsigma_h} \left[\sum_{i=h}^{m-1} \left(\left(F_h^i - R_h^i P_h \right) \mathbf{x}_m - R_h^i Q_h \mathbf{x}_{h-1} \right)^T W_i^{-1} \left(\left(F_h^i - R_h^i P_h \right) \mathbf{x}_m - R_h^i Q_h \mathbf{x}_{h-1} \right) \right] \tag{6.6}$$

Now, if we set $F_{h-1}^{h-1} = P_h$, $R_{h-1}^{h-1} = \mathrm{e}^{\delta_{h-1} A_{\sigma(h-1)}} - Q_h$, $F_{h-1}^i = F_h^i - R_h^i P_h$, and $R_{h-1}^i = R_h^i Q_h$, for all $i = h, \ldots, m-1$, Equation (6.6) can be rewritten as in (6.3), that is,

$$V_{h-1}^*(\mathbf{x}_{h-1}) = \mathop{\mathrm{E}}_{\varsigma_h} \left[\sum_{i=h-1}^{m-1} \left(F_{h-1}^i \mathbf{x}_m - R_{h-1}^i \mathbf{x}_{h-1} \right)^T W_i^{-1} \left(F_{h-1}^i \mathbf{x}_m - R_{h-1}^i \mathbf{x}_{h-1} \right) \right]. \tag{6.7}$$

From (6.2), and setting $F_{m-1}^{m-1} = I_N$ and $R_{m-1}^{m-1} = \mathrm{e}^{\delta_{m-1} A_{\sigma(m-1)}}$, we know that (6.3) holds for $h = m - 1$. By induction, the thesis follows. □

6.2 Description of the numerical setting

To show the effectiveness of our approach in controlling temporal networks in the stochastic setting, we perform numerical simulations both on synthetic and empirical data set.

Empirical data set

Protein network of Figure 4.1: The raw data set is the time series of gene expression (GSE4987) coming from GEO (Gene Expression Omnibus) repository and consists of 6228 probes at 50 different time points [49]. To reconstruct the temporal network, we filter the data employing the method presented in [44]. Namely,

1) At each time point $t \in \{1, \dots, 50\}$, we compute the activity level $\mathrm{act}_i(t)$ of the i-th gene, for all $i = 1, \dots, 6228$, following [44];
2) We compare $\mathrm{act}_i(t)$ with a global activity threshold τ for all the genes. At each snapshot, we say that there is an undirected edge between nodes j and h if $\mathrm{act}_i(t) > \tau$ for $i = j, h$.
3) Finally, according to the gene ontology terms, we consider a reduced network obtained by considering only the genes sharing the same *Biological Process*.

Although our optimal solution also works for unstable dynamics, we focus on networks associated to stable (dissipative) dynamics. Therefore, we add suitable self-loops so as to make the adjacency matrix Hurwitz in all the snapshots.

Synthetic data set

To perform our analyses on synthetic temporal networks, we build a pool of three ER-like undirected graphs with average degree 6 and $n = 100$ nodes. The edge weights of each graphs are randomly selected in the interval $(0, 1]$. Their adjacency matrices are manipulated so as to obtain laplacian row-stochastic matrices.

For the numerical analysis portrayed in Figure 4.2, we build the three snapshots starting from the obtained three laplacian matrices stabilizing their standalone dynamics according to the Gershgorin disks theorem, that is, adding to their diagonal elements the scalars $\{-3, -1, -2\}$.

For the numerical analysis of Figure 4.3, we start from the same set of three laplacians. From these matrices we create 19 pools of 3 snapshots stabilizing their standalone dynamics so that each matrix in the same pool shares the same maximum eigenvalue $\lambda_{\max}$, each pool being characterized by different $\lambda_{\max}$. The maximum eigenvalues selected for each pool are

$$\{-20, -18, -16, -13, -12, -10, -8, -6, -4, -2 \\ -1.8, -1.6, -1.4, -1.2, -1, -0.8, -0.6, -0.4, -0.2\}.$$

In this way, the dynamics associated to each pool are characterized by increasing dominant time constants $\tau_{\max} = 1/|\lambda_{\max}|$.

For all numerical analyses performed on synthetic networks (Figures 4.2 and 4.3), each snapshot of a temporal network is extracted from its pool according to a uniform distribution. Moreover, a common set of 10 driver nodes has been selected so to ensure controllability of each snapshot of all the pools.

Part II

Coevolving networks: modeling and control

7 Coevolving networks

Temporal networks are a suitable modeling framework when the network topology commutes between a set of graphs. However, in several applications, it is essential to explicitly account for the inertia associated to changes in the graph topology. For instance, the topology of mutual influence among traders in a financial markets is based, among the others, on the concept of trust and reputation, which both need time to be built, and depend dynamically from a node state variable, such as the trader's wealth, which is a proxy of its success. Similarly, during a political campaign, the preferences are built as the result of individual opinion dynamics, combined with the dynamic evolution of the cobweb of interaction between the voters. To capture the interlaced dynamics of the nodes and their interconnected topology, we associate a state variable also to the edges of a network. Since the evolution of nodes and edges state variables is in general mutually interdependent, we call this kind of network *coevolving*. Formally, we give the following definition:

Definition 7.1 (Coevolving networks). *Given a graph $\mathcal{G} = \{\mathcal{V}, \mathcal{E}\}$, a coevolving network $C(G)$ associates a state variable $\mathbf{x}_i \in \mathbb{R}^n$ to each node $i \in \mathcal{V}$ and a state variable $\boldsymbol{\sigma}_{ij} \in \mathbb{R}^q$ to each edge $(i, j) \in \mathcal{E}$. Denoting, $\mathbf{x} \in \mathbb{R}^{|\mathcal{V}|n}$ the stack vector of the nodes' states and $\boldsymbol{\sigma} \in \mathbb{R}^{|\mathcal{E}|q}$ the stack vector of the edges' states, it can be described by the following equations*

$$\begin{aligned} \dot{\mathbf{x}}(t) &= \phi(\mathbf{x}, \boldsymbol{\sigma}, t) \quad \mathbf{x} \in \mathbb{R}^{|\mathcal{V}|n} \\ \dot{\boldsymbol{\sigma}}(t) &= \gamma(\boldsymbol{\sigma}, \mathbf{x}, t) \quad \boldsymbol{\sigma} \in \mathbb{R}^{|\mathcal{E}|q}. \end{aligned} \tag{7.1}$$

The concept of coevolving network aims to concurrently take into account the adaptive nature of the real-world complex systems, the virtuous feed-back loop between the networks structure and the nodes dynamics, and the possibility for a network topology to evolves. D. Siljak, in his pioneering work [50] , made a paramount first step toward the concept of coevolving network, by introducing the *dynamic graphs*, defined as a set of weighted graphs, with a given number of nodes, whose weights dynamically evolve. Later work [51, 52] has further expanded this concept and introduced the *evolving dynamical networks* that encompass a wider set of networks compared to coevolving networks as described in Definition 7.1. For instance, while coevolving networks use ODEs for modeling the network evolution, evolving dynamical networks can also consider

a Markovian update of the network structure. It is worth pointing out that, when there is a time-scale separation between the node and edge dynamics, the coevolving networks becomes a traditional (static) complex network. Indeed, when the edge evolution is much slower compared to node dynamics, the network system can be viewed as dynamical nodes interacting on a static graph. The same happens when the node evolution is much slower than the edge dynamics, with the only caveat that now the edges dynamically evolves, and are statically coupled through their common endpoints.

This chapter focuses instead on the case in which there is no time-scale separation between node and edge dynamics, so that their intricate interdependence cannot be neglected.

In Chapter 8, we will show how coevolving networks can be effectively used to model the dynamics of an artificial financial markets. In Chapter 9, we will show how network coevolution can be leveraged in control problems over networks. Specifically, in Section 9.1 we will show how, with a suitable choice of the edges dynamics, we can pinning synchronize a dynamical networks in an *efficient* way, that is, by minimizing the control energy required to reject a local perturbation [53]. Then, in Section 9.2, in the context of pinning controllability, we illustrate a distributed approach to dynamically evolve the edge weights to maximize the class of systems that can be pinning synchronized [54].

8 Coevolving networks to model financial market dynamics

In this Chapter we offer an example of application of coevolving networks to model real-world phenomena in which the relations among the actors (i.e., the nodes) dynamically evolve and depends upon the agents' states. As a paradigmatic example, we present how in a financial market (viewed as a coevolving network) we are able to show how the delicate interplay between the decisions of the investors (i.e., the nodes) and the cobweb of intricate relations (i.e., the edges) among them affects the overall market dynamics. Specifically, by incorporating in the network edges dynamics we are able to describe a bunch of realistic aspects that actually lack in the neoclassical economics [55]. The finding reported in this Chapter have been published in [2, 3].

8.1 Behavioral financial markets

In the modern and contemporary economic history there is plenty of evidence in apparent contradiction with the main hypotheses of neoclassical economics [55]. As examples, we mention some of the speculative bubbles and market crushes that cannot be explained with the neoclassical theory. In 1637, the first big speculative bubble of the history erupted, the so-called *Tulip bubble*, making the price of a bulb comparable with that of houses, fields and livestocks [56], while, around 1720, in the United Kingdom the overwhelming euphoria of the investors fostered the *South Sea Bubble* which caused substantial losses even to Isaac Newton [57]. More recently, the worldwide crises which followed the Wall Street's crush of 1929 represents a stunning example of unpredicted and sudden market crushes. The analysis of these and of more recent historical events, (*e.g.*, the 2008 financial crisis), seriously questioned the model of the *homo oeconomicus* and convinced the economists of the necessity of additional and interdisciplinary tools to make quantitative the novel concepts coming from *behavioral econonomics* [58, 59]. Indeed, psychological studies illustrate that the decision-making process, which is the determinant of financial dynamics, cannot be described as perfectly rational [60] and conceptual models of bounded rationality have been proposed in [61]. Our way of taking decisions is imperfect due to the presence of uncertainties, approximation errors, emotions, and cognitive biases. Inspired by the early concepts of the *Prospect Theory* [62, 63], and,

thanks to the collaborative work of Economists, Psychologists and Sociologists, a new discipline, *Behavioral Finance*, was born with the goal of investigating the reasoning patterns of the financial agents to unravel their mental and emotional processes and the way they influence their trading strategies [59].

Among the revealed cognitive bias and emotional processes that lies outside rationality and are related to markets' crushes we will focus on

1. How the *reputation* of financial agents, when based on individual charisma rather than on objective evaluations, can spur the emergence of an unmotivated leadership in the market. Indeed, while the imitation of a best performing agent could produce a general improvement of the financial agents' conditions, being myopically influenced by charismatic peers can of course have detrimental effects on market dynamics.
2. The effect on market dynamics of one of the most studied cognitive bias, that is, overconfidence [64], which is the attitude of an individual to strongly believe in her inaccurate evaluations. This often leads to performing overoptimistic judgements of life prospects which ultimately affect financial decisions. Overconfidence is associated with a body of related effects, which includes overplacement, that is, overestimation of one's rank in a population. Clearly, this directly impacts on the assessment of her own trading abilities compared to those of her competing peers [65, 66], and reflects on her trading patterns: overconfident agents tend to be stubborn rather than open-minded [67].

Therefore, we will build a behavioral market, that is, an artificial financial market model that can atomically account for the presence of cognitive biases affecting the investor decision process, and we will show how such behavioral nuances shape their interactions and then their investing strategies.

8.2 Why coevolving networks?

Developing quantitative models capable of translating the principles of Behavioral Finance into helpful instruments that may inform policy makers, is a pressing open problem, see for instance [68]. A relevant contribution to this field has been given by the community of the Physicists, who looked at financial markets as complex systems that can be studied through the tools of statistical mechanics [69–71]. A novel discipline, Econophysics, was born in 1995 [72] and tried to elucidate the macroscopic emerging features of financial markets from the behavior of its micro constituents, i.e., the financial agents. Using tools from agent-based modeling [73–75], artificial financial markets were developed to reproduce and explain the so-called *stylized facts* observed in real markets [73, 76–84]. For instance, in [81] the authors showed how scaling in finance arises from mutual interactions of market participants, while in [82] a realistic trading mechanism for price formation was reproduced. The study of financial markets represents an intriguing challenge for the Engineering community as well, which also started to contribute to this field, see for instance [82, 84, 85] and references therein. We wish to remark that, even though the effort of several scientific communities is producing noticeable work that is clarifying certain aspects of the market fluctuations, a thorough

understanding of the cause-effect relationship between the agents' behavior, decision of policy makers, and market dynamics is still missing. One of the unanswered questions is the impact of the cobweb of relationship among the agents on the market evolution. Indeed, the bias induced by the social interactions among individuals may strongly affect individual decision making [86]. In the literature, the interaction network among investors is frequently considered static [87] or varies according to the rate of transmission of information [88]. However, in real markets the influence among the agents may dynamically change [89, 90], thus determining an adaptive topology whose evolution driven, among other exogenous factors, by the perceived successfulness of the agents, with some central nodes of the network loosing their leadership in favor of other agents that are climbing the market [91–93]. Differently form the existing literature, we model the edge dynamics through the edges snapping mechanism, firstly introduced in [94] to model edges evolution in complex networks, to describe the variable patterns of influence among financial agents. Indeed, starting from the assumption that the relations among the agents play a crucial rule, we will design two types of input driving the edges dynamics and corresponding to two different behavioral features observed in real markets to be the determinants of its evolution. Moreover, we endow the agents with different *degrees of rationality*, which affect their ability of objectively assess the reputation of an agent. We illustrate how the different degrees of investors' rationality impact on macroscopic market observables (e.g., the wealth distribution, the overall transaction volumes) [2]. Finally, we show how the presence of overconfident agents in the market affects the overall market dynamics [3].

8.3 Market model

Leveraging tools from agent-based modeling and complex networks theory, we model the investment market as a coevolving network, see Definition 7.1, where the node state variables describe the current wealth and investing attitude of each financial agent, while the edge state variables determine the dynamical evolution of the cobweb of influence relationship among the agents (see a schematic of the investment market model in Figure 8.1). In what follows, after describing the node and edge dynamics, we detail the driving forces triggering the market evolution and the taxation scheme regulating the market.

8.3.1 Node dynamics

We consider a market populated by N financial agents. At each trading session, an agent can decide whether investing a fraction δ of her capital in one of the alternative financial portfolios from the finite set $\mathcal{L} = \{1, ..., m\}$. The m-th portfolio is virtual, corresponding to no-investment, which, differently from the other (proper) investments, has unlimited availability. Every agent will chose among one of the available portfolios depending on her risk attitude $r_i(k)$. In turn, the risk attitude dynamics are described by

$$r_i(k+1) = \begin{cases} (1-w)r_i(0) + \frac{w}{\mathcal{N}_i(k)} \sum_{h=1}^{N} a_{hi}(k) r_h(k), & \text{if } \mathcal{N}_i(k) > 0, \\ r_i(0) & \text{otherwise,} \end{cases} \tag{8.1}$$

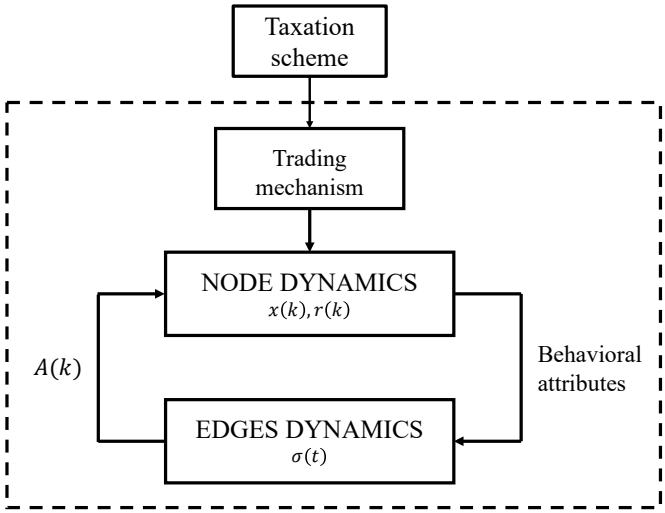

Figure 8.1: **Schematic of the investment market.** The node dynamics describe the evolution of the agent wealth $x(k)$ and of its risk attitude $r(k)$ which are updated at discrete steps, corresponding, e.g., to trading sessions. The edge dynamics evolve continuously in time, and determine whenever an agent is affected or not by another investor, with the corresponding component of $\sigma(t)$ converging to one or zero, respectively. The edge state at time k determines the adjacency matrix $A(k)$ at the k-th trading session.

for $i = 1, \dots, N$, where $0 < w < 1$ is the interaction weight, $r_i(0)$ is the innate risk attitude of agent i, $a_{hi}(k)$ is the hi-th element of a time-varying adjacency matrix $A(k) \in \mathbb{R}^{N\times N}$ describing the current mutual influences among the agents at time k, and it is 1 if agent i is influenced by agent h at time k, while it is zero otherwise, and $\mathcal{N}_i(k) = \sum_h a_{hi}(k)$, is the in-degree of agent i. In general, $a_{hi}(k)$ is involved in a virtuoso feed-back loop as it will be clear later[1]. At trading session k, the current risk attitude $r_i(k)$ shapes the utility function that agent i seeks to maximize, thus determining the selection of the portfolio $\ell_i(k) := \ell_i(r_i(k))$ in which she invests a fraction δ of her capital. According to this trading mechanism, the wealth dynamics will be then given by

$$x_i(k) = \phi(x_i(k-1), \tau_i(r_j(k-1))), \tag{8.2}$$

where the function ϕ accounts for the specific structure of the market; and $\tau_i(k-1)$ is the investing strategy she adopts on the basis of her risk attitude $r_i(k-1)$.

During the trading sessions, each agent is characterized by a behavioral attribute.

- The *reputation* of each agent $\rho_i(k)$, which is a time-varying attribute conferred to i by the *other* agents. To avoid an overly complex modeling, we consider the reputation of the agent independent from the agent assessing it. Specifically, the reputation is computed as a convex combination of her current wealth, that is a proxy of the effectiveness of its trading history, and the intensity c_i of her *charisma*, which is a personal quality that magnifies the capability of influencing her peers independently from her trading skills. Namely,

  $$\rho_i(k) = (1-\nu)x_i(k) + \nu c_i, \quad i = 1, \dots, N, \tag{8.3}$$

  where $0 \le \nu \le 1$ is the *irrationality coefficient* that quantifies the extent of irrationality permeating the market,[2]. Depending on the selection of the reputation of an agent will be more or less influenced by the intensity of her charisma.
- The level of *self-confidence*, s_i of agent i, which is her resistance to learn from the trading strategies of her neighbors, thus overestimating her own abilities respect with those of her neighbors. Given two thresholds $\underline{s} < \bar{s}$, we define the sets of overconfident and underconfident agents as

  $$\mathcal{O} = \{i \ : \ s_i > \bar{s}\} \subseteq \mathcal{V}, \qquad \mathcal{U} = \left\{i \ : \ s_i < \underline{s}\right\} \subseteq \mathcal{V},$$

  respectively. As it will be clear from the next sections, both the market irrationality and the self-confidence will affect the way the influence matrix $A(k)$ evolves, thus indirectly impacting on the node dynamics, see equation (8.1).

[1] We remind the reader that $A(k)$ is the output of the edge dynamics, which will be described in the next section.

[2] Differently from the conceptual models in [61], here we use a single parameter to quantify the extent of rationality in the market.

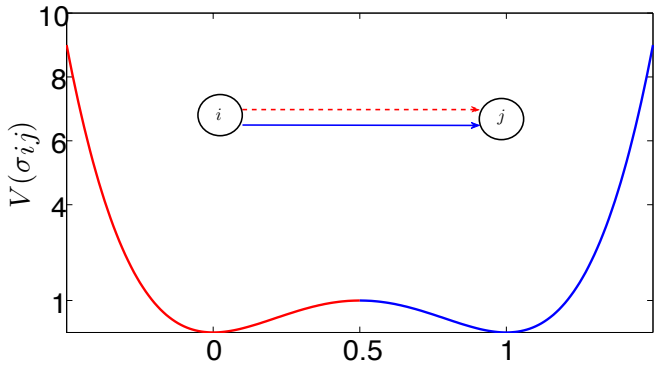

Figure 8.2: **Potential driving the edge evolution with $b = 16$.** The red dotted arrow corresponds to an inactive edge, while the blue solid arrow to an active one.

8.3.2 Edge dynamics

To mimic the variable patterns of aggregation observed in financial markets [95], at every trading session, edges between agents can be added or removed. Namely, the topology of the influence network among the agents can evolve depending on the relative agent reputations. Typically, each agent cannot interact with all the others: in real social networks the interaction mechanism is selective and not all-to-all, as individuals have a finite communication capacity [96–99]. Accordingly, we introduce the graph $\mathcal{P} = \{\mathcal{V}, \mathcal{E}_p\}$ describing the *social capacity* of every agent, where $\mathcal{V}$ is the set of agents, and $\mathcal{E}_p$ is the set of edges (the relations) that can be activated.

The activation or deactivation of an edge $(i, j) \in \mathcal{E}_p$ depends on the value of the state variable $\sigma_{ij} \in \mathbb{R}$ associated to each potential edge in the network. To capture the evolutive dynamics of the mutual influence among financial agents, we leverage the edge snapping mechanism proposed in [94] to model the edge evolution in complex networks. Specifically, the following set of differential equations governs the edge dynamics[3]:

$$\ddot{\sigma}_{ij}(t) + d\dot{\sigma}_{ij}(t) + \frac{\mathrm{d}V(\sigma_{ij}(t))}{\mathrm{d}\sigma_{ij}(t)} = u_{ij}(\lfloor t \rfloor), \tag{8.4}$$

for all $(i, j) \in \mathcal{E}_p$, where d is a damping parameter, V is a bistable potential, and $u_{ij} : \mathbb{R} \times \mathbb{R} \to \mathbb{R}$ is a driving force, which is a function of the reputation of the agents' pair. The bistable potential $V : \mathbb{R} \to \mathbb{R}$ is

$$V(\sigma_{ij}) = b\sigma_{ij}^2(\sigma_{ij} - 1)^2, \tag{8.5}$$

where b sets the height of the barrier separating the two equilibrium points, see Figure 8.2. The edge dynamics, in turn, determines the adjacency matrix $A(k)$ describing the

[3]Notice that, while the agents' state are updated at discrete time steps (at each trading session), the cobweb of interactions among the agents evolves continuously with time.

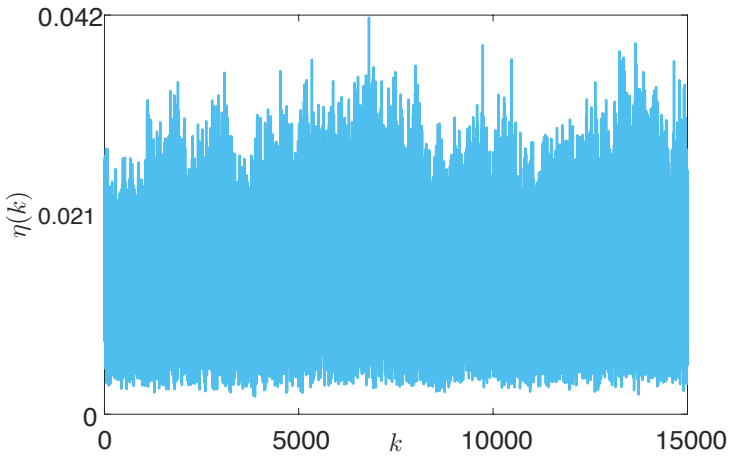

Figure 8.3: **Network variability $\eta(k)$ in the rational market.**

active edges at time k. Specifically, its element $a_{ij}(k)$ is computed as follows:

$$a_{ij}(k) = \begin{cases} 1 & \text{if } (i,j) \in \mathcal{E}_p \text{ and } \sigma_{ij}(k) > 0.5 \\ 0 & \text{otherwise} \end{cases} \tag{8.6}$$

Indeed, at time k, the edge $(i, j) \in \mathcal{P}$ is *active* if $\sigma_{ij}(k) > 0.5$, while it is *inactive* otherwise, as illustrated in Figure 8.2. The time varying matrix $A(k)$ is associated to the graph $\mathcal{G}(k) = \{\mathcal{V}, \mathcal{E}(k)\}$ defining the *influence network* among the agents. Namely, (i, j) belongs to $\mathcal{E}(k) \subseteq \mathcal{E}_p$ if $a_{ij}(k) = 1$. Notice that the update of $A(k)$ (and then of $\mathcal{G}(k)$) has a direct influence on the node dynamics, see Equation (8.1) and Figure 8.1.

8.3.3 Driving forces

The drivers of the edge evolution embedded in the function u_{ij} in Equation (8.4) can determine the emergence and/or the dissolution of an influence relation between financial agents [100] and can vary depending on the behavioral attribute we are taking into account. Specifically, as stated in Section 8.3.1, we consider two alternative inputs, one shaped by the relative reputation among the financial agents and one shaped by the self-confidence of the agents in their own trading abilities.

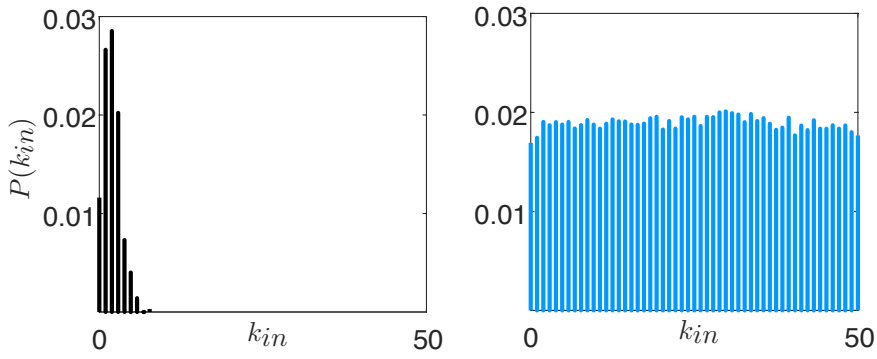

Figure 8.4: **Indegree distribution of the network in the rational market.** In (a) at $k = 1$ and in (b) at $k = 15000$.

Reputation

When we consider the reputation as the major behavioral attribute determining the relation among the financial agents, the force driving the edge evolution is selected as follows:

$$u_{ij}(k) = (-1)^{a_{ij}(k)} \max\left\{0, (-1)^{a_{ij}(k)}\big(\rho_i(k) - \rho_j(k)\big)\right\}, \tag{8.7}$$

for all $(i, j) \in \mathcal{E}_p$. In simple words, the absence of the edge (i, j) at time k that is, $a_{ij}(k) = 0$, implies that agent i does not influence agent j, although agent i belongs to the social network of agent j. In that case, an input $u_{ij}(k) = \rho_i(k) - \rho_j(k)$ may induce the activation of the edge (i, j) in a future trading session only if the reputation of i is higher than that of j ($\rho_i > \rho_j$). Symmetrically, if $a_{ij}(k) = 1$, an edge may be deactivated only when $\rho_j > \rho_i$. We emphasize that the edge activation or deactivation is not instantaneous, as it is regulated by the dynamical system (8.4). This models the effect of memory in social dynamics [101]: the difference of reputation has to persist for a sufficient time-span to determine a variation in the network topology.

Looking at Eqs. (8.3) and (8.7), we notice that by varying the value of ν in Equation (8.3), we can move on what we call the *spectrum of market rationality*: its origin corresponds to a market populated by agents behaving as the *homo oeconomicus* ($\nu = 0$), while at the end of the spectrum the agents are solely inspired by their subjective perceptions ($\nu = 1$). Indeed, in a perfectly rational market, the relative reputation is measured by the wealth differences ($\rho_i - \rho_j = x_i - x_j$), which become the only driver of the edge evolution through Equation (8.7). When irrationality dominates the market, the different intensities of the agents' charisma ($\rho_i - \rho_j = c_i - c_j$) determine the edge evolution. We emphasize that low values of the irrationality coefficient could trigger a potentially virtuous phenomenon of rational adaptation, in which the agents tend to account for the investing strategies of the most wealthy investors. On the other hand, as irrationality pervades the market, the agents start to follow charismatic leaders irrespectively of the trading outcome, a scenario that we call irrational herding [102].

Self-confidence

When, the self-confidence is the behavioral feature that mostly affects the relations among the financial agents the driving force becomes:

$$u_{ij}(k) = (-1)^{a_{ij}(k)} \max\left\{0, (-1)^{a_{ij}(k)}\left(x_i(k)/s_j - x_j(k)\right)\right\}, \tag{8.8}$$

where s_j is the *self-confidence* of j, that is, a parameter quantify the level of confidence of agent j in her trading ability. To clarify how this mechanism works, for the sake of clarity, we refer to the case of an agent j not being influenced by agent i at time k (i.e. $a_{ij}(k) = 0$, $\sigma_{ij}(k) < 0.5$), and having to decide whether she wants to account for agent i's risk attitude at time $k+1$, thus activating the edge (i, j) (the case of a deactivation is specular). In this case, Equation (8.8) becomes

$$u_{ij}(t) = \max\left(0, \frac{x_i(k)}{s_j} - x_j(k)\right), \qquad t \in [k, k+1[. \tag{8.9}$$

Indeed, in our mechanical analogy, when the mass is closer to the first well ($\sigma_{ij}(k) < 0.5$), then j is not influenced by i. To make j change her mind at the next trading session, a necessary condition is that $u_{ij}(t) > 0$, that is, she believes that i has better trading abilities than her own. This happens when $x_i(k)/s_j > x_j(k)$. Notice that a neutrally confident agent ($s_j = 1$) just compares her wealth with that of i, thus objectively evaluating their relative past trading abilities. Differently, an overconfident agent (i.e. $s_j \gg 1$) will consider being influenced by i only if agent i's trading strategies proved to be way more successful than that of agent j (i.e. $x_i(k) \gg x_j(k)$). The opposite happens for underconfident agents. However, we emphasize that those are only necessary conditions for activating the edge: as the update is not instantaneous, but dynamical according to Equation (8.4), the perceived difference in trading abilities has to be intense enough and persist for a sufficient time span.

8.3.4 Trading mechanism and taxation

Following the work in [103], we focus on a simplified competitive market where the agents can choose to invest on a set of alternative portfolios of financial assets, characterized by a limited availability and different expected return and volatility. The market is regulated by a taxation scheme that redistributes the wealth while keeping its total unchanged. In particular, the generic wealth dynamics in (8.2) become

$$\begin{aligned} x_j^-(k) &= x_j(k-1) + \beta_j(k)\delta x_j(k-1)(a_\ell - 1) \\ &\quad - (1 - \beta_j(k))\delta x_j(k-1)(1 - b_\ell), \end{aligned} \tag{8.10}$$

$$x_j(k) = \chi(x_j^-(k)), \tag{8.11}$$

where δ is the fraction of the current wealth that j decides to invest in the portfolio ℓ, whose win and loss rates are a_ℓ and b_ℓ, respectively, $\beta_j(k)$ is a realization of a uniform Bernoulli random variable B describing the output of the trade, and χ is a function describing the considered taxation scheme. At each trading session, the agents can decide to invest on the available portfolio that corresponds to the highest expected value of a power-low utility function [103] (see Section 10.1, Appendix 10 for details).

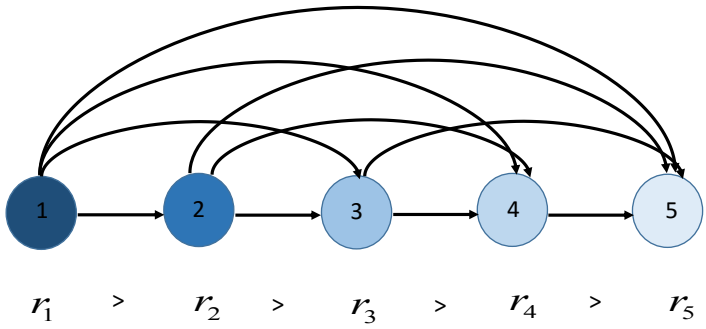

Figure 8.5: **Example of graph with uniform indegree and outdegree distributions.**

8.4 Numerical set up

We consider an artificial investment market populated by $N = 1000$ agents with average wealth $\bar{x} = 100$. At each trading session, they can choose among three alternative portfolios of investments. The agents are grouped in three classes (of equal size) depending on their innate risk attitudes, which are uniformly distributed in the interval $[0.5, 1]$ as in [103]. Namely, they are classified as audacious if $r_{j0} \in [0.83, 1]$, ordinary if $r_{j0} \in [0.67, 0.83)$, and prudent otherwise. These three agent classes are chosen so that the prudent agent will only consider investing in the less risky portfolio, the ordinary will also consider the averagely risky portfolio, while the audacious agents will invest in the riskiest one as well. The selected taxation scheme is Tobin-like and determines the investing strategy. Within this frame, we aim at testing the effect of the irrationality of the market and of the self-confidence of the investors on the overall market dynamics with a special focus on the properties of the emerging network. In both cases, the social capacity topology $\mathcal{P}$ is randomly generated applying a degree-preserving rewiring algorithm to a nearest neighbor graph with average degree $\langle k \rangle = 52$, and we randomly select initial conditions for all the σ_{ij} such that $(i, j) \in \mathcal{E}_p$. The number of trading sessions T is selected so that the investment market evolves for a sufficient time span to achieve a steady-state wealth distribution.

8.4.1 The effect of irrationality

As the reputation of agent i depends on her charisma (8.3), we randomly selected parameter c_i from an exponential distribution of parameter $\lambda = 1$. The mean of this distribution is amplified of a factor 100 to coincide with the expected value of the wealth. Moreover, the impact of the edge dynamics on the market will be tested for increasing values of the irrationality coefficient ν. Indeed, the extent of rationality in the market affects the way the agents evaluate their reputation. Accordingly, we select $\nu = 0$ and $\nu = 1$ to model the purely rational and irrational investment markets, respectively, while we choose $\nu = 0.75$

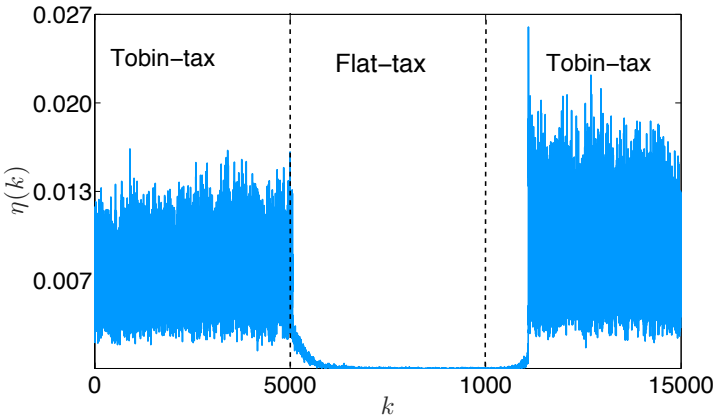

Figure 8.6: **Network variability $\eta(k)$ in the rational market under variable taxation schemes.**

as a representative example of partially rational market.

To isolate the effect of the snapping evolution from that of other possible drivers, as for instance the selected taxation scheme, we evaluate the results against two reference scenarios: i) a market with non-interacting agents and ii) a market where the interaction is triggered on an Erdös and Rènyi (ER) random undirected topology [104]. All the results reported below are averaged over 100 repetitions for each value of ν.

Rational market evolution ($\nu = 0$)

In what we called a perfectly rational market, subjective factors like the agent charisma should not affect the edge evolution. We model this scenario by setting the irrationality coefficient ν to zero so that the reputation of each agent is solely determined by its current wealth, that is, $\rho_j(k) = x_j(k)$. In what follows, we explain the effect of perfect rationality on market dynamics.

Impact on the network topology

In a perfectly rational market, the reputation of the agents, which drives the edge dynamics, is quantified by an objective and measurable variable, that is, their wealth. As the agents' wealth persistently changes, because of the stochastic nature of the investment outcome (see the variable $\beta_j(k)$ in Equation (8.10)), the network topology will persistently vary along the trading sessions. To quantify these variations, we defined the *network variability* $\eta(k)$ as the fraction of potential edges activated or deactivated at every session, that is,

$$\eta(k) := \frac{\|A(k) - A(k-1)\|_1}{|\mathcal{E}_p|}.$$

As illustrated in Figure 8.3, $\eta(k)$ is persistently greater than zero at every trading session, with an average value of 0.01.

However, while the network continues to change, some topological properties remain almost unchanged throughout the evolution. For instance, it is interesting to discuss the steady-state distribution of the indegree (similar considerations hold for the outdegree distribution). At the onset of the network evolution, as the initial conditions are randomly selected, the indegree distribution is Poisson-like, see the left panel of Figure 8.4. Then, after a transient, the indegree distribution settles, and, averaging the distribution in the 100 simulations, we observe an almost uniform distribution in the interval [0 51], right panel of Figure 8.4. This distribution shows striking similarities with the degree distribution of the corporate elite network in the US, which was also shown to be close to the uniform [105]. A possible explanation of this common behavior is that in networks of influence, like the one considered in this work or the real corporate elite network studied in [105], the nodes are ranked based on what we call reputation, and the links almost always points from nodes with a higher reputation (the *influencers*) to nodes with a lower reputation (the *followers*). In case this unwritten rule were always followed, and every link could be in principle activated, a perfectly uniform degree distribution would be obtained, as for the graph illustrated in Figure 8.5. However, in real influence networks, this rule is less compelling, and the interaction is selective, that is, not every link in the network may be activated [97], thus leading to a moderate deviation from a perfectly uniform distribution. Our edge snapping mechanism is capable of reproducing this second, and more realistic, degree distribution. Indeed, the topology is not instantly updated, as its evolution is filtered by the dynamical system (8.1), which adds an inertia to the activation or deactivation of links. Therefore, a higher reputation of node i compared to that of node j implies a higher likelihood of edge (i, j) compared to (j, i), but does not guarantee its activation. In combination with the selective interaction due to the limited social capacity of the agents, this allows the model to display moderate deviations from a uniform distribution, thus making it closer to a real influence network.

As the degree distribution is determined by the snapping mechanism, a question naturally arises: what is the cause of the persistent network variability shown in Figure 8.3? We argue that the variability of the network topology is an indirect measure of the chances that the wealth ranking among the agents changes. Indeed, due to the stochastic nature of the investments and the redistributive effect of Tobin-like taxation schemes [106], the poorest nodes may increase their wealth, thus *climbing* the pyramidal network structure: in the limit example of Figure 8.5, one or more nodes climbing the market would only correspond to a relabeling of the nodes, but would have no effect on the network structure. Different market structures, which would translate into different shapes of the function ϕ in (8.2), may hinder agent recovery from poverty, thus reducing the network variability. A striking example can be obtained by considering the impact of a less fair taxation scheme. For instance, we report in Figure 8.6 the outcome of a single run of the market simulation, in which at time 5000 the taxation scheme is changed to a flat tax, and then is switched back to a Tobin-like tax at time 10000. Differently from the Tobin-like tax, the flat tax has no redistributive effect, as the rate of the tax is independent from the agents' wealth [107]. This dramatically reduces the opportunities for an agent to

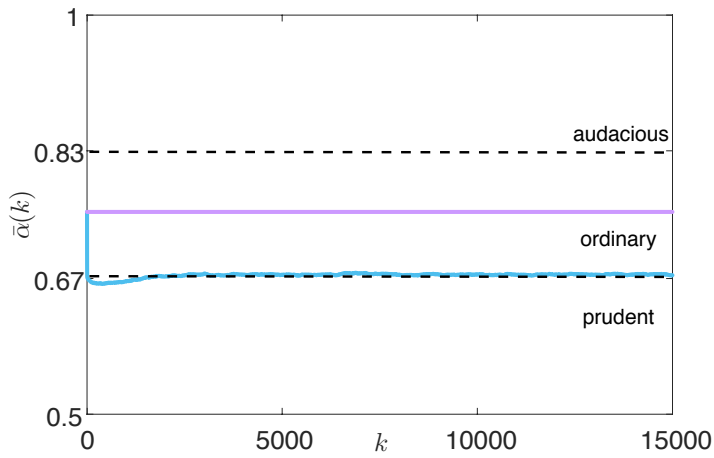

Figure 8.7: **Average risk attitude $\bar{r}(k)$ of the network.** In magenta for the reference scenarios and in blue for the rational market.

climb the wealth rankings. Accordingly, the network variability strongly decreases when the flat tax is introduced, and then slowly returns to oscillating in the usual range when the Tobin-like tax is introduced again.

Impact on the risk attitudes

The evolution of the influence network has a direct impact on the risk attitude of the agents. Indeed, Equation (8.1) implies that the risk attitude of the j-th agent is updated through a weighted average between its innate attitude and the current average attitude of the set $\mathcal{N}_j(k)$ of its neighbors. Therefore, as the edge states evolve, $a_{ij}(k)$ is updated, with the effect of a persistent variation of the set $\mathcal{N}_j(k)$, which in turn implies that risk attitude dynamics never settle. Moreover, we observe that the average risk attitude decreases if compared with the case of no interaction among the agents, and with the case of an ER undirected random influence topology, in which it remains constant, see Figure 8.7. Indeed, in a rational market the reputation is built based only on the agents' wealth: when a Tobin-like tax is considered, the prudent agents are favored [103], and therefore the edge snapping dynamics steer the agents attitude towards prudence, with the poorest agents trying to emulate the successful strategy of the richest ones. We emphasize that, when $\nu = 0$, the snapping dynamics are also capable of adapting to possible variation in the trading mechanism: for instance, we observe that, when the taxation scheme changes, the most effective investing strategy changes, and the risk attitudes start drifting accordingly, see Figure 8.9. Indeed, when the flat tax, which rewards more audacious traders [103], replaces the original taxation scheme, the average risk attitude starts to increase, with this tendency reversed when the Tobin-like tax is reintroduced.

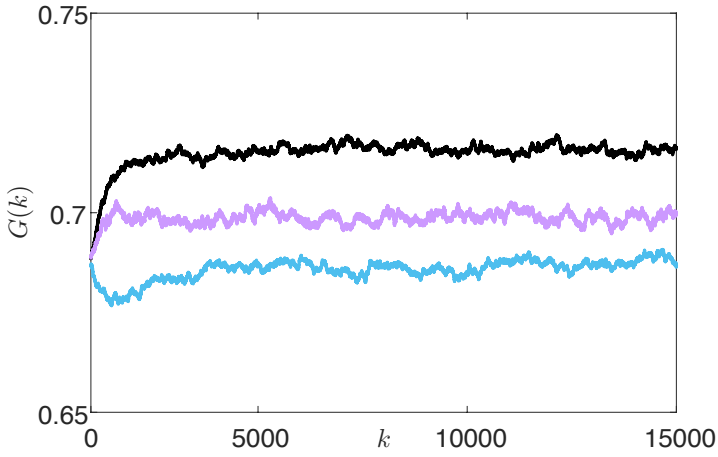

Figure 8.8: **Evolution of the Gini coefficient.** In black for a market without interaction, in magenta for a market with random interaction, and in blue for the rational market.

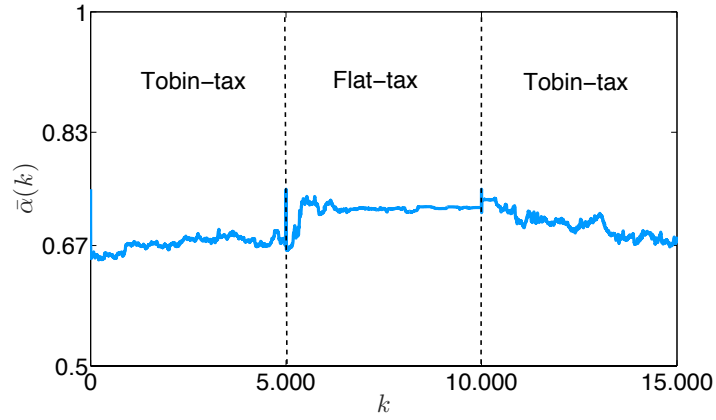

Figure 8.9: **Average risk attitude $\bar{r}(k)$ in the rational market under variable taxation schemes.**

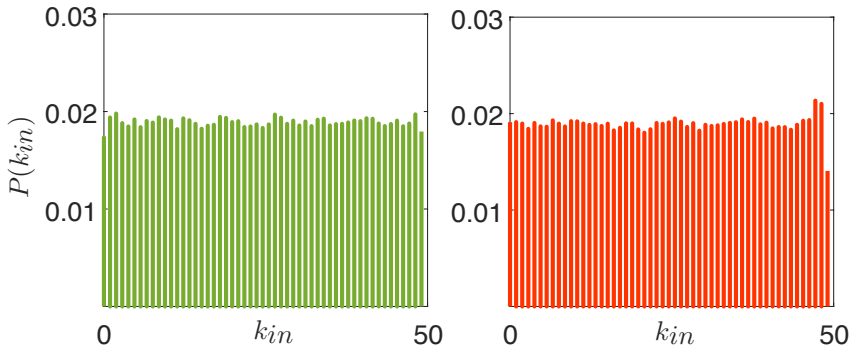

Figure 8.10: **Indegree distribution.** In (a) for the partially rational market and in (b) for the irrational market at $k = 15000$.

Impact on the wealth distribution

The modification of the risk attitude induced by the introduction of the snapping mechanism has an impact on the overall dynamics of the market, and in particular on the wealth distribution. To quantify the extent of the inequalities among the agents, we used the Gini coefficient, introduced by Corrado Gini in [108], which can vary between 0 (perfect equality among the agents' wealth) and 1 (all the wealth belongs to one agent). As expected, because of the learning mechanism, the topological adaptation is beneficial and induces wealth redistribution in the market: from Figure 8.8 we notice that the Gini coefficient decreases if compared with both the reference scenarios.

The onset of irrationality ($\nu > 0$)

As irrationality pervades the market, the reputation of each agent becomes more and more influenced by a subjective variable, that is, the innate intensity of its charisma. An analysis of the steady-state degree distribution demonstrates that it is approximately uniform regardless of the level of irrationality in the market, see Figures 8.4 and 8.10. Although the structural properties of the graph do not change, the ranking of the nodes in the hierarchical structure of Figure 8.5 becomes less and less related to the agents' wealth as the irrationality increases. To clearly illustrate this point, in Figure 8.11 we report the average wealth of an agent as a function of its indegree (symmetrical considerations hold for the outdegree), and we observe that the dependence between the two quantities becomes weaker and weaker as ν gets closer to 1. Indeed, a higher indegree means that the agent is influenced by a large fraction of her neighbors. In presence of rationality, this happens when she is significantly poorer than her neighbors. This is not the case when irrationality increases. An interesting common denominator across all the levels of irrationality is that the nodes with very low indegree (and high outdegree), tend to

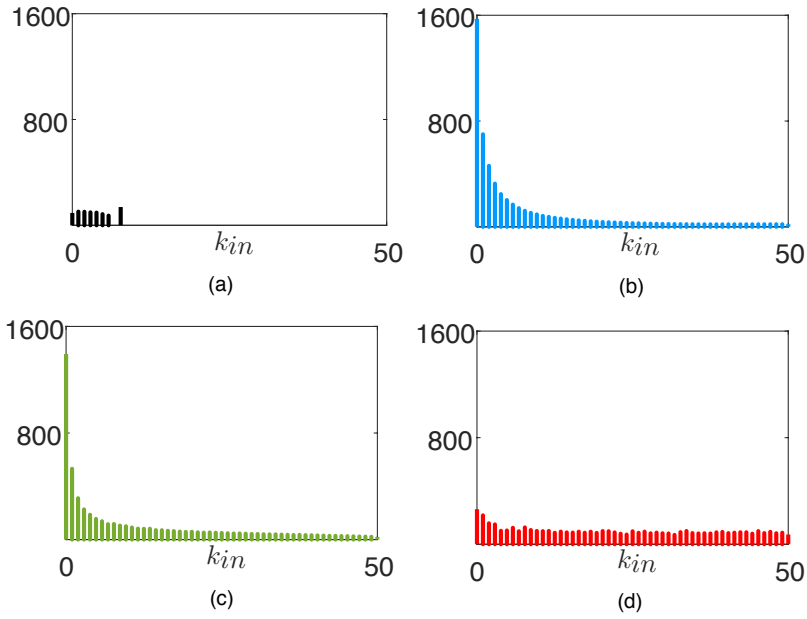

Figure 8.11: **Average wealth of an agent as a function of her indegree.** In the rational market at $k = 1$ (a) and in (b) at $k = 15000$, and in the partially rational market (c) and irrational market (d) at $k = 15000$.

have a wealth that is remarkably higher than the average. This can be easily explained in a rational market, in which the edge dynamics are driven by the wealth difference, and then the absence of ingoing links is associated to the richest nodes. When ν approaches to one, the explanation is less trivial, and can be obtained by observing that only low indegree agents preserves a relevant fraction of agents with the best (prudent) attitude, see Figure 8.12. Indeed, the random interaction taking place when $\nu = 1$ has the main effect of averaging the attitudes, dramatically increasing the fraction of ordinary nodes. The nodes that are less affected by this effect are the most charismatic, who maintain their initial investing strategies regardless of what the others do. In other words, this means that when irrationality pervades the market, the best strategy is to avoid herding.

The reduced rationality also impacts on the investing strategies selected by the agents: compared with the perfectly rational case, the average risk attitude increases and, when $\nu = 1$, becomes equivalent to the innate one, see Figure 8.16. Accordingly, the distribution of the investing strategies is not anymore steered towards the more prudent (and rewarded) ones, and becomes comparable to that obtained with a random undirected ER influence network. Consistently, we observe that the redistributive effect of rational adaptation illustrated in Figure 8.8 is hampered as irrationality increases, giving place to what we call *irrational herding*, where the potential benefits of the interaction are ruled out by

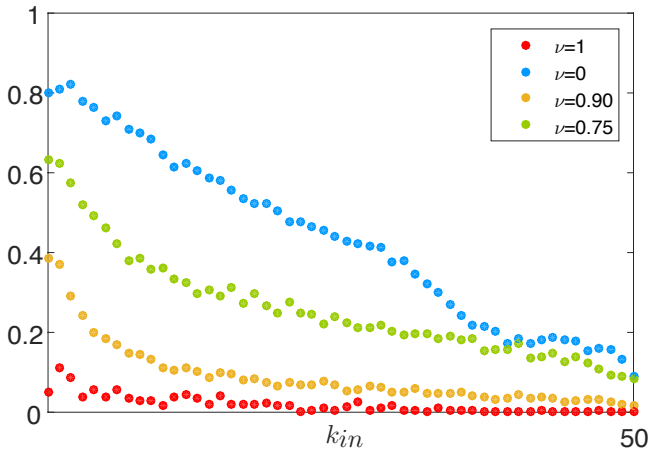

Figure 8.12: **Average fraction of prudent agents as a function of their indegree for different values of ν at $k = 15000$.**

its randomness, see Figure 8.17. On the other hand, the increased irrationality mitigates one of the known drawbacks of the introduction of Tobin-like tax schemes, that is, the reduction of the trading volumes [106]. Indeed, the irrationality leads to the permanence of a relevant fraction of audacious agents, thus increasing the total volume of trades, see Figure 8.18.

8.4.2 The effect of overconfidence

In our simulations, we set $\bar{s} = 2.5$. To test the effect of overconfidence, we selected two reference scenarios:

a) All the agents are neutrally confident, that is, $s_i = 1$ for all i. In this case, the agents are perfectly rational, and they rank their trading ability by only considering the output of their past investments, that is, their wealth.
b) The agents mildly deviate from rationality, as, s_i for $i = 1, \ldots, N$, are randomly selected from an inverse uniform distribution with median 1, where the overconfident agents represent a minority in the market.

These reference scenarios are compared with cases in which the overconfident are prevalent, as often occurs in real markets [109]. In particular, we consider

c) An extremely overconfident market, in which all the agents are overconfident, as we selected the coefficients s_i, $i = 1, \ldots, N$, from an inverse uniform distribution with values in $[\bar{s}, +\infty)$.
d) A prevalently overconfident market, in which, for each class of agents (audacious, ordinary, and prudent), half of the agents are selected as in Scenario b) and half as in c).

In our analysis, we have run 100 simulations for each of the four scenarios, where all the agents start with the same initial wealth. Before the interaction is triggered, the agents trade without mutual influence for 1000 sessions to diversify their wealth x_j, $j = 1, \dots, N$. At time $k = 1001$ the edges dynamics (8.4) are activated for all the pair of nodes $(i, j) \in \mathcal{E}_p$, and we let the market evolve for further 14000 sessions, so that a steady-state wealth distribution is achieved and that the network parameters analyzed in the following settle. We first investigate how overconfidence shapes the network of influence among the agents, and then analyze the subsequent effect on the risk attitude and wealth of the agents.

Impact of overconfidence on the network

The considered scenarios differ for both the percentage of overconfident, and for the variability of the self-confidence, which could be quantified by the sample standard deviation. In what follows, we aim at elucidating how these reflects on the network properties, with a specific focus on

- the network density, quantified by its average degree d_{ave}.
- the network asymmetry, that determines the directionality of the relations in the influence network, and that, following [110], we quantify through the *absolute binary network asymmetry* as

$$s_b = \frac{1}{2}\frac{N+1}{N-1}\left(\frac{\left\|A - A^T\right\|_F}{\|A\|_F}\right)^2,$$

  where $\|\cdot\|_F$ is the Frobenius norm. Notice that s_b spans from 0, that is the case of an undirected network, to 1, which corresponds to the case where there are no mutual links, i.e. the activation of edge (i, j) implies the absence of (j, i).
- the network clustering, that is quantified by the average clustering coefficient C. We remind that the clustering coefficient of a node, say i, is computed as the ratio between the number of directed triangles in the graph and the total number of possible triangles that i could form;
- the correlation $cor(x, d_{\text{o}})$ between the out-degree distribution and wealth.

The effects of the different distribution of self-confidence are summarized in Table 8.1 and discussed below. The first immediate consequence of overconfidence is an increased sparsity of the network. Indeed, the abnormal level of self-confidence makes the agent reluctant to be influenced by their neighbors. Consistently, we observed a dramatic reduction of the average degree d_{ave} as the fraction of overconfident agents increases. Indeed, when all the agents are overconfident (Scenario (c)), given the pair of edges $(i, j), (j, i) \in \mathcal{E}_p$ with agent i richer than j, it happens that i will decide not to be influenced by j, but often we will also observe that $a_{ij} = 0$. This behavior produces a sparse network, populated by stubborn investors, but the network remains perfectly asymmetric, with s_b being equal to 1 as in the Scenario (a). Consistently, we observe that the presence of bidirectional links is caused by the presence of a set of underconfident agents (in our simulations we set $\underline{s}_i = 0.65$). Indeed, underconfident agents overestimate

Table 8.1: Legend. d_{ave} is the average degree of the network; s_b is the absolute binary network asymmetry; C and C_r are the clustering coefficient of the network and of the corresponding ER graph with equivalent degree, respectively; $cor(x, d_{\text{o}})$ is the correlation between the wealth of an agent and her out-degree, C_o, C_m, C_i, and C_o are the number of cycle, middleman, in, and out pattern over the total number of possible triangles, respectively; $|O|/N$ and $|\mathcal{U}|/N$ are the fraction of overconfidence and underconfident agents, respectively. Confidence intervals with significance level 0.05 are also reported when needed.

Scen.	**(a)**	**(b)**	**(c)**	**(d)**
d_{ave}	26.00 [25.61, 26.39]	23.46 [22.87, 24.05]	5.50 [4.95, 6.05]	14.40 [13.87, 14.93]
s_b	1.00 [0.98, 1.00]	0.80 [0.78, 0.81]	1.00 [0.98, 1.00]	0.91 [0.90, 0.92]
$10^3 C$	25.80 [25.59, 26.01]	28.10 [27.56, 28.64]	4.18 [3.57, 4.79]	24.10 [23.28, 24.92]
$10^3 C_c$	0.07 [0.05, 0.09]	0.85 [0.75, 0.95]	0 [0, 0]	0.19 [0.16, 0.22]
$10^3 C_m$	8.58 [8.51, 8.65]	8.86 [8.74, 8.98]	1.50 [1.19, 1.81]	8.11 [7.84, 8.38]
$10^3 C_i$	8.58 [8.51, 8.65]	6.50 [6.38, 6.62]	2.53 [1.98, 3.08]	4.05 [3.87, 4.23]
$10^3 C_o$	8.58 [8.51, 8.65]	11.85 [11.43, 12.27]	0.15 [0.13, 0.17]	11.75 [11.02, 12.48]
$10^3 C_r$	26.05	23.51	5.51	14.28
$cor(x, d_o)$	0.41 [0.39, 0.43]	0.51 [0.49, 0.54]	0.71 [0.69, 0.73]	0.62 [0.60, 0.64]
$\lvert O\rvert/N$	0	0.22	1.00	0.62
$\lvert\mathcal{U}\rvert/N$	0	0.20	0	0.10

the trading abilities of their neighbors, thus considering being influenced also by less successful investors: this leads to an increased probability of the presence of mutual links, and therefore to the reduction of s_b as the fraction of underconfident increases.

As for the clustering coefficient C, we observed that, when the agents behave homogeneously, it is always of the same magnitude as the expected one in an ER random graph with the same size and expected degree. This happens in Scenarios (a) and (c), where the agents are all rational or all overconfident, respectively. On the contrary, the increased heterogeneity of the agent behaviors in Scenarios (b) and (d) increases the likelihood of encountering triangles of agents, see Table 8.1. However, the differences becomes even more relevant if we decompose the overall clustering coefficient in the four possible patterns that can be formed in directed networks, see Figure 8.13. The absence of underconfident agents in Scenarios (a) and (c) makes almost impossible the formation of cycles, which instead appear in (b) and are significantly higher in (d), which is the scenario characterized by the highest fraction $|\mathcal{U}|/N$ of underconfident. Moreover, we notice that in a market dominated by overconfidence as in Scenario (c), the possibility of having (at least) two outgoing edges is limited only to the richest agents, that may influence those who are significantly poorer overcoming their overconfidence: consequently, this strongly reduces the fraction of *out* patterns C_o, which are instead favored in Scenarios (b) and (d), where the underconfidence of a non-negligible minority of agents increases the chances of having *out* patterns.

Finally, we observe the correlation between outdegree and wealth. Intuition would suggest this correlation to be higher in a market where most of the agents are capable of correctly assessing their trading ability and where the richer are more likely to have a higher out-going degree. On the contrary, we observe that the ρ increases as long as the fraction of overconfident agents increases. The explanation is that in a market populated by overconfident agents, agent i may have outgoing edges only if her wealth is much higher than that of her neighbors, thus increasing the correlation between out-degree and wealth.

The impact of overconfidence on agent success

The different distribution of self-confidence in the four considered scenarios shapes the network topology which, in turns, affects the way agents' trade through Equation (8.1). From [2, 103], we know that in a rational market the Tobin-like tax regulating the market favors the prudent agents, that consider investing only in the less risky asset. Therefore, prudent agents have in average more outgoing links, and therefore the average risk attitude $\bar{r}$ settles around 0.67, see the blue line in Figure 8.14, which is significantly lower than the average innate attitude of the agents, that is 0.75. An interesting effect is observed as the fraction of overconfident agents pervades the market: the average risk attitude further reduces, see Figure 8.14 when all the agents are overconfident (red line) we observe the lowest settling value for $\bar{r}(k)$. This is explained by the fact that overconfident agents are only influenced by the agents who are significantly richer than them: this means that an overconfident agent i is very likely to only imitate the trading patterns of the agents with the best strategy, and not of agents with wrong strategy, but that are temporary richer than i due to a better luck.

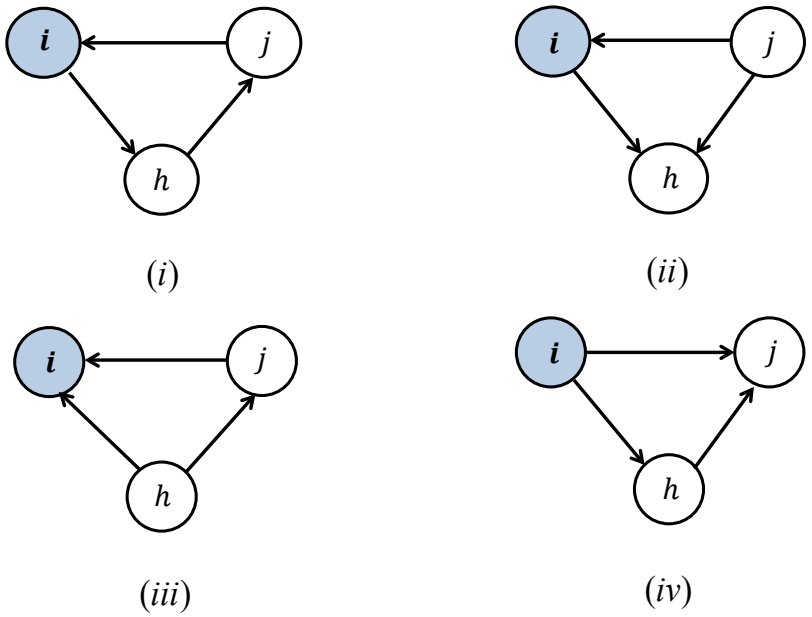

Figure 8.13: Example of the four possible patterns in triangles from the perspective of node i [111]: cycle (i), middleman (ii), in (iii), and out (iv).

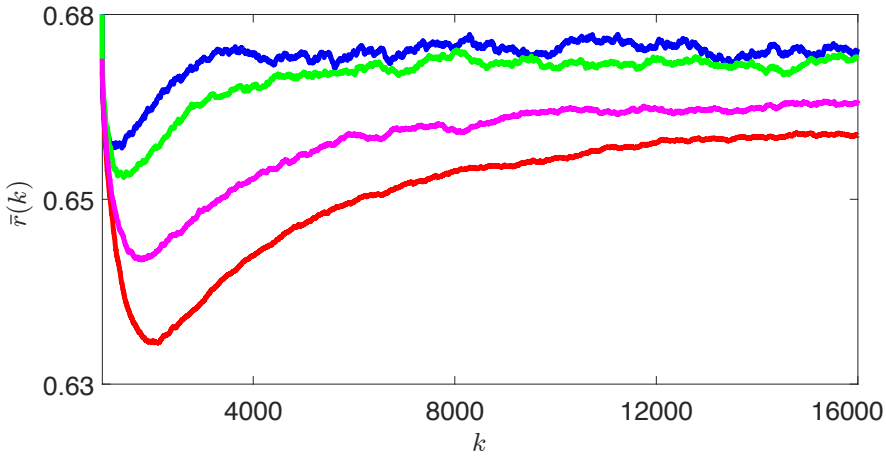

Figure 8.14: **Evolution of the average risk attitude $\bar{r}(k)$.** Scenario (a) (blue line), (b) (green line), (c) (red line), and (d) (magenta line).

Next, we focus on Scenario (d) to understand whether overconfidence hinders agent's wealth. To this aim, we evaluated the average wealth for each class of agents (prudent, ordinary, and audacious) and checked whether being overconfident were an advantage or not in each class, see Figure 8.15. In agreement with the findings of behavioral finance [65, 66, 109, 112], we find that an excess of confidence is detrimental when agents' own valuations are mistaken: in this case, being open-minded can make up for wrong evaluations. On the other hand, skilled traders benefit from self-confidence, as they stand on their own correct evaluations.

8.5 Discussion

We explored the interplay between the evolution of the cobweb of relations among financial agents and the overall market dynamics. Taking a new perspective, we exploited the edge snapping mechanism, firstly introduced in [94], to model the edges dynamics: each link is viewed as a mass moving in a double-well potential, with the first well corresponding to an inactive link and the second to an active one. We considered two behavioral features shaping the edge evolution, that is, the extent of the agent's ratioanlity and their self-confidence, respectively. Then, the driver of link evolution depends on a behavioral feature of the agents. Specifically, in one case we consider the relative reputation between possibly coupled nodes, while in the other the self-confidence of the agent in her own trading strategy.

As for the role of rationality, we observed that

- the network topology at steady state displays a fairly uniform indegree distribution.

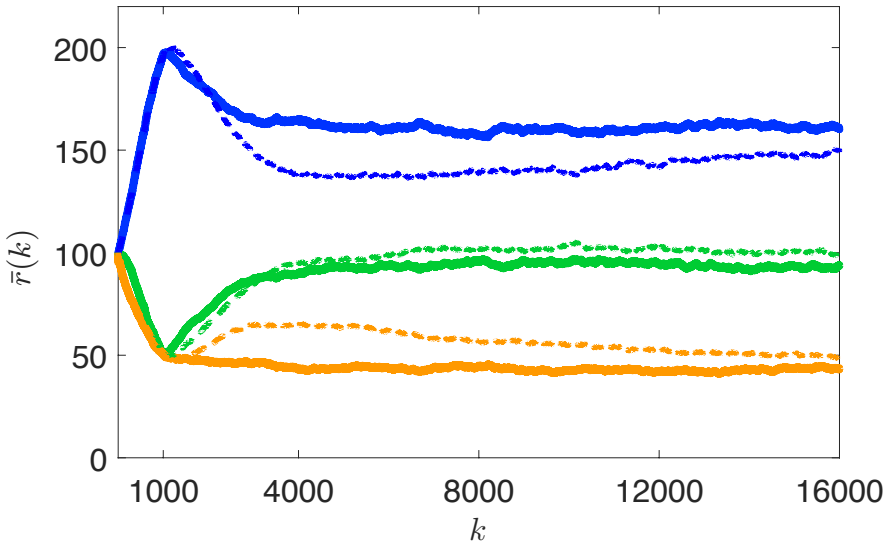

Figure 8.15: **Scenario (d). Evolution of the average risk attitude.** Blue, green, and orange lines, correspond to prudent, ordinary and audacious agents, respectively, while solid and dotted lines refer to overconfident and non-overconfident agents, respectively.

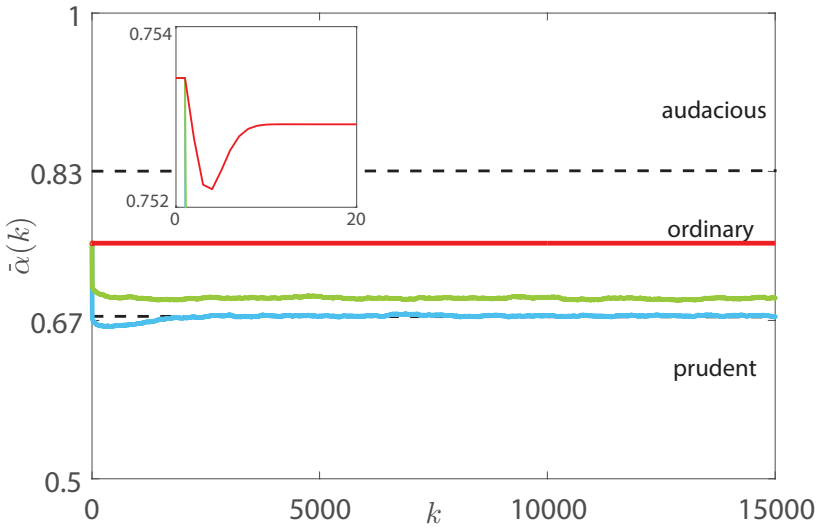

Figure 8.16: **Average risk attitude.** In the rational (in blue), partially rational (in green) and irrational (in red) markets.

This result is due to the fact that the snapping dynamics tend to assign an indegree which is inversely proportional to agents' reputation (the opposite happens for the outdegree). This result is consistent with the typical structure of influence networks, in which the agents are ranked based on their reputation, see for instance the network of corporate elite in the US [105]. A different level of rationality only has the effect of modifying the wealth ranking of the agents, but not the topology of the interaction graph.

- The rate of the network variability, defined as the number of edges activated or deactivated at each trading session, quantifies the permeability of the market to agents climbing the reputation ranking. Indeed, in a rational market less fair taxation schemes, such as the flax tax, hamper wealth redistribution, thus reducing network variability. As irrationality pervades the market, the reputation is prevalently determined by the agent innate charisma, and therefore this also hinders the network variability, as modifications of the agents' wealth have little impact on their reputation.
- Rational adaptation is beneficial for the market stability. Indeed, it favors wealth redistribution and steers the investing strategies towards the most efficient. Moreover, it confers to the agents the capability of learning from the environment: they react to variations of the market scenario (e.g. changes in the regulations) and adapt their investing strategies accordingly. On the other hand, irrational herding fosters inequalities, nullifying the potential benefits of mutual interactions. Indeed, the agents start to follow the strategies of the most charismatic agents, which are not necessarily those with the most effective investing strategies. Interestingly, the nodes with the lowest indegree, that are the charismatic market leaders, who refuse to herd, shows a significantly higher average wealth. This means that in an irrational market it is better not to herd and to be an influencer rather than a follower, according to the empirical findings that illustrate how bubbles may appear in conjunction with irrational herding [113].

Next, we tested the influence of a second behavioral parameter, the agent's level of overconfidence. We observed that

- overconfidence induces network sparsity: agents tend to become stubborn, thus reducing the connections with their neighbors;
- networks pervaded by overconfident agents are strongly asymmetric, as underconfident (and wealthy) agents are crucial for the formation of mutual influence among pairs of agents;
- a more heterogeneous distribution favors clustering. The presence both underconfident and overconfident agents promotes the emergence of triangle motifs and, more specifically, allows the presence of cycles;
- a highly overconfident market is characterized by a stronger correlation between out-degree and wealth: indeed, only the richest agents are capable of influencing stubborn overconfident agents.
- The average risk attitude reduces as the fraction of overconfidence increases: indeed, overconfidence is accompanied by a more selective coupling which implies that most of the influence links depart from edges having the best (prudent) trading strategy.

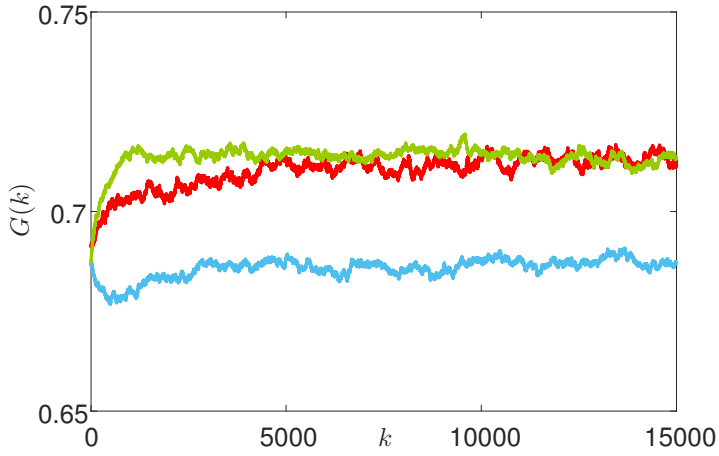

Figure 8.17: **Evolution of the Gini coefficient.** In the rational (blue line), partially rational (green line), and irrational (red line) markets.

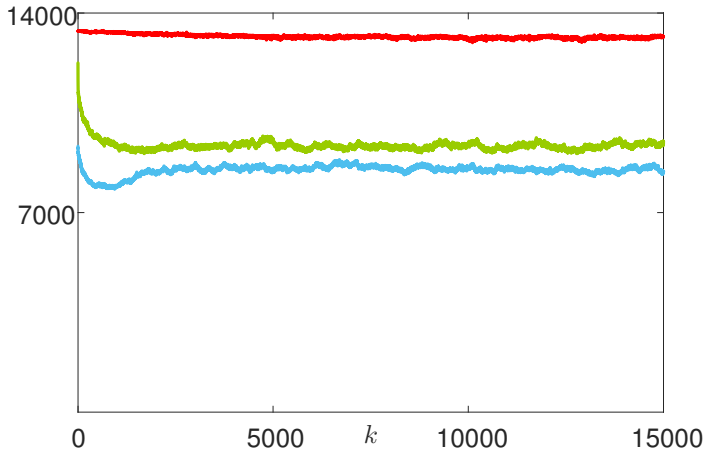

Figure 8.18: **Evolution of the trading volumes.** In the rational (blue line), partially rational (green line), and irrational (red line) markets.

However, we numerically illustrated that overconfidence is indeed detrimental when it has the effect of sticking the agent on her own mistaken valuation.

9 Optimal control of coevolving networks

In this Chapter, we focus on the case in which the edge dynamics of the coevolving network can be tailored so as to achieve the control goal. Special instances of control of coevolving networks are the synchronization and the pinning control problem with adaptive coupling gains. In these contexts, the coupling gain between neighboring nodes corresponds to the edge state, and is often chosen to monotonically increases with the relative error norm [51, 94, 114–116]. Although effective in controlling the network, these adaptive approaches cannot regulate the steady-state values of the edge state, which will depend on the initial conditions, and might end up to be excessively large. In this chapter, we aim to explore two alternative approaches to control the edge dynamics in an optimal way. In Section 9.1, we consider the problem of controlling the node dynamics toward a desired equilibrium point. Specifically, we optimally select the target value for the edge dynamics. The selection is optimal in the sense that it minimizes the control energy required to reject local perturbations from the desired equilibrium point of the node dynamics [53]. Then, in Section 9.2, we consider the problem of optimally evolving the edge dynamics so as to maximizing pinning controllability in the network. Different from existing approaches, the optimal adaptation is obtained in a completely distributed fashion [54].

9.1 Optimal selection of the target edge state

9.1.1 Linear node dynamics: the classic consensus case

To describe our approach, we start with the simplest node dynamics, that is, we consider a coevolving network of coupled integrators on a graph $\mathcal{G} = \{\mathcal{V}, \mathcal{E}\}$. We refer to a specific class of coevolving networks whose dynamics fall within Definition 7.1. Specifically, the node dynamics are described by

$$\dot{x}_i(t) = u_i(t) \qquad \forall i \in \mathcal{V} \tag{9.1}$$

where $x_i(t)$ is the state of the i-th node and

$$u_i(t) = -\sum_{j=1}^{N} \sigma_{ij}(t)\left(x_i(t) - x_j(t)\right) \tag{9.2}$$

with $\sigma_{ij}(t)$ being the state of edge $(i, j) \in \mathcal{E}$. Then, we select the edge dynamics so that the only possible equilibrium of the network are $x_1 = \cdots = x_N$ and $\sigma_{ij} = 0$ for all $(i, j) \in \mathcal{E}$, that is

$$\dot{\sigma}_{ij}(t) = -b\sigma_{ij}(t) + k\left(x_i(t) - x_j(t)\right)^2, \tag{9.3}$$

where b and k are two positive scalars. This means that, when consensus is achieved, the network topology is completely disconnected.

Note that the node dynamics can be rewritten in matrix form as

$$\dot{\mathbf{x}}(t) = -L^{\sigma}\mathbf{x}(t) \tag{9.4}$$

where L^{σ} is a time-varying Laplacian matrix (when unnecessary, we omit the dependence on time for brevity) with its generic ij-th element being

$$l_{ij}^{\sigma} = \begin{cases} \sum_{k=1,k\neq i}^{N} \sigma_{ik}(t) & i = j \\ -\sigma_{ij}(t) & i \neq j. \end{cases} \tag{9.5}$$

Note that, independent of $\sigma_{ij}(t)$, if $\mathcal{G}$ is undirected and connected, L^{σ} is a Laplacian matrix, that is, it is zero row-sum and its diagonal elements are non-negative.

When $\mathcal{G}$ is connected, the only possible consensus value is $\bar{x} = \frac{1}{N}\sum_{i=1}^{N} x_i(0)$. Defining the disagreement vector, $\mathbf{e}(t) = [e_1(t), \ldots, e_N(t)]^T \in \mathbb{R}^N$ with $e_i(t) := x_i - \bar{x}$, we can show that, under the edge dynamics (9.3), the network achieves consensus by proving that the error, described by the following dynamics,

$$\dot{\mathbf{e}}(t) = -L^{\sigma}\mathbf{e}(t) \tag{9.6}$$

converges towards zero. Before illustrating the proof, we provide the following useful Lemma:

Lemma 9.1. *For all non-negative initial conditions $\sigma_{ij}(t_0) \geq 0$, the dynamical system in (9.3) is positive.*

Proof. The proof follows from [117], Part I, Theorem 2. □

Theorem 9.2. *Given the network in (9.1–9.3), if $\mathcal{G}$ is undirected and connected, and $0 \leq k < 2$, the equilibrium $\{\bar{x}\mathbf{1}_N, \mathbf{0}_M\}$ is globally asymptotically stable.*

Proof. To prove the thesis, we show that both $\mathbf{e}(t)$ and $\boldsymbol{\sigma}(t)$ globally asymptotically converge to zero. Combining together (9.6) and (9.1–9.3), we can rewrite the network dynamics as

$$\begin{aligned} \dot{e}_i(t) = & \quad -\sum_{j=1}^{N} l_{ij}^{\sigma} e_j(t) & \forall\, i \in \mathcal{V} \\ \dot{\sigma}_{ij}(t) = & \quad -b\sigma_{ij}(t) + k(e_i(t) - e_j(t))^2 & \forall\, (i,j) \in \mathcal{E}. \end{aligned} \tag{9.7}$$

where l_{ij}^{σ} is the generic element of the time-varying Laplacian matrix defined in (9.5). Next, let us consider the candidate Lyapunov function

$$V(t) = \frac{1}{2}\left(\mathbf{e}(t)^T\mathbf{e}(t) + \boldsymbol{\sigma}(t)^T\boldsymbol{\sigma}(t)\right) = \frac{1}{2}\mathbf{e}(t)^T\mathbf{e}(t) + \frac{1}{2}\sum_{(i,j)\in\mathcal{E}} \sigma_{ij}(t)^2.$$

Differentiating, we can write

$$\begin{aligned} \dot{V}(t) = & -\mathbf{e}(t)^T L^{\sigma}\mathbf{e}(t) - b\sum_{(i,j)\in\mathcal{E}} \sigma_{ij}(t)^2 + k\sum_{(i,j)\in\mathcal{E}} \sigma_{ij}(t)(e_i(t) - e_j(t))^2 \\ = & -\mathbf{e}(t)^T L^{\sigma}\mathbf{e}(t) + \frac{1}{2}k\mathbf{e}^T(t)L^{\sigma}\mathbf{e}(t) - b\boldsymbol{\sigma}^T(t)\boldsymbol{\sigma}(t) \\ = & \left(\frac{1}{2}k - 1\right)\mathbf{e}^T(t)L^{\sigma}\mathbf{e}(t) - b\boldsymbol{\sigma}^T(t)\boldsymbol{\sigma}(t) \\ \leq & -b\boldsymbol{\sigma}^T(t)\boldsymbol{\sigma}(t) := w(\mathbf{e}(t),\boldsymbol{\sigma}(t)) \leq 0 \end{aligned} \tag{9.8}$$

where the last inequality comes from Lemma 9.1.1. Now, for the generalized LaSalle Theorem [118] $\lim_{t\to+\infty} w(\mathbf{e}(t),\boldsymbol{\sigma}(t)) = 0$, which implies

$$\lim_{t\to+\infty} \boldsymbol{\sigma}(t) = 0. \tag{9.9}$$

From (9.6) and (9.9), we also have that $\lim_{t\to+\infty} \dot{\mathbf{e}}(t) = 0$, $\lim_{t\to+\infty} \mathbf{e}(t) = \bar{\mathbf{e}}$, where $\bar{\mathbf{e}}$ is a vector in $\mathbb{R}^N$. We prove that $\bar{\mathbf{e}} = 0$ by contradiction. Indeed, if $\bar{\mathbf{e}} \neq 0$, we would have $\lim_{t\to+\infty} \dot{\boldsymbol{\sigma}}(t) \neq 0$, and this would contradict (9.9). □

Figure 9.1 compares the traditional adaptive coupling in [51] which corresponds to setting $b = 0$ in Equation (9.3), with our approach ($b > 0$). Note that the selection of a positive b make the coupling strength between the network nodes asymptotically vanishing. On the other hand, in the classic adaptive approach (right panels of Figure 9.1), the coupling gains monotonically increase, and this could yield to their divergence, e.g., in the case of persistent noise acting on the network system, see Figures 9.2 and 9.3. This also has implications on the overall control energy spent to lead the network to consensus, defined as

$$\mathrm{E} = \int_0^T \mathbf{u}(t)^T\mathbf{u}(t)\mathrm{d}t \tag{9.10}$$

with $\mathbf{u}$, the stack vector of u_i for all $i \in \mathcal{V}$. In Figure 9.4, we show that the control energy in (9.10) is significantly lower when $b > 0$.

When the control objective is to steer the node dynamics toward the state of a given node in the network, rather than to the average of the initial conditions, the control problem is called *leader-followers* consensus [119, 120]. In this context, the controlled network can be viewed as an augmented system, in which an extra node, the leader, is added to the graph $\mathcal{G}$, and is unidirectionally coupled with a (limited) fraction of the rest of the nodes, the followers. To keep the notation consistent with the existing literature, we use a different letter p, for the state of the edges connecting the leader to the the rest of the network, and we use a single subscript to identify which node is coupled with the leader. In formal terms, we rewrite (9.1–9.3) as

$$\dot{x}_i(t) = -\sum_{j=1}^{N} l_{ij}^{\sigma} x_j - p_i \delta_i (x_i - x_\ell(t)) \tag{9.11}$$

$$\dot{\sigma}_{ij} = -b\sigma_{ij}(t) + k\,(|x_i(t) - x_\ell(t)|)^2 \quad \forall (i,j) \in \mathcal{E} \tag{9.12}$$

$$\dot{p}_i = -b_p p_i(t) + k_p\,(|\,x_i(t) - x_\ell(t)\,|)^2 \quad \forall i \in \mathcal{P} \tag{9.13}$$

where $\mathcal{P} \subseteq \mathcal{V}$ is the subset of the p followers, that is, nodes that are directly connected with the leader; $x_\ell(t) = x_\ell(0)$ is the state of the leader, which is constant since, having no incoming links, its dynamics are given by $\dot{x}_l(t) = 0$; δ_i is the Kroncker delta, that is, it is equal to 1 if $i \in \mathcal{P}$, while it is 0 otherwise; and b_p, k_p are nonnegative tunable parameters.

Definition 9.3. *Network (9.11– 9.13) globally asymptotically achieves consensus onto the state of the leader if, for all* $\mathbf{x}(0) \in \mathbb{R}^N$,

$$\lim_{t \to +\infty} |x_i(t) - x_\ell(0)| = 0 \quad \forall i \in \mathcal{V}. \tag{9.14}$$

Note that, defining this time the disagreement vector with respect to leader's state, that is, as $\mathbf{e}(t)$=$[e_1(t), \ldots, e_i(t), \ldots, e_N(t)]$, with $e_i(t) := x_i(t) - x_\ell(0)$, imposing condition (9.14) for all initial conditions $\mathbf{x}(0) \in \mathbb{R}^N$ and for all $i \in \mathcal{V}$ is equivalent to the global asymptotic convergence of $\mathbf{e}(t)$ to the origin. The error dynamics can be written as

$$\dot{\mathbf{e}}(t) = -L^{\sigma}\mathbf{e}(t) - P\mathbf{e}(t) = -M^{\sigma}\mathbf{e}(t) \tag{9.15}$$

where $M^{\sigma} := L^{\sigma} + P$, with P a diagonal matrix whose i-th diagonal entry is p_i if $i \in \mathcal{P}$, while it is 0 otherwise. Now, we are ready to give a convergence result for network (9.11–9.13) similarly to what has been done in Theorem 9.10.

Lemma 9.4. *For all nonnegative initial conditions* $p_i(t_0) \geq 0$*, the dynamical system in (9.13) is positive.*

Proof. The proof follows from [117], Part I, Theorem 2. □

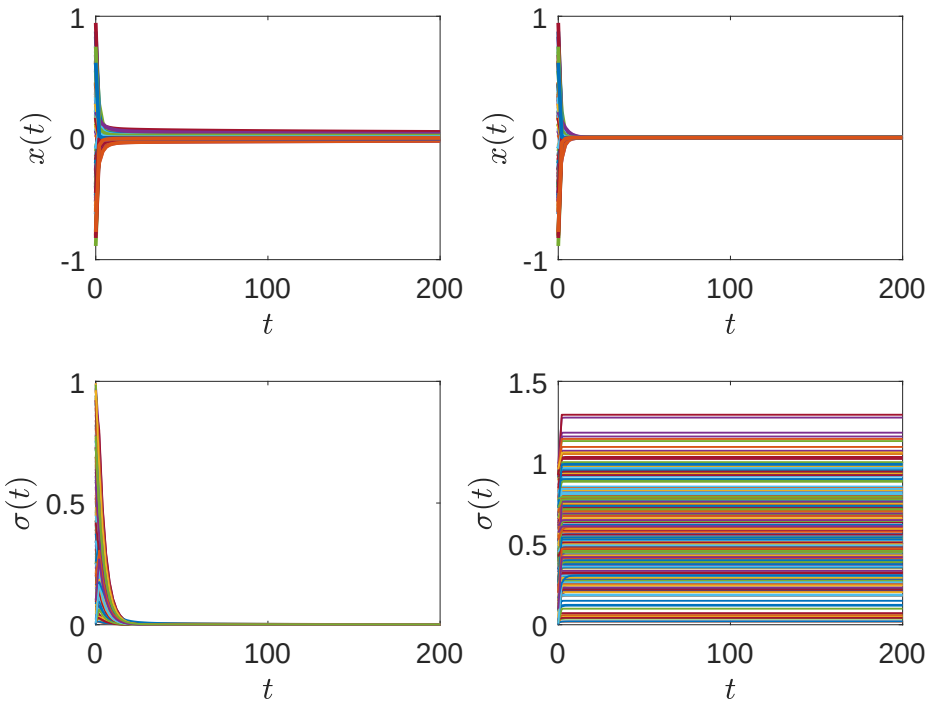

Figure 9.1: Time evolution of the coevolving network (9.1,9.3) on an ER graph with $N = 100$ when $b = 0.5$ (left panels) and when $b = 0$ (right panels). Top and bottom panels corresponds to node and edge evolution, respectively. Node initial conditions are normally distributed with 0 mean and standard deviation equal to 0.5, while edge initial conditions are uniformly distributed in [0 1].

Theorem 9.5. *Given the network in (9.11–9.13), if $\mathcal{G}$ is undirected and connected and k and k_p are such that $0 \leq (k + k_p) < 2$, the equilibrium $\{x_\ell(0)\mathbf{1}_N, \mathbf{0}_M, \mathbf{0}_p\}$ is globally asymptotically stable.*

Proof. The proof comes from the proof of Theorem (9.2) by considering the following Lyapunov function

$$V(t) = \frac{1}{2}\left(\mathbf{e}(t)^T\mathbf{e}(t) + \boldsymbol{\sigma}(t)^T\boldsymbol{\sigma}(t) + \mathbf{p}(t)^T\mathbf{p}(t)\right)$$

invoking Lemma 9.4, Equation (9.15) and using the fact that $M^\sigma = L^\sigma + P$. □

Figure 9.5 and 9.6 show that, as in the leaderless case, setting 0 as the equilibrium point of the edge dynamics yields a reduction in the overall control energy required to drive the network to consensus and to respond to external disturbances.

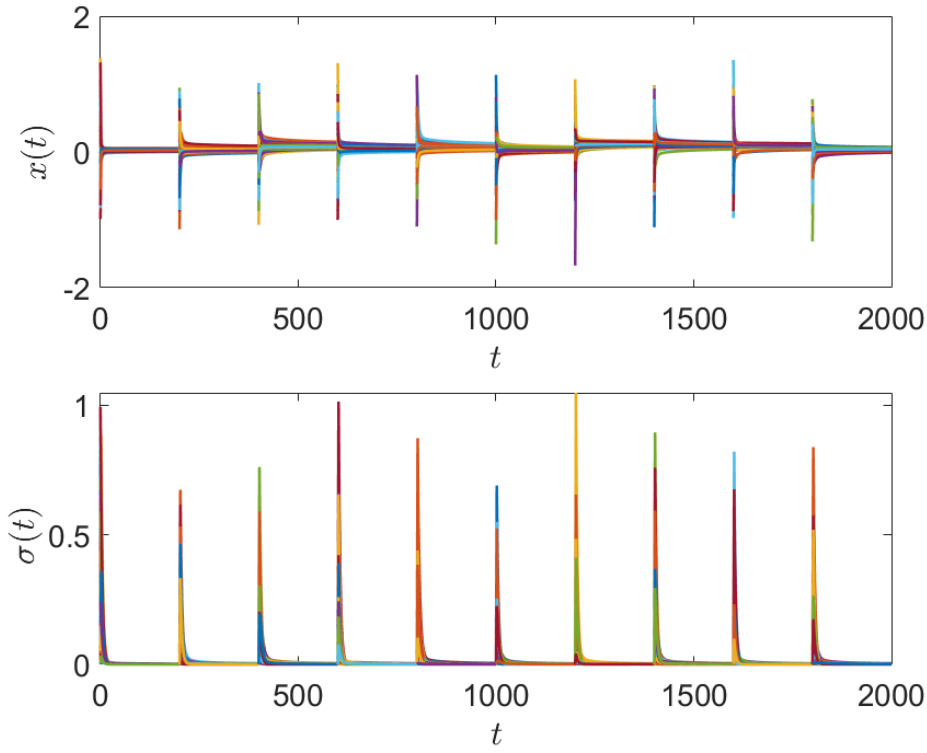

Figure 9.2: Time evolution of the state of the nodes (top panel) and edges (bottom panel) of the coevolving network (9.1–9.3) on an ER graph with $N = 100$ when $b = 0.5$, and, every 200 time units, an impulsive disturbance acts on each node. The amplitude of the disturbance is randomly selected from a normal distribution with zero mean and standard deviation equal to 0.5.

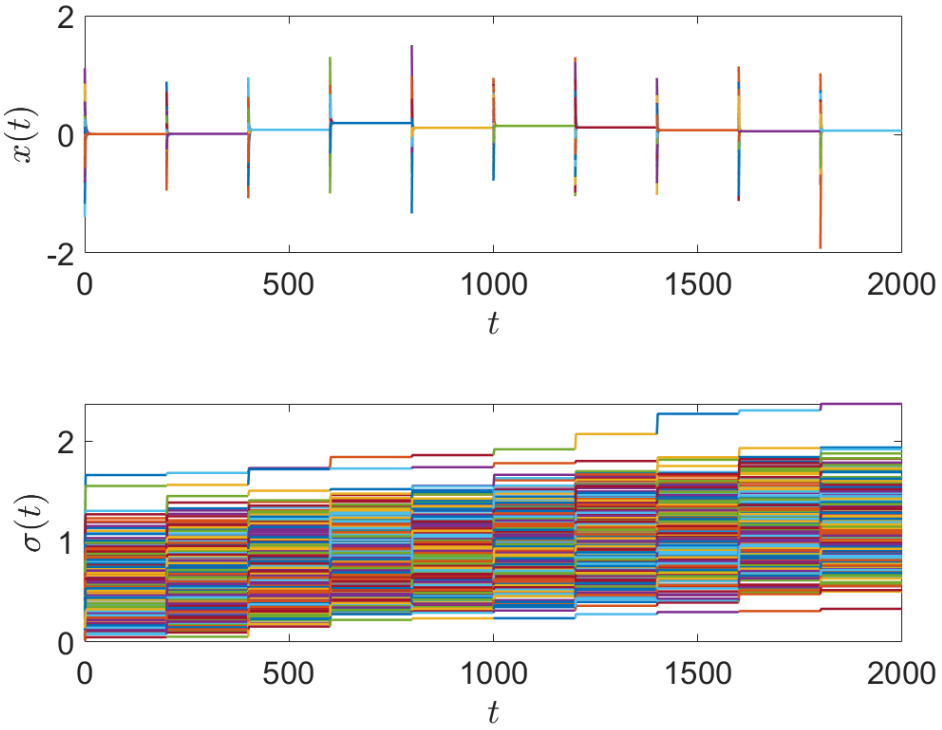

Figure 9.3: Time evolution of the state of the nodes (top panel) and edges (bottom panel) of the coevolving network (9.1–9.3) on an ER graph with $N = 100$ when $b = 0$, and, every 200 time units, an impulsive disturbance acts on each node. The amplitude of the disturbance is randomly selected from a normal distribution with zero mean and standard deviation equal to 0.5.

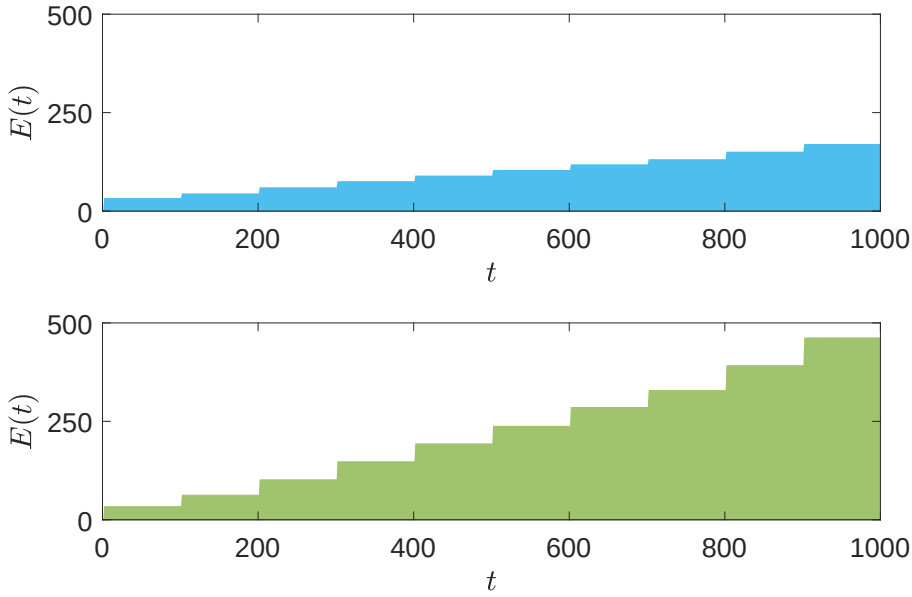

Figure 9.4: **Control energy comparison.** Time evolution of the energy E spent to control the coevolving network (9.1–9.3) on an ER graph with $N = 100$ when $b = 0.5$ (left panel) and $b = 0$ (right panel). Every 200 time units, an impulsive disturbance acts on each node. The amplitude of the disturbance is randomly selected from a normal distrubution with zero mean and standard deviation equal to 0.5.

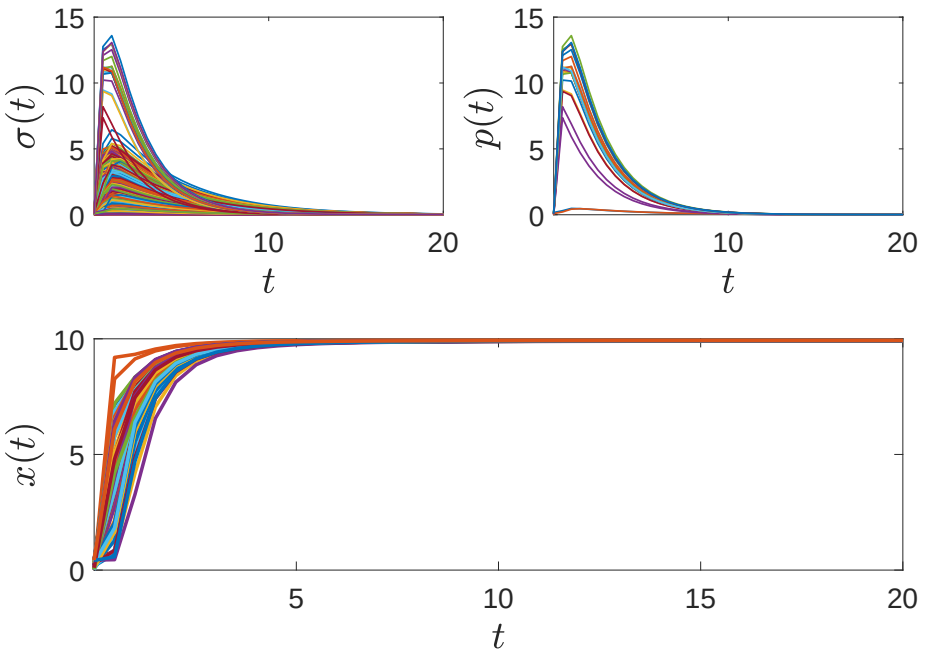

Figure 9.5: Time evolution of the coevolving network (9.11–9.13) with $b = b_p = 0.5$, $k = k_p = 0.8$. The followers are coupled through the same topology as in Figure 9.1–9.4. The set $\mathcal{P}$ of followers directly connected with the leader has cardinality $0.2N$, that is, the number of followers is equal to $0.2N$.

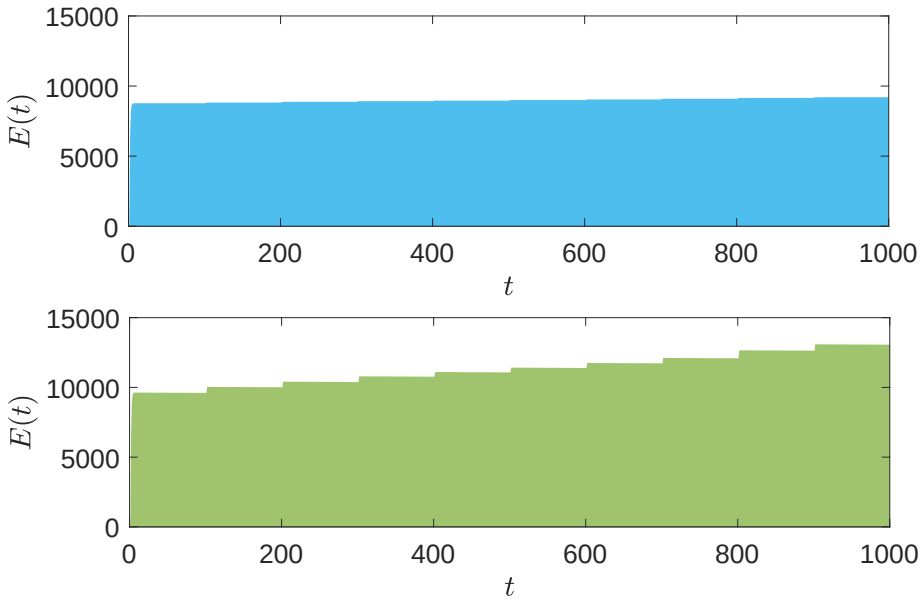

Figure 9.6: **Energy comparison.** Time evolution of the energy spent to control coevolving network (9.11–9.13) with $k = 0.8$. The followers are coupled through the same topology as in Figure 9.1–9.4. The set $\mathcal{P}$ of followers directly connected with the leader has cardinality $0.2N$. The parameter b is set to 0.5 (top panel) and 0 (bottom panel), respectively.

9.1.2 Nonlinear node dynamics: pinning control of synchronization

Note that in the classic consensus problem it is possible to choose the origin as the target state for the edge dynamics since the disagreement dynamics are marginally stable when the system is decoupled. This is not true, in general, for synchronization of nonlinear systems, where the synchronization error might be unstable in the absence of coupling. In that case, the problem arises of appropriately selecting the target point for the edge dynamics. In the context of nonlinear node dynamics, leader-follower problems take the name of pinning control [17, 121–126], where the role of the leader is played by a virtual node, the pinner, that exerts a feedback control action only on a small fraction of the nodes which then propagates to the rest of the nodes by leveraging the existing connections among them. The objective here is to drive the node dynamics towards the trajectory identified by the pinner. As explained above, to achieve this aim, since we are considering now generic nonlinear node dynamics, we need to modify the design of the edge dynamics (9.11–9.13) so as to change the setpoint for the edge states. Specifically, the dynamics of the coevolving network become

$$\dot{\mathbf{x}}_i = F(\mathbf{x}_i, t) - \sum_{j=1}^{N} l_{ij}^{\sigma} \mathbf{x}_j - p_i \delta_i (\mathbf{x}_i - \mathbf{s}) \qquad \forall\, i \in \mathcal{V} \tag{9.16}$$

$$\dot{\sigma}_{ij} = -b(\sigma_{ij} - \varsigma_{ij}) + k\|\mathbf{x}_i - \mathbf{x}_j\|^2 \qquad \forall\, (i,j) \in \mathcal{E} \tag{9.17}$$

$$\dot{p}_i = -b_p(p_i - \rho_i) + k_p\|\mathbf{x}_i - \mathbf{s}\|^2 \qquad \forall\, i \in \mathcal{P} \tag{9.18}$$

where $\mathbf{x}_i \in \mathbb{R}^n$ is the state of node i, $F(\cdot) : \mathbb{R}^n \times \mathbb{R}^+ \to \mathbb{R}^n$ is the vector field describing the individual dynamics, $\mathcal{P} \subseteq \mathcal{V}$ is now called the set of pinned nodes and $\mathbf{s}(t) \in \mathbb{R}^n$ is the reference trajectory identified by the pinner, that is the solution of the following Cauchy problem

$$\begin{aligned} \dot{\mathbf{s}}(t) &= F(\mathbf{s}, t) \\ \mathbf{s}(0) &= \mathbf{s}_0. \end{aligned} \tag{9.19}$$

Finally, ς_{ij} and ρ_i are the setpoints for the dynamics of the edges among followers, and among the pinner and the followers, respectively and, b, k, b_p, k_p are tunable parameters.

The synchronization error is defined as $\mathbf{e}(t) = \left[\mathbf{e}_1(t)^T, \ldots, \mathbf{e}_i(t)^T, \ldots, \mathbf{e}_N(t)^T\right]$, where $\mathbf{e}_i(t) = \mathbf{x}_i - \mathbf{s}(t) \quad \forall i \in \mathcal{V}$, that is described by the following dynamics

$$\dot{\mathbf{e}}_i = F(\mathbf{x}_i, t) - F(\mathbf{s}, t) - \sum_{j=1}^{N} m_{ij}^{\sigma} \mathbf{e}_j \quad \forall\, i \in \mathcal{V} \tag{9.20}$$

where m_{ij}^{σ} is the ij-th element of the extended Laplacian M^{σ}. Let us now give some definitions that will turn out to be useful for the next results

Definition 9.6 (Pinning controllability). *[127] The coevolving network (9.16–9.18) is said to be locally asymptotically controlled to the pinner trajectory* $\mathbf{s}(t) \in \mathbb{R}^n$ *with*

$t \geq 0$ if there exists a constant $\Delta(t_0)$ for any $t_0 \geq 0$ such that

$$\lim_{t \to +\infty} \|\mathbf{e}(t)\| = 0 \tag{9.21}$$

for $\|\mathbf{e}(t_0)\| < \Delta(t_0)$. When, additionally, there exists $r > 0$ such that

$$\|\mathbf{e}(t)\|_2 \leq \|\mathbf{e}(0)\|_2 \mathrm{e}^{-rt} \tag{9.22}$$

then the network is locally exponentially controlled to the pinner trajectory. Finally, if (9.22) holds for all $\|\mathbf{e}(t_0)\| \in \mathbb{R}^{nN}$, then network (9.16–9.18) is globally exponentially controlled to the pinner trajectory.

In what follows, we consider the case in which the vector field $F(\cdot)$ admits an unstable equilibrium point $\bar{\mathbf{s}}$, and that $\mathbf{s}(0) = \bar{\mathbf{s}}$. In other words, we consider the problem of pinning controllability towards an unstable equilibrium point. Specifically, our problem consists in a suitable selection of the setpoints ς_{ij} and ρ_i for the edge dynamics. First, we provide lower bounds on the setpoints guaranteeing local pinning controllability to the equilibrium point, thus identifying an admissible set of values for ς_{ij} and ρ_i. Then, within this set, we optimally select the edge setpoints so that the network rejects local perturbation with the minimum control energy.

Lower bounds on the edge setpoints.

To study the local pinning controllability of network (9.16–9.18) (see Definition 9.6), we consider infinitesimal perturbations from the unstable equilibrium point $\bar{\mathbf{s}}$ identified by the pinner. Defining $\boldsymbol{\varsigma}$ as the stack of all ς_{ij}, and $\boldsymbol{\rho}$ as the stack of all the ρ_i, we linearize network (9.16–9.18) around $(\mathbf{x}, \boldsymbol{\sigma}, \boldsymbol{\rho}) = (\bar{\mathbf{s}}, \bar{\boldsymbol{\sigma}}, \bar{\boldsymbol{\rho}})$, thus obtaining

$$\delta\dot{\mathbf{x}} = \left[\mathbf{I}_N \otimes JF(\mathbf{s}) - M^{\delta} \otimes \mathbf{I}_N\right] \delta\mathbf{x} \tag{9.23}$$

$$\delta\dot{\boldsymbol{\sigma}} = -b(\boldsymbol{\sigma} - \boldsymbol{\varsigma}) \tag{9.24}$$

$$\delta\dot{\mathbf{p}} = -b_p(\mathbf{p} - \boldsymbol{\rho}) \tag{9.25}$$

where $JF(\mathbf{s})$ is the time-invariant Jacobian of $F(\cdot)$ evaluated in $\mathbf{s}$ and M^{δ} is the time-invariant extended Laplacian whose weights correspond to the asymptotic edge and gain states. Moreover, we denote $\delta\mathbf{x} = [\delta\mathbf{x}_1, \ldots, \delta\mathbf{x}_i, \ldots, \delta\mathbf{x}_N]$, with $\delta\mathbf{x}_i = \mathbf{x}_i - \bar{\mathbf{s}}$, $\delta\boldsymbol{\sigma} = \boldsymbol{\sigma} - \bar{\boldsymbol{\varsigma}}$ and $\delta\mathbf{p} = \mathbf{p} - \bar{\boldsymbol{\rho}}$. Moreover, we assume that the target edge states are identical for all $(i, j) \in \mathcal{E}$, i.e., $\varsigma_{ij} = \varsigma$, and that the target gains states are identical for all $i \in \mathcal{P}$ and are equal to the target edge state, i.e., $\rho_i = \varsigma$. Therefore, the asymptotic edge and gain states are equal to $\mathbf{1}_M \varsigma$ and $\mathbf{1}_p \varsigma$[1].

To study the local stability of (9.16–9.18), we study the stability of (9.23–9.25) that are decoupled and can be studied separately. Diagonalizing M^{δ}, equation (9.23) can be rewritten as

$$\dot{\boldsymbol{\xi}}_i = (JF(\mathbf{s}) - \varsigma\lambda_i(M^{\delta})\mathbf{I}_N)\boldsymbol{\xi}_i, \tag{9.26}$$

[1]Note that the equilibrium point $\bar{\boldsymbol{\sigma}}$ and $\bar{\mathbf{p}}$ are independent on the control parameters b and b_p.

for all $i = 1, \dots, N$, where $\boldsymbol{\xi}_i$ is the i-th modal coordinate of the network corresponding to the i-th eigenvalue of M^δ. Now, if we assume $\mathcal{G}$ connected and undirected, the eigenvalues of M^δ are positive and real [125] and can be ordered as $0 < \lambda_1 \leq \dots \leq \lambda_i \leq \lambda_N$. Substituting $\varsigma\lambda_i$ with a nonnegative parameter η, we obtain the following master stability equation

$$\dot{\boldsymbol{\xi}}_i = (JF(\mathbf{s}) - \eta(M^\delta)\mathbf{I}_N)\boldsymbol{\xi}_i, \tag{9.27}$$

The master stability function (MSF) [12, 124] is a function that associates to each value of η the largest Lyapunov exponent, $\Lambda(\eta)$, of (9.27). In this way, rather than studying the N variational equations in (9.26), we can study the parametric behavior of $\Lambda(\eta)$ as η changes. We are now ready to give the following result:

Theorem 9.7. *The coevolving network (9.16–9.18) is locally asymptotically controlled to the unstable equilibrium $\bar{s}$ if,*

1) *$\mathcal{G}$ is connected and undirected;*
2) *$F(\cdot)$ is such that $\Lambda(\eta)$ is monotonically decreasing, and there exists $\eta^\star > 0$: $\Lambda(\eta^\star) = 0$;*
3) *$\varsigma_{ij} = \varsigma > \dfrac{\eta^\star}{\lambda_1(M^\delta)}$ for all $(i, j) \in \mathcal{E}$;*
4) *$\rho_i = \varsigma > \dfrac{\eta^\star}{\lambda_1(M^\delta)}$ for all $i \in \mathcal{P}$.*

Proof. As $F(\cdot)$ is such that $\Lambda(\eta)$ is monotonically decreasing and by setting $\rho_i = \varsigma_{ij} = \varsigma > \dfrac{\eta^\star}{\lambda_1(M^\delta)}$, all the transversal eigenmodes to the synchronization manifold in (9.26) become stable as $\Lambda(\eta) < 0$ for $\eta = \varsigma\lambda_i(M^\delta)$, $i = 1, \dots, N$. Moreover, the edge (9.17) and the gain (9.18) dynamics are asymptotically locally stable at ς. □

Theorem 9.7 provides a sufficient condition to select the edge setpoints. In the following, within the admissible setpoints (i.e., those fulfilling the bound given in Theorem 9.7), we select those minimizing the control energy required to reject local perturbations.

Optimal selection of the setpoints

Here we select the edge setpoints $\boldsymbol{\varsigma}$ so that the controller reacts spend the minimum possible energy to recover from local perturbations of the node states from the desired node setpoint $\bar{\mathbf{s}}$. More specifically, we find $\boldsymbol{\varsigma}^\star$ by minimizing the control energy required

as follows

$$\begin{aligned}
&\min_{\varsigma} \max_{\|\delta \mathbf{x}_0\|} \int_0^{+\infty} \mathbf{u}(t,\varsigma)^T \mathbf{u}(t,\varsigma) \mathrm{d}t \\
&s.t. \\
&\delta \dot{\mathbf{x}}(t) = \left[\mathbf{I}_N \otimes JF(\mathbf{s})\right] \delta \mathbf{x}(t) + \mathbf{u}(t,\varsigma) \\
&\delta \mathbf{x}(0) = \delta \mathbf{x}_0 \\
&\mathbf{u}(t,\varsigma) = -\left[M^{\delta}(\varsigma) \otimes \mathbf{I}_n\right] \delta \mathbf{x}(t) \\
&\varsigma > \mathbf{1}_M \left(\eta^*/\lambda_1(M^{\sigma})\right)
\end{aligned} \tag{9.28}$$

where η^* is needed to enforce local pinning synchronization and comes from Theorem 9.7[2]. The min-max problem (9.28) consists in selecting a unique setpoint ς^* for the edge dynamics so as to minimizing the energy required to reject a local perturbation along the least favorable direction.

Although in general problem (9.28) has to be numerically solved, we show how in the case of scalar node dynamics it can be analytically treated. Indeed, in this case we have that the node set point $\bar{s} \in \mathbb{R}$ and $JF(s) \in \mathbb{R}$. Furthermore, since the edge setpoints are selected to be identical for all $(i,j) \in \mathcal{E}$, we can then write $M^{\delta} = \varsigma M = \varsigma(L+P)$. Hence problem (9.28) becomes

$$\begin{aligned}
&\min_{\varsigma} \max_{\|\delta \mathbf{x}_0\|=1} \varsigma^2 \delta \mathbf{x}_0^T W(\varsigma) \delta \mathbf{x}_0 \\
&s.t. \\
&\varsigma > \eta^*/\lambda_1(M)
\end{aligned} \tag{9.29}$$

where

$$W(\varsigma) = \int_0^{+\infty} \mathrm{e}^{(JF(s)\mathbf{I}_N - \varsigma M)t} M M^T \mathrm{e}^{(JF(s)\mathbf{I}_N - \varsigma M)^T t} \mathrm{d}t$$

is a positive semi-definite matrix, solution of the following Lyapunov equation

$$(JF(s)I_N - \varsigma M)^T W(\varsigma) + W(\varsigma)\left(JF(s)\mathbf{I}_N - \varsigma M\right) + MM^T = 0. \tag{9.30}$$

Following the chain of the min – max problems, we start by solving

$$\max_{\|\delta \mathbf{x}_0\|=1} \delta \mathbf{x}_0^T W(\varsigma) \delta \mathbf{x}_0. \tag{9.31}$$

By applying the Lagrange Multipliers method, we obtain that

$$W \delta \mathbf{x}_0^{\star} = \lambda(W(\varsigma)) \delta \mathbf{x}_0^{\star} \tag{9.32}$$

that is the eigenvalues equation. In other words, the maximum of (9.31) is attained at the eigenvector $\delta \mathbf{x}_0^{\star}$ of $W(\varsigma)$ corresponding to the maximum eigenvalue of $W(\varsigma)$. Indeed, the maximum value of the objective function is $\lambda_{\max}(W(\varsigma))$, as $\delta \mathbf{x}_0^{\star T} W(\varsigma) \delta \mathbf{x}_0^{\star} = \lambda_{\max}(W(\varsigma))$. Now, we are ready to solve

$$\min_{\varsigma} \varsigma^2 \lambda_{\max}(W(\varsigma)). \tag{9.33}$$

[2]Note that the solution of problem (9.28) is independent of the selection of ϵ, and therefore in the following we will set $\epsilon = 1$.

Let us note that we can diagonalize (9.30) left multiplying it by V^T and right multiplying it by V, that is the matrix of the right eigenvectors of $(JF(s)\mathbf{I}_N - \varsigma M)$ to obtain:

$$(JF(s)\mathbf{I}_N - \varsigma\Lambda)\, Q + Q\,(JF(s)\mathbf{I}_N - \varsigma\Lambda) + V^T M M^T V = 0 \tag{9.34}$$

where $Q = V^T W(\varsigma) V$ and Λ is the diagonal matrix containing the eigenvalues of M. As $M = M^T$, the eigenvectors of M^2 are the same of M (i.e., are those contained in V) while the eigenvalues are the squared eigenvalues of M. Therefore, Q is a diagonal matrix containing the eigenvalues of the Gram matrix $W(\varsigma)$ with generic element equals to

$$Q_i = \lambda_i(W(\varsigma)) = -\frac{\lambda_i^2(M)}{2(JF(s) - \varsigma\lambda_i(M))}. \tag{9.35}$$

that is, the eigenvalues of $W(\varsigma)$ are function of the eigenvalues of M. As (9.35) are not a monotonic function of $\lambda_i(M)$, problem (9.33) becomes

$$\begin{aligned} \min_{\varsigma} \max_{i} \mathrm{L}_i &:= -\frac{\varsigma^2 \lambda_i(M)^2}{2(JF(s) - \varsigma\lambda_i(M))} \\ &\frac{\eta^\star}{\lambda_1(M)} - \varsigma < 0. \end{aligned} \tag{9.36}$$

Problem (9.36) can be solved by noting that for $\varsigma \in (\eta^\star/\lambda_1(M), +\infty)$, and for all $i = 1, \ldots, N$, L_i is convex, and has a unique minimum point at $\varsigma_i^\star = \dfrac{2JF(s)}{\lambda_i(M)}$. Furthermore, the minimum is the same for all i, and correspond to $2JF(s)$. This implies that, defining $\bar{\varsigma} := \dfrac{JF(s)\,(\lambda_1(M) + \lambda_N(M))}{(\lambda_1(M)\lambda_N(M))}$ as the value of ς such that $\mathrm{L}_1 = \mathrm{L}_N$, we have

$$\max_i \mathrm{L}_i = \begin{cases} \mathrm{L}_1, & \text{if } \varsigma \le \bar{\varsigma}, \\ \mathrm{L}_N, & \text{if } \varsigma > \bar{\varsigma}. \end{cases} \tag{9.37}$$

Since $\varsigma_N^\star \le \bar{\varsigma} \le \varsigma_1^\star$, the solution of (9.36) is $\varsigma^\star = \bar{\varsigma}$.

To illustrate our findings, we consider a simple example over the pinned 4-nodes graph depicted in Figure 9.7, where the individual dynamics are described by the normal form of the supercritical pitchfork bifurcation, that is,

$$F(x, t) = rx - x^3, \tag{9.38}$$

where we select $r = 2$, so that the origin is the unstable equilibrium point towards which we aim at steering the network dynamics. In Figure 9.8, we show function L_i for $i = 1, \ldots, N$, with the red dashed line identifying $\max_i \mathrm{L}_i$. In this case, we obtain $\varsigma^\star = 14.85$, and to illustrate the optimality of this selection, we compare in Figure 9.9 the energy required to reject a sequence of impulsive perturbations, when $\varsigma = \varsigma^\star$ and $\varsigma = 20 > \varsigma^\star$, respectively. We conclude this example by showing in Figure 9.9 that the control energy required to react to infinitesimal perturbations of the node states from the desired setpoint is doubled when it is selected an edge setpoint $\varsigma > \varsigma^\star$.

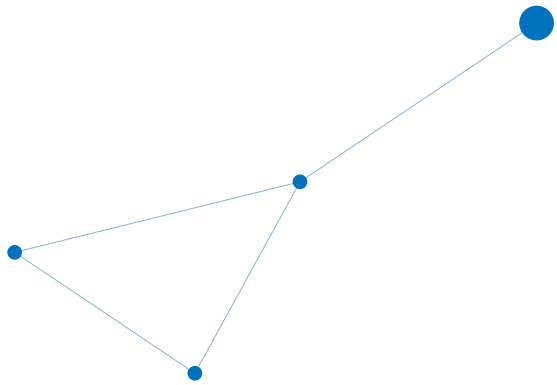

Figure 9.7: 4-nodes network: the largest dot identifies the pinned node.

9.2 Optimal pinning controllability of complex networks

Here, we consider the problem of optimally evolving the edge dynamics to maximize traditional measures of pinning controllability. Different from existing approaches, we aim at achieving this goal in a completely distributed fashion. In this case, the controlled network is static, and thus the node dynamics coevolve only with the edges connecting the pinner node to the nodes of the controlled network. In pinning control problems over static networks, sufficient conditions for local and global convergence of the nodes to the desired trajectory have been derived in the literature [124–126, 128]. In particular, it was shown in [128] that, under suitable assumptions on the individual node dynamics, a crucial parameter for controlling the network is the smallest eigenvalue λ_1 of an extended Laplacian matrix, which encompasses information on the network topology, the set of pinned nodes, and the coupling and control gains. The largest λ_1, the easier is to control the network. Although it is apparent that a smart choice of the *value* of the control gains might increase λ_1, most of the previous works on optimal pinning control focuses on optimizing the selection of the pinned nodes (i.e., the nodes to be targeted by the control action), see for instance [129], while lower bounds on the (typically uniform) coupling gains are provided. However, when the control gains cannot be arbitrarily large, a uniform choice is indeed detrimental and might prevent the achievement of the control goal.

In this Section, we propose a fully decentralized approach for tuning online the control gains in an optimal adaptive fashion. Inspired by the work on optimal consensuability and synchronizability of Kempton et al. [130–132], we built a multilayer approach where i) the first layer employs a decentralized version of the power iteration algorithm [133] to evaluate the sensitivity of λ_1 to the variation of the gains and ii) the second layer dynamically tunes the control gains, which are then used for pinning control. The effectiveness of the approach is demonstrated through a representative example of a network of Chua's circuits.

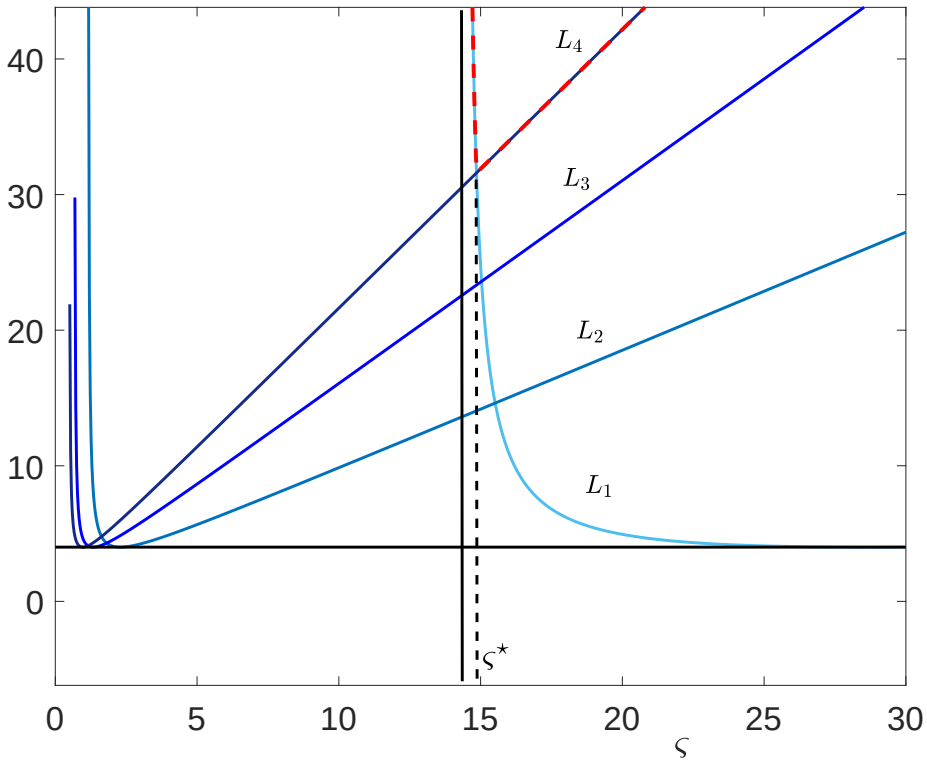

Figure 9.8: Optimal selection of the edge setpoint for the network depicted in Figure 9.7 when $F(\cdot)$ corresponds to (9.38). Plot of the functions $\mathrm{L}_1, \ldots, \mathrm{L}_4$, with the solid horizontal line identifying their minimum $2JF(s) = 4$, and the solid vertical line the threshold on ς at 14.36 as defined in problem (9.36). The red dashed line corresponds to $\max_i \mathrm{L}_i$, while the vertical dashed lines identifies the optimal value $\varsigma^\star = 14.85$.

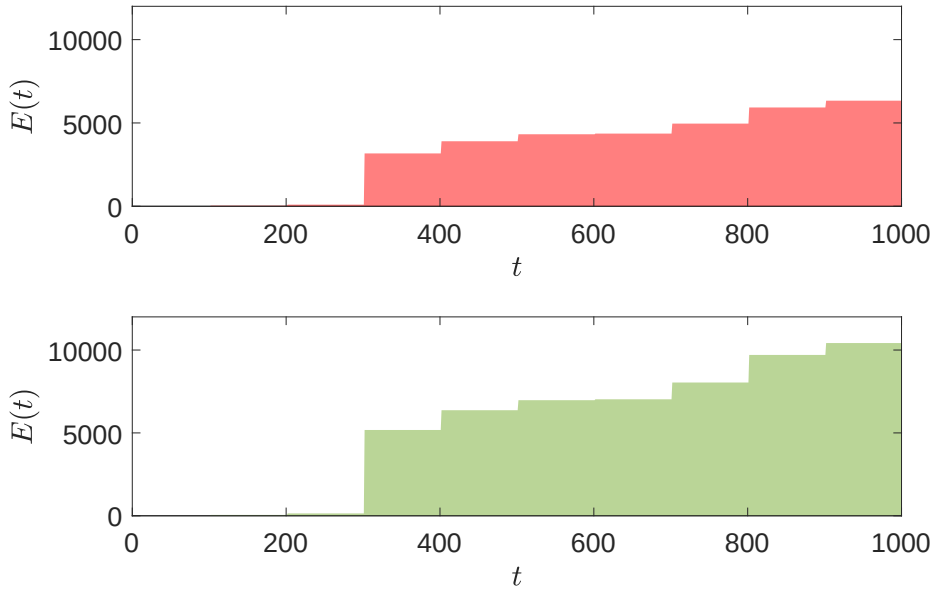

Figure 9.9: Control energy required to the 4-nodes network with vector field as in (9.38) for rejecting a sequence of impulsive perturbations from the node equilibrium point $x = 0$. The edge setpoint is set to $\varsigma^\star = 14.85$ (top panel) and to $\varsigma = 20$ (bottom panel), respectively.

9.2.1 Pinning controllability in static networks

Let us consider network (9.16) when the edges are time-invariant, that is

$$\dot{\mathbf{x}}_i(t) = \begin{cases} F(\mathbf{x}_i, t) - \sigma \sum_{j=1}^{N} l_{ij}\mathbf{x}_j(t) - p_i(\mathbf{x}_i - \mathbf{s}(t)), & \text{if } i \in \mathcal{P}, \\ F(\mathbf{x}_i, t) - \sigma \sum_{j=1}^{N} l_{ij}\mathbf{x}_j(t), & \text{otherwise.} \end{cases} \tag{9.39}$$

In pinning control, a well-assessed assumption on the node dynamics ensuring that global exponential pinning controllability (see Definition 9.6) can be achieved is the so-called QUAD inequality, , which is defined as follows:

Definition 9.8. *A vector function $F(\cdot)$ is QUAD [114] if there exists a diagonal matrix $Q \in \mathbb{R}^{n\times n}$ such that*

$$(\mathbf{x} - \mathbf{y})^T (F(\mathbf{x}, t) - F(\mathbf{y}, t)) \leq (\mathbf{x} - \mathbf{y})^T Q(\mathbf{x} - \mathbf{y})$$

for all $\mathbf{x}, \mathbf{y} \in \mathbb{R}^n$.

Notice that the pinning error dynamics can be written as in (9.20) with m_{ij} instead of m_{ij}^{σ}. The following Lemma shows that, when the individual dynamics are QUAD, the magnitude of the smallest eigenvalue of M, $\lambda_1(M)$, plays a key role in guaranteeing global pinning controllability.

Lemma 9.9. *If $\mathcal{G}$ is undirected and connected, the vector function $F(\cdot)$ is QUAD and $\lambda_1(M) > q_{\max} := \max_i Q_{ii}$, then network (9.39) is globally exponentially pinning controlled to the desired trajectory $\mathbf{s}(t)$ with rate $(\lambda_1(M) - q_{\max})/2$.*

Proof. Consider the candidate Lyapunov function

$$V(t) = \frac{1}{2}\mathbf{e}(t)^T \mathbf{e}(t).$$

Differentiating, and exploiting the assumption that $F(\cdot)$ is QUAD, we can write

$$\begin{aligned} \dot{V}(t) &= \mathbf{e}^T(t)\dot{\mathbf{e}}(t) \\ &\leq \mathbf{e}^T(t)[(\mathbf{I}_N \otimes Q) - (M \otimes \mathbf{I}_n)]\mathbf{e}(t) \\ &\leq q_{\max}\mathbf{e}(t)^T \mathbf{e}(t) - \lambda_1(M)\mathbf{e}(t)^T \mathbf{e}(t) \\ &= -(\lambda_1(M) - q_{\max})\,\mathbf{e}(t)^T \mathbf{e}(t) \end{aligned} \tag{9.40}$$

where we leveraged the fact that $\mathbf{e}(t)^T\ (M \otimes I_n)\,\mathbf{e}(t) \geq \lambda_1(M \otimes I_n) = \lambda_1(M)$ with $\lambda_1(M)$ being positive as $\mathcal{G}$ is undirected and connected. As $\lambda_1(M) > q_{\max}$, then inequality (9.40) implies the thesis. □

Lemma 1 explains that optimizing $\lambda_1(M)$ is crucial to enlarge the set of node dynamics we can control (i.e., we can pick larger $q_{\max}$), and to improve their convergence rate towards $\mathbf{s}(t)$. Clearly, if there are no constraints on the set of pinnable nodes $\mathcal{P}$ and on the

gains p_i, a trivial solution would be to pin all the nodes with the highest possible control gains. However, not all the nodes may be accessible, that is, $\mathcal{P} \subset \mathcal{V}$, and the sum of the control gains, which can be viewed as a proxy of the control effort, must be lower than some upper bound, say $\bar{p}$. Hence, we formulate the following optimization problem for the selection of the control gains:

$$\begin{aligned} \mathbf{p}^* &= \arg\min_{\mathbf{p}} -\lambda_1(M(\mathbf{p})) \\ &\text{s.t.} \\ &\mathbf{1}_p^T \mathbf{p} \leq \bar{p} \\ &\mathbf{p} \geq \mathbf{0}, \end{aligned} \tag{9.41}$$

where $\mathbf{p} \in \mathbb{R}^p$ is the vector with elements $\{p_i\}_{i\in\mathcal{P}}$, and $p = |\mathcal{P}|$.

Notice that $\lambda_1(M)$ depends both on the network topology and the control gains, thus in principle the pinner should have global topological information for solving the optimization problem in (9.41). This assumption is often unrealistic, hence we avoid it and solve problem (9.41) by designing a distributed strategy where the only edge states that can evolve are those associated to the pinner, i.e., the edge states corresponding to the control gains of the pinner. Specifically, our approach optimally tune the control gains, solving problem (9.41) in a completely distributed fashion.

9.2.2 Distributed adaptation of the control gains

Note that the objective function in (9.41) is a convex function of the eigenvalues of M, which in turn are a monotone function of p_i, for all $i \in \mathcal{P}$ [134]. This also implies convexity of the objective function with respect to $\mathbf{p}$. Moreover, the fact that the set of feasible control weights

$$\mathbf{p} \in \left\{\mathbf{p} \geq 0 \wedge \bar{p} - \mathbf{1}^T \mathbf{p} \geq \mathbf{0}\right\}$$

is convex, implies that the optimization problem (9.41) is also convex, and thus its global minimum can be found through the gradient descent algorithm [130]. To implement a distributed version of the algorithm, we first need to evaluate the sensitivity of $\lambda_1(M)$ to variations of the control gains.

9.2.3 Layer 1: Distributed estimation of $\partial\lambda_1(M)/\partial p$

Here, we present a continuous-time version of the power iteration algorithm, which adapts the implementation of [135] to obtain a decentralized estimation of $\partial\lambda_1(M)/\partial\mathbf{p}$.

Let us denote by $\underline{v}_1$ the right eigenvector corresponding to $\lambda_1(M)$, and define $\hat{\mathbf{v}}_1 := \mathbf{v}_1/(\mathbf{v}_1^T\mathbf{v}_1)^{1/2}$. We can then write:

$$\hat{\mathbf{v}}_1^T M \hat{\mathbf{v}}_1 = \lambda_1(M)\hat{\mathbf{v}}_1^T\hat{\mathbf{v}}_1 = \lambda_1(M). \tag{9.42}$$

Now, computing the derivative of the above expression with respect to the the pinner control gain vector $\mathbf{p}$, and omitting for brevity the dependency upon M, we have

$$\frac{\partial\lambda_1(M)}{\partial\mathbf{p}} = \frac{\partial\hat{\mathbf{v}}_1^T}{\partial\mathbf{p}} M\hat{\mathbf{v}}_1 + \hat{\mathbf{v}}_1^T \frac{\partial M}{\partial\mathbf{p}}\hat{\mathbf{v}}_1 + \hat{\mathbf{v}}_1^T M \frac{\partial\hat{\mathbf{v}}_1}{\partial\mathbf{p}}. \tag{9.43}$$

Now,

$$\frac{\partial \hat{\mathbf{v}}_1^T}{\partial \mathbf{p}} M \hat{\mathbf{v}}_1 + \hat{\mathbf{v}}_1^T M \frac{\partial \hat{\mathbf{v}}_1}{\partial \mathbf{p}} = \lambda_1(M) \frac{\partial \left(\hat{\mathbf{v}}_1^T \hat{\mathbf{v}}_1 \right)}{\partial \mathbf{p}} = 0,$$

and from (9.43) we get:

$$\frac{\partial \lambda_1(M)}{\partial \mathbf{p}} = \hat{\mathbf{v}}_1^T \frac{\partial M}{\partial \mathbf{p}} \hat{\mathbf{v}}_1. \tag{9.44}$$

Noting that $\dfrac{\partial M}{\partial p_i} = \text{diag}\{0_{i-1}, 1, 0_{N-i}\}$, we can rewrite (9.44) as

$$\frac{\partial \lambda_1(M)}{\partial p_i} = \hat{\mathbf{v}}_1^T \frac{\partial M}{\partial p_i} \hat{\mathbf{v}}_1 = \hat{v}_{i,1}^2 = \frac{v_{i,1}^2}{\mathbf{v}_i^T \mathbf{v}_i}, \tag{9.45}$$

for $i = 1, \ldots, N$. Therefore, to estimate the sensitivity of $\lambda_1(M)$ to variations of the control gains, we need to perform an estimate of $\mathbf{v}_1$. To this aim, we propose to apply the power iteration algorithm from [135] to matrix $(\mathbf{I}_N - \alpha M)$, for some sufficiently small α. Let $\mathbf{y} = (y^1, \ldots, y^N)^T \in \mathbb{R}^N$ be the estimate of the eigenvector $\mathbf{v}_1$. The classical steps of the power iteration algorithm are

$$\begin{aligned} \dot{\mathbf{y}} &= -\alpha M \mathbf{y}, && \textit{(apply } M\textit{)}, \\ \dot{\mathbf{y}} &= -\left(\mathbf{y}^T \mathbf{y}/N - 1 \right) \mathbf{y}, && \textit{(renormalization)}, \end{aligned} \tag{9.46}$$

where α is a positive scalar. To run (9.46) simultaneously, we combine them in a linear way as

$$\dot{\mathbf{y}} = -k_1 M \mathbf{y} - k_2 \left(\frac{\mathbf{y}^T \mathbf{y}}{N} - 1 \right) \mathbf{y}, \tag{9.47}$$

where k_1 and k_2 are scalar gains. As M is real and symmetric, it is diagonalizable, that is, $M = T^T M_\text{d} T$ with $M_\text{d} = \text{diag}\{\lambda_1, \ldots, \lambda_N\}$ and T being an orthonormal matrix. Therefore, after performing a change of coordinates $\tilde{\mathbf{y}} = (\tilde{\mathbf{y}}^1 \ldots \tilde{\mathbf{y}}^N)^T = T\mathbf{y}$, we can rewrite (9.47) as

$$\dot{\tilde{\mathbf{y}}} = -k_1 M_\text{d} \tilde{\mathbf{y}} - k_2 \left(\frac{\tilde{\mathbf{y}}^T \tilde{\mathbf{y}}}{N} - 1 \right) \tilde{\mathbf{y}}. \tag{9.48}$$

Now, we are ready to give the following theorem that provides the necessary and sufficient condition for the convergence of $\mathbf{y}$ to $\mathbf{v}_1$.

Theorem 9.10. *Given any initial condition $y(t_0)$ such that $\mathbf{v}_1^T \mathbf{y}(t_0) \neq 0$, and positive gains k_1 and k_2, the solution of (9.47) will converge to the eigenvector $\mathbf{v}_1$ corresponding to λ_1 of M with norm $\|\mathbf{v}_1\|_2 = \sqrt{N(k_2 - k_1\lambda_1)/k_2}$ iff*

$$k_2 > k_1 \lambda_1. \tag{9.49}$$

Proof. See the Appendix. □

In view of implementing (9.47) in a decentralized manner, we emphasize that an upper bound for $\lambda_1(M)$ is given by $\bar{p}$, and therefore condition (9.49) can be met without any information on the graph topology by simply setting $k_2 > k_1\bar{p}$. Now, considering that $M = \bar{L} + P$, we expand Equation (9.47) as

$$\dot{\mathbf{y}} = -k_1\bar{L}\mathbf{y} - k_1 P\mathbf{y} - k_2\left(\mathbf{y}^T\mathbf{y}/N - 1\right), \tag{9.50}$$

and then analyze each of the terms of the right-hand side, and observe that

i) The first term can be computed in a decentralized manner from the definition of graph Laplacian.
ii) The second term $-k_1 P\mathbf{y}$ is also decentralized, if we only make the reasonable assumption that each node knows if it belongs to the set $\mathcal{P}$ or not.
iii) The third term requires computing a centralized average of $\mathbf{y}^T\mathbf{y}$. However, this computation can be performed in a decentralized fashion by employing the following PI average consensus estimator [135, 136]

$$\begin{aligned} \dot{z}^i &= \gamma((y^i)^2 - z^i) - k_P \sum_{j\in\mathcal{N}_i}(z^i - z^j) \\ &\quad + k_I \sum_{j\in\mathcal{N}_i}(w^i - w^j), \\ \dot{w}^i &= -k_I \sum_{j\in\mathcal{N}_i}(z^i - z^j), \end{aligned} \tag{9.51}$$

where $\mathcal{N}_i$ is the set of neighbors of node i, z^i is the estimate of $\mathbf{y}^T\mathbf{y}/N$ carried out by node i; $\gamma > 0$ is the rate at which new information replaces old information, while $k_P > 0$ and $k_I > 0$ are the proportional and the integral estimator gains, respectively.

These considerations yield the following decentralized version of Equation (9.47):

$$\dot{y}^i = \begin{cases} -k_1\sum_j l_{ij}y^j - k_2(z^i - 1)y^i & \text{if } i \notin \mathcal{P}, \\ -k_1\sum_j l_{ij}y^j - k_2(z^i - 1)y^i - k_1 p_i y^i & \text{if } i \in \mathcal{P}, \end{cases} \tag{9.52}$$

which, paired with (9.51), allows to perform a decentralized estimate of $\mathbf{v}_1$, where at each time instant each agent i receives a triplet of variables $\{y^j, z^j, w^j\}$ from each of its neighbors $j \in \mathcal{N}_i$.

Notice that, crucially, every agent i is capable of computing an estimate y^i of $v_{i,1}$, and therefore every pinned node can transmit a decentralized estimation of the sensitivity of $\lambda_1(M)$ to p_i back to the pinner. Namely,

$$\widehat{\frac{\partial\lambda_1(M)}{\partial p_i}} = \frac{(y^i)^2}{Nz^i}, \tag{9.53}$$

where we exploit the decentralized estimation z_i of $\mathbf{y}^T\mathbf{y}/N$.

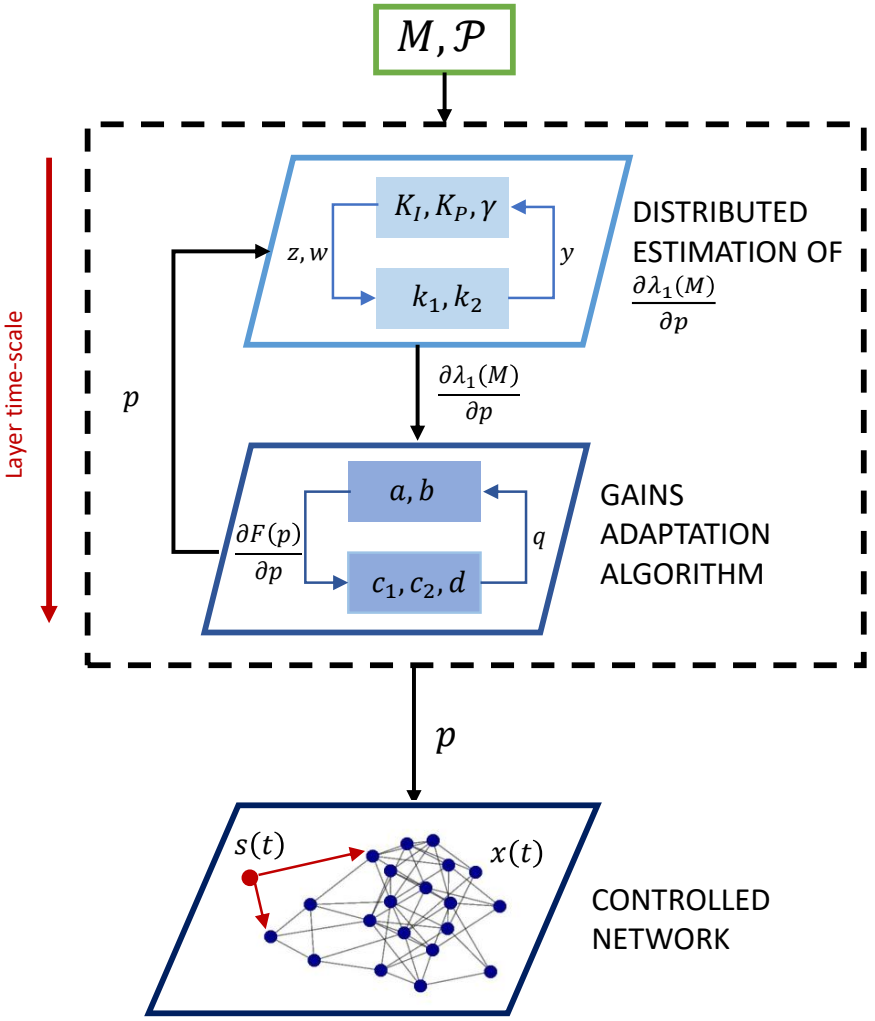

Figure 9.10: **Schematic of the multilayer algorithm described in Subsection 9.2.5.** The two estimation and adaptations layers (enclosed by a dashed rectangle) provide the values of the control gains to be used by the pinner, which steers the trajectories of the nodes in the controlled network (at the bottom) towards the desired solution $\mathbf{s}(t)$.

9.2.4 Layer 2: Decentralized gain adaptation

The second layer exploits the information provided by (9.53), to solve (9.41) through a decentralized implementation of the steepest descent method. First, we incorporate the inequality constraints in the objective function, thus obtaining the modified cost function

$$\mathrm{J}(\mathbf{p}) = -\lambda_1(M) + \Phi_1(\mathbf{p}) + \Phi_2(\mathbf{p}), \tag{9.54}$$

where

$$\Phi_1(\mathbf{p}) = \frac{1}{q(t)} \sum_{i \in \mathcal{P}} \log(p_i), \Phi_2 = \frac{1}{q(t)} \log\left(\bar{p} - \sum_{i \in \mathcal{P}} p_i\right)$$

are the logarithmic barriers, and $q(t)$ is an adaptive parameter determining their severity. The minimum of (9.54) is the stationary point of the following second order differential equation [131]:

$$\ddot{\mathbf{p}} = -a \frac{\partial \mathrm{J}(\mathbf{p})}{\partial \mathbf{p}} - b\dot{\mathbf{p}}, \quad a > 0,\ b > 0. \tag{9.55}$$

In view of our distributed implementation, we derive a decentralized estimation of $\partial \mathrm{J}(\mathbf{p})/\partial \mathbf{p}$ which exploits the estimator (9.53) from Layer 1. Namely,

$$\widehat{\frac{\partial \mathrm{J}(\mathbf{p})}{\partial p_i}} = -\widehat{\frac{\partial \lambda_1(M)}{\partial p_i}} - \frac{1}{q(t)} \left(\frac{1}{p_i} - \frac{1}{\bar{p} - \sum_{i \in \mathcal{P}} p_i} \right). \tag{9.56}$$

Now, we decentralize (9.55) as

$$\ddot{p}_i = a \left(\widehat{\frac{\partial \lambda_1(M)}{\partial p_i}} \right) + \frac{a}{q_i(t)} \left(\frac{1}{p_i} - \frac{1}{\bar{p} - \sum_{i \in \mathcal{P}} p_i} \right) - b\dot{p}_i, \tag{9.57}$$

where the barriers steepness function $q_i(t)$ is adapted as

$$\ddot{q}_i = \frac{c_1}{\left| \widehat{\partial \mathrm{J}/\partial p_i} \right| + d} - c_2 \dot{q}_i, \quad q_i(0) = 1,\ \dot{q}_i(0) = 0, \tag{9.58}$$

see [130] for a detailed discussion on steepness functions.

9.2.5 Overall pinning control scheme

A schematic of the optimal pinning control scheme developed in this work is reported in Figure 9.10. Once the nodes to be pinned have been selected, layer 1 runs equations (9.51)-(9.53) and outputs the sensitivity of $\lambda_1(M)$ to variations of $\mathbf{p}$. This output is transmitted to Layer 2 that adapts the control gains to maximize $\lambda_1(M)$ through the adaptive equations (9.57) and (9.58). The gains $\mathbf{p}$ are then fed to the pinning controller, which drives network (9.39) towards the prescribed solution $\mathbf{s}(t)$. Note that for the multilayer approach to work smoothly, it is necessary to guarantee a sufficient time-scale separation between the processes involved. Specifically, the fastest time-scale should be that of the PI average estimator (9.51): this allows an accurate estimation of the sensitivity

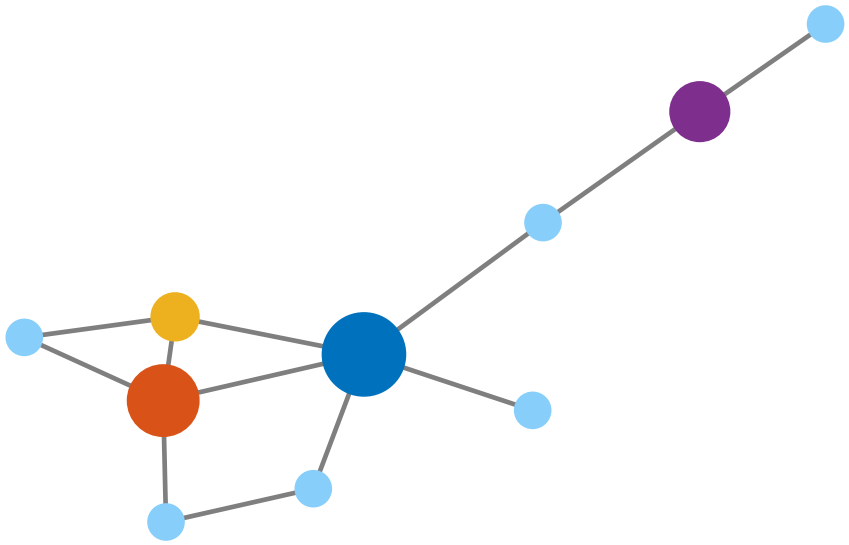

Figure 9.11: **Topology of the controlled network.** The pinned nodes are colored consistently with the plot of $p_i(t)$ in Figure 9.12, with their sizes being proportional to the corresponding p_i^*.

of the cost function to variations of the control gains. Finally, the slowest time-scale should be that of Layer 2, thus providing sufficient time for $\lambda_1(M)$ to converge. Notice that it is always possible to tune the time-scale separation of the processes involved in the two layers, and numerical explorations suggests keeping their time-scales separated by an order of magnitude to be sufficient. Nevertheless, a formal proof is beyond the scope of this thesis.

9.2.6 Numerical example

In this section, we illustrate the effectiveness of the proposed pinning control scheme via a representative example.

Node dynamics

we select Chua's chaotic circuits [115] as nodes of the controlled network. Thus, the vector dynamics in Equation (9.39) can be written in adimensional form as

$$F(\mathbf{x}_i, t) = \begin{bmatrix} \alpha_1 \left(-x_{i1} + x_{i2} - \varphi(x_{i1})\right) \\ x_{i1} - x_{i2} + x_{i3} \\ -\alpha_2 x_{i2} \end{bmatrix}, \quad i = 1, \ldots, N,$$

where $\varphi(x_{i1}) = \beta_1 x_{i1} + 0.5(\beta_2 - \beta_1)\left(|x_{i1} + 1| - |x_{i1} + 1|\right)$. We select $\alpha_1 = 10$, $\alpha_2 = 18$, $\beta_1 = -3/4$, and $\beta_2 = -4/3$ to ensure chaotic behavior of the nodes when decoupled.

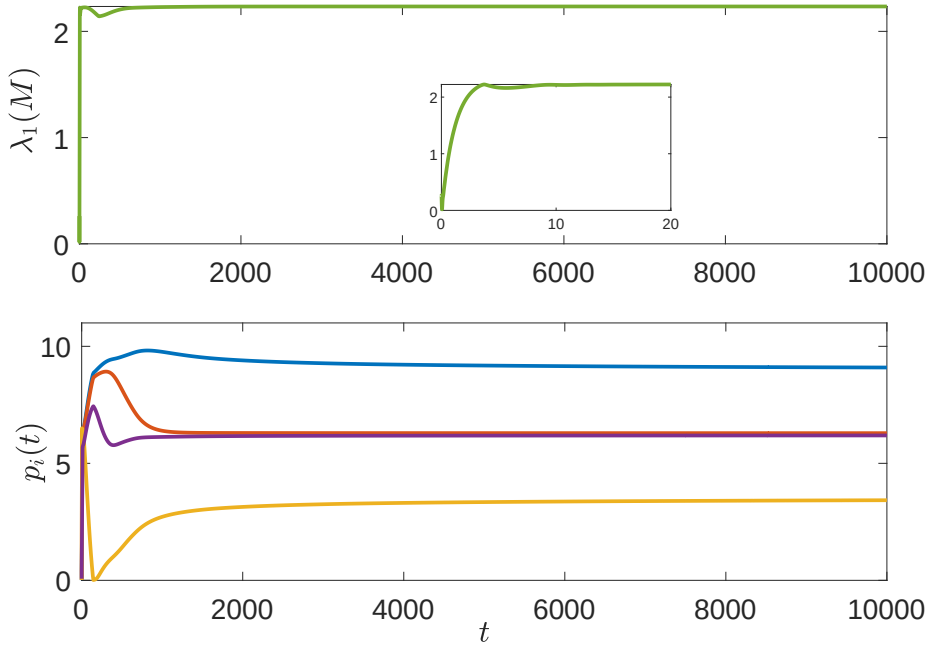

Figure 9.12: Evolution of $\lambda_1(M)$ (top panel) and of the control gains p_i, $i = 1, \ldots, 4$ (bottom panel). The initial conditions are set to $p_i(0) = 10^{-2} \times [1.0\ 1.5\ 2.0\ 7.0]^T$, while $\dot{p}_i(0)$ are uniformly distributed in $[0, 0.7]$ for all $i = 1, \ldots, 4$.

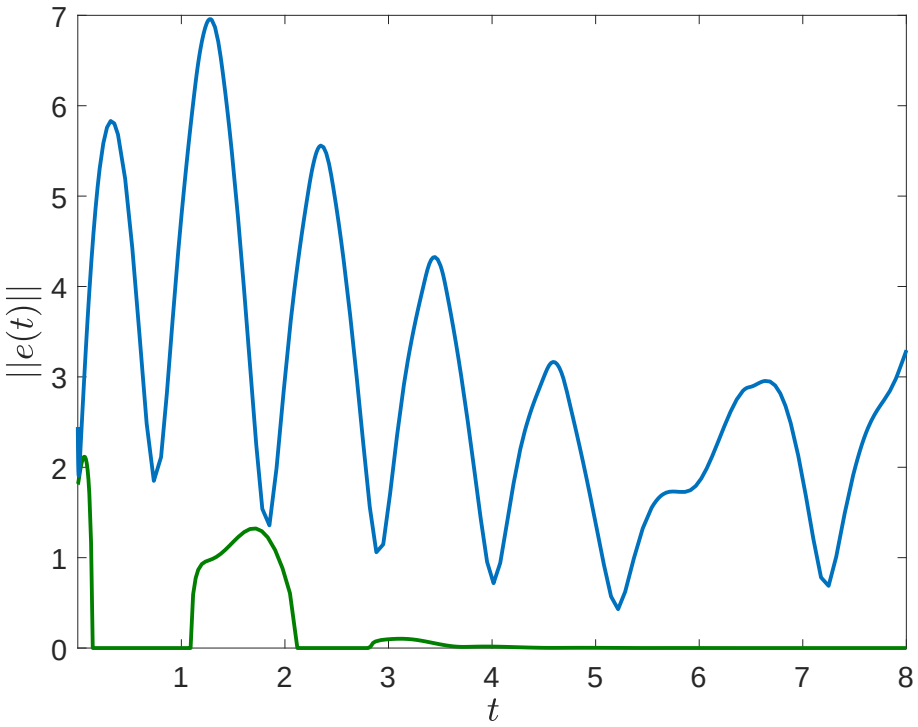

Figure 9.13: **Norm of the network pinning error**. The green line corresponds to the case in which the control gains, starting from initial conditions $\mathbf{p}(0)$, evolve according to the multi-layer approach described in Figure 9.12, while the blue line corresponds to a static pinning control strategy with $\mathbf{p} = \mathbf{p}(0)$.

The initial conditions are uniformly distributed in $[-0.5, 2.5]$. The Chua's circuit fulfills the QUAD assumption [114], therefore an optimal selection of the control gains can be crucial to achieve the pinning control goal.

Network topology

We consider a randomly selected undirected and connected graph of $N = 10$ nodes, whose topology is depicted in Figure 9.11. We set the number m of pinned nodes to 4 and the maximum sum $\bar{p}$ of the control gains to 25. The pinned nodes are randomly selected from a discrete uniform distribution and depicted in Figure 9.11.

Multilayer estimation and gain adaptation

By exploring the parameter space numerically, we tuned the parameters of both layers so as to allow sufficient time-scale separation between the processes. In particular, we set $k_P = 200$ and $k_I = 20$ for the PI estimator (Layer 1, equations (9.51)), $k_1 = 2$ and $k_2 = 40$ for the estimation of the eigenvector v_1 (Layer 1, Equation (9.47)), and $a = 2$, $b = 1$, $c_1 = 1$, $c_2 = 2$, and $d = 0.01$ for the adaptive tuning of the gains (Layer 2, Equations (9.57) and (9.58)). Moreover, we set the initial conditions of the control gains such that, in the absence of any adaptation, the synchronization error would not converge to the origin (i.e., the network would not be pinning controllable).

Results

Figure 9.12 illustrates the effectiveness of the proposed approach, with $\lambda_1(M)$ converging very close to the constrained maximum (compared to a centralized approach, the error is below 1%) thus distributedly solving problem (9.41). We also observe the control gains asymptotically settle to steady-state optimal values. Figure 9.13 illustrates how the adaptation can be beneficial from a control viewpoint. Indeed, while with the initial control gains $\mathbf{p}(0)$ the error exhibits chaotic oscillations (blue line), optimizing the coupling gains all the oscillators converge towards the desired trajectory, with the error asymptotically settling to zero (green line).

10 Appendix

10.1 Wealth dynamics

The proposed artificial financial market is populated by a set of n agents, who can choose among alternative portfolios. The agents behave according to the Von Neumann and Morgenstern utility theory [137]. At each time step $k = 1, 2, ...$, a simulated trading session is performed. Each agent, in a sequential random order, evaluates the convenience of investing a given fraction δ of its current wealth $x_j(k)$ in one of the portfolios from the set $\mathcal{L} = \{1, \ldots, m\}$. The portfolios in $\mathcal{L}$ are characterized by a limited availability $\Upsilon_i, i = 1, ..., m$, where $\Upsilon_m = +\infty$ is associated to a virtual portfolio, corresponding to no-investment. Each agent is allowed to invest in one of the available portfolios, that is, in any element of $\mathcal{L}$ such that $\Upsilon_i \geq \delta x_j(k)$. Agents' access to trading is randomly permuted at each time step k, so that, on average, no agent is favored. After each trading, the availability of the selected portfolio is updated before the next agent is allowed to trade. A power-law utility function characterizes the risk attitude of each agent. At each trading session k, agent j decides to invest a fraction δ of its current wealth $x_j(k)$ in the most profitable portfolio $i \in \mathcal{L}$, selected by comparing the expected utilities

$$E[U_j(x_j(k), i)] = 0.5 \left[(a_i \delta x_j(k))^{\alpha_j(k)} + (b_i \delta x_j(k))^{\alpha_j(k)} \right], \; i = 1, ..., m, \qquad (10.1)$$

where $\alpha_j(k)$ is the risk attitude of the j-th agent, a_i and b_i are the win and loss rates associated to the i-th portfolio, $i = 1, \ldots, m$[1]. Namely, at each trading session agent j, based on its risk attitude $\alpha_j(k)$, selects the investment

$$\ell_j(\alpha_j(k)) = \arg\max_{i \in \mathcal{S}} E[U_j(x_j(k), i)], \qquad (10.2)$$

where $\mathcal{S} \subseteq \mathcal{L}$ is the set of portfolios that the moment of the trade have an availability higher than $\delta x_j(k)$. We emphasize here that an agent may decide not to invest (formally, to invest in the m-th portfolio), if $E[U_j(x_j(k), m)] \geq E[U_j(x_j(k), i)]$ for all the $i \in \mathcal{S} - \{m\}$.

The outcome of the trade is the realization $\beta_j(k)$ of a uniform Bernoulli random variable B. Therefore, the wealth $x_j^-(k)$ of the agent j at time k before the taxation is given by

$$\begin{aligned} x_j^-(k) = x_j(k-1) &+ \beta_j(k) \delta x_j(k-1)(a_{\ell_j(k)} - 1) \\ &- (1 - \beta_j(k)) \delta x_j(k-1)(1 - b_{\ell_j(k)}), \end{aligned}$$

[1]Notice that the win and loss rates associated to the virtual portfolio are $a_m = b_m = 1$.

where we omit the dependence of ℓ_j on $\alpha_j(k)$. At this point, the taxation scheme determines the wealth at iteration k as

$$x_j(k) = \chi(x_j^-(k)). \tag{10.3}$$

In the next sections, we clarify the taxation mechanism of the Tobin-like and flat taxes considered in this work, that is, we specify function χ.

10.2 Tobin-like taxation scheme

The Tobin-like tax employed in this work is a financial transaction tax, which reduces the current wealth of the winning agents by a profit fraction $\rho(k)$ given by

$$\rho(k) = \begin{cases} \frac{p(k)}{\sum_{j=1}^n s_j(k)}, & p(k) > 0, \\ 0, & p(k) \leq 0, \end{cases} \tag{10.4}$$

where $s_j(k) = x_j^-(k) - x_j(k-1)$, and $p(k) = \sum_{j=1}^n (x_j^-(k) - x_{j0})$. Accordingly, (10.3) becomes

$$x_j(k) = x_j^-(k) - H(s_j(k))s_j(k)\rho(k), \tag{10.5}$$

where H is the Heaviside step function. For the sake of brevity, in what follows we refer to this financial transaction tax as Tobin-like Tax (TT).

10.3 Flat taxation scheme

Adopting a flat tax, the amount of the tax is proportional to the total wealth of the individual. Specifically, it is a non-progressive wealth tax (WT), proportional to the current wealth $x_j^-(k)$ of each agent j, with $j = 1, \ldots, n$. Accordingly, (10.3) becomes

$$x_j(k) = \gamma(k)x_j^-(k), \tag{10.6}$$

where

$$\gamma(k) = \frac{\sum_{j=1}^n x_{j0}}{\sum_{j=1}^n x_j^-(k)}.$$

Notice that, to allow for a proper comparison between the two taxation schemes, the time-varying coefficients $\rho(k)$ and $\gamma(k)$ in (10.4) and (10.6), respectively, are selected so as to keep the average wealth constant over time, that is, $\frac{1}{n}\sum_{j=1}^n x_j(k) = \bar{x}$.

10.4 Stability of system (9.47)

Here, we present some results on the stability of system (9.47) that are instrumental for the subsequent proof of Theorem 9.10.

Proposition 10.1. *System* (9.47) *has an equilibrium point* $y = 0$ *which is locally unstable when* $k_2 > k_1\lambda_1$.

Proof. Linearizing the equivalent system (9.48) around a generic equilibrium point $\bar{y}$, we obtain the following Jacobian:

$$J = -k_1 M_{\mathrm{d}} - k_2 \left(\bar{y}^T \bar{y} I + 2\bar{y}\bar{y}^T \right) / N + k_2 I.$$

When $\bar{y} = 0$, the linearized system (9.48) can then be written as

$$\dot{\tilde{y}} = \left(-k_1 M_{\mathrm{d}} + k_2 I\right) \tilde{y}. \tag{10.7}$$

Therefore, setting $\bar{y} = 0$ in (10.7), we obtain that the origin is a locally unstable equilibrium point of (9.47) if $k_2 > k_1\lambda_1$. □

Proposition 10.2. *If* (9.49) *holds, then system* (9.48) *has* N *pairs of nonzero equilibrium points* $\tilde{y}_i$, $i = 1, \ldots, N$, *given by*

$$\tilde{y}_i^j = \begin{cases} 0 & \text{if } 1 \le j \le N,\ j \neq i, \\ \pm\sqrt{N\left(k_2 - k_1\lambda_i\right)/k_2} & \text{if } j = i. \end{cases} \tag{10.8}$$

Moreover, among the N *pairs of equilibria, only* $\tilde{y}_1$ *is locally stable.*

Proof. Setting $\dot{\tilde{y}} = 0$ one gets

$$M_{\mathrm{d}}\tilde{\mathbf{y}} = -\frac{k_2}{k_1}\left(\frac{\tilde{\mathbf{y}}^T\tilde{\mathbf{y}}}{N} - 1\right)\tilde{\mathbf{y}}.$$

As for any unit eigenvector $\hat{\tilde{v}}_i$ of M_{d}, $M_{\mathrm{d}}\hat{\tilde{v}}_i = \lambda_i\hat{\tilde{v}}_i$, and considering that condition (9.49) holds, then $\tilde{y}_i = \pm\sqrt{N(k_2 - k_1\lambda_i)/k_2}\hat{\tilde{v}}_i$. As $\hat{\tilde{v}}_i$ is the i-th versor of $\mathbb{R}^N$, it follows that (10.8) are the set of nonzero equilibria of (9.48). Now, to study the stability of those equilibria, we can look at the eigenvalues of the diagonal Jacobian

$$\mu_i^j = \begin{cases} -2(k_2 - k_1\lambda_i) & \text{if } i = j, \\ k_1(\lambda_i - \lambda_j) & \text{if } i \neq j, \end{cases}$$

that are all negative only for $i = 1$, that is $\tilde{y}_1$ is the only stable equilibrium of (9.48). □

Proposition 10.3. *Given any initial condition* $\mathbf{y}(t_0)$ *and any positive gains* k_1, k_2, *the trajectory of system* (9.47) *is bounded over time as*

$$\|\mathbf{y}(t)\| \leqslant \max\left\{\|\mathbf{y}(t_0)\|, \sqrt{N}\right\}.$$

Proof. Consider the following candidate Lyapunov function

$$V = \mathbf{y}^T\mathbf{y} = \tilde{\mathbf{y}}^T\tilde{\mathbf{y}}.$$

Differentiating, we get

$$\dot{V} = 2\tilde{\mathbf{y}}^T\dot{\tilde{\mathbf{y}}} = 2\tilde{\mathbf{y}}^T\left[-k_1 M_d - k_2\left(\tilde{\mathbf{y}}^T\tilde{\mathbf{y}}/N - 1\right)\mathbf{I}\right]\tilde{\mathbf{y}}.$$

If $\|\tilde{\mathbf{y}}(t_0)\| > \sqrt{N}, \left(\tilde{\mathbf{y}}^T\tilde{\mathbf{y}}/N - 1\right) > 0$ and then $\dot{V} < 0$ until $\|\tilde{\mathbf{y}}(t)\| \leq \sqrt{N}$ (an invariant set for system (9.47)). Moreover, if $\|\tilde{\mathbf{y}}(t_0)\| \leq \sqrt{N}$ then $\|\tilde{\mathbf{y}}(t)\| \leq \sqrt{N}$ and so $\|\mathbf{y}(t)\| \leq \sqrt{N}$ for all $t > t_0$. □

Proof of Theorem 1

As $\mathbf{y} = T^T\tilde{\mathbf{y}}$, showing that condition (9.49) is necessary and sufficient for the convergence of $\mathbf{y}$ to the eigenvector $\mathbf{v}_1$ with norm $\sqrt{N(k_2 - k_1\lambda_1)/k_2}$ is equivalent to showing that it is a necessary and sufficient condition for the convergence of $\tilde{\mathbf{y}}$ to $\tilde{y}_1$, which is what we are going to prove next.

Sufficiency

Consider any two $\tilde{y}^1$ and $\tilde{y}^2$. Then, we can write

$$\frac{d}{dt}\left(\ln\frac{\tilde{y}^1}{\tilde{y}^2}\right) = \frac{\dot{\tilde{y}}^2\tilde{y}^1 - \dot{\tilde{y}}^1\tilde{y}^2}{\tilde{y}^2\tilde{y}^1} = -k_1\lambda_2 - k_2\left(\frac{\tilde{y}^T\tilde{y}}{N} - 1\right)$$
$$+ k_1\lambda_1 + k_2\left(\tilde{y}^T\tilde{y}/N - 1\right) = k_1(\lambda_2 - \lambda_1) > 0$$

that implies that $\tilde{y}^1/\tilde{y}^2 \to \infty$ and as $\tilde{y}^1$ is bounded, see Proposition 10.3, $\tilde{y}^2 \to 0$. This holds for all $i > 1$, that is $\tilde{y}^1/\tilde{y}^i \to \infty$ and $\tilde{y}^i \to 0$. Therefore, $\tilde{\mathbf{y}}^T\tilde{\mathbf{y}} \to \left(\tilde{y}^1\right)^2$ and as (9.49) holds, the expression of $\tilde{y}^1$ over time can be reduced to

$$\dot{\tilde{y}}^1 = \frac{k_2}{N}\left(\sqrt{N\left(k_2 - k_1\lambda_1\right)/k_2} + \tilde{y}^1\right)\left(\sqrt{N\left(k_2 - k_1\lambda_1\right)/k_2} - \tilde{y}^1\right)\tilde{y}^1.$$

As $\tilde{\mathbf{y}}(t_0) \neq 0$ and being the origin unstable, see Proposition 10.1, then $\tilde{y}^1 \to \pm\sqrt{N\left(k_2 - k_1\lambda_1\right)/k_2}$.

Necessity

If $\tilde{y}^1 \to \pm\sqrt{N\left(k_2 - k_1\lambda_1\right)/k_2}$, then condition (9.49) automatically holds. ■

Part III

Further challenges for network control: considering symmetries and antagonistic interactions

11 Background

In Part III we will conclude our trip into the complexity of the networks structure. In Parts I and II we saw that the advantages gained from a modeling and control perspective are worth the effort of conisidering the mathematical paradigm of evolving networks. Specifically, in Part I we shed out that the range of situations in which a stochastic temporal network can be efficiently controlled is limited and in Part II we pointed out how the flexibility of coevolving networks turns to be useful in modeling intricate real phenomena in performing a more efficient network control. In both cases, the key ingredient to overcome the obstacle of facing with a higher complexity is to devise optimization problems able to exploit the features of the network to our advantage.

Along the same lines of argument, in Part III, we will show how an *ad hoc* design of the control action allows us at the same time to overtake and to exploit two kinds of networks that seem to hinder our ability to achieve a desired collective behavior: networks with symmetries or signed interconnections. In the first case, provided that the presence of symmetries in the network causes loss of controllability, we show how to deal with a control goal known as *group consensus* (a collective behavior where clusters of nodes sharing the same value of their state variables arise) [33]. In the second case, that is, when the graph of the network is signed, we define the *partial containment control* and propose an algorithm to solve it, that is, steering the states of a subset of the network nodes in the convex hull defined by the states of what we will define as the leaders of the network [34].

11.1 Networks with symmetries

It can be observed in nature and in several real-world applications that networks have a certain degree of symmetry in their structures (see Table 11.1). The concept of symmetry is perhaps one we all have in mind, having learned it in daycare (See Figure 11.1). Mathematically speaking, the symmetry properties of a network are defined in terms of the existence of certain automorphisms of the nodes set $\mathcal{V}$ of the graph $\mathcal{G} = \{\mathcal{V}, \mathcal{E}\}$. Indeed, an *automorphism* is a permutation of the nodes that leaves the networks unchanged (that is, maps edges to edges and nonedges to nonedges [139]). The set of all authomorphisms forms a permutation group $\mathrm{aut}(\mathcal{G})$ generated by all the network symmetries. Indeed, the set of all the permutations in the automorphism group will only permute certain subsets of nodes among each other. Consistently with the existing literature [140–142], we will

Network	N	$\lvert\mathrm{aut}(\mathcal{G})\rvert$
Biological Networks		
Caenorhabditis elegans Genetic (Cele)	2060	6.9985×10^{161}
Yeast Protein Interactions (Yeast)	1458	1.2607×10^{254}
BioGRID Human(BGHum)	7019	1.207×10^{485}
Technological Networks		
Internet (AS Level) (IntAS)	22332	1.2822×10^{11298}
US Power Grid (USPow)	4941	5.1851×10^{152}
www.EPA.gov subnet(EPA)	4253	$1.277772 \times 10^{2321}$
Social Networks		
Media ownership (Media)	4475	3.3638×10^{4818}
PhD network (PhD)	1025	2.9810×10^{292}
Erdös Collaboration (Erdös)	6927	3.4610×10^{42222}

Table 11.1: Table extracted by Table 1 of [30] where in the third column the order of magnitudes of the size of automorphism groups, $\lvert\mathrm{aut}(\mathcal{G})\rvert$, of some real networks are given. Note that the symmetries of most of the listed networks are order of magnitudes higher than the estimated number of atoms in the visible universe, that is, $\sim [10^{72}, 10^{87}]$ [138].

denote these subsets as *orbits* or *clusters* (more details will be given in Chapter 12). The abundance of symmetries in real world networked systems (see Table 11.1) spurred the scientific communities to investigate (as usual) if the structure of such networks could be exploited to our advantage. Paradigmatic is the example of the *cluster synchronization* in which all the nodes belonging to the same orbit synchronize to the same trajectory essentially by employing the symmetry structure of the network [140, 141, 143]. However, coping with networks with symmetries can also prevent from their control. Backpedaling to Chapter 1, one issue is represented by the inability of controlling a network with a limited set of drivers to a desired behavior. Indeed, in [31, 32, 144] it is pointed out that symmetries cause loss of controllability and sufficient conditions for uncontrollability are provided. A recent work [142] showed that although the presence of symmetries in linear networks hampers controllability, it has the power to favor the emergence of group consensus, i.e.,

Definition 11.1 (Group consensus). *The nodes in a cluster C_k achieve group consensus if $\lim_{t\to+\infty} \|x_i(t) - x_j(t)\| = 0$ for all i and j in C_k. Moreover, group consensus is possible for either stable, marginally stable, or unstable node dynamics, as long as the trajectories converge to each other.*

Therefore, it does naturally arise the question: is it possible to control the group consensus of such networks? This is the research question we answered in [33] and that we report in Chapter 12. A byproduct of our study regards another chance offered by the presence of symmetries in networks. Indeed, given a graph with symmetries, the clusters C_k of

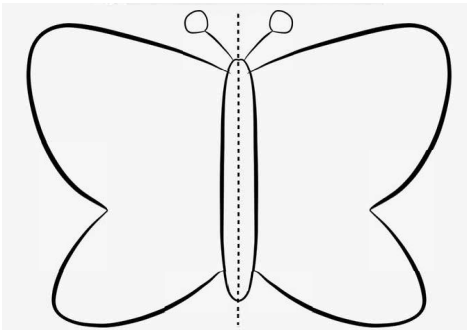

(a)

(b)

Figure 11.1: Daycare exercise to train the concept of symmetry in 11.1a and a nice natural example of symmetry in the star fish in 11.1b

symmetric nodes such that $\cup_{k=1}^{K} C_k = \mathcal{V}$ and $\cap_{k=1}^{K} C_k = \emptyset$ define a partition, Π, of $\mathcal{V}$. The graph whose nodes are the K cells of Π is called the quotient graph, $\mathcal{Q}$, of $\mathcal{G}$. As, generally, the dimension of $\mathcal{Q}$ is smaller than that of $\mathcal{G}$, we can take advantage from such dimensionality reduction also from a control prospective, by designing the required control input on the quotient network rather than on the original network as we will see in Section 12.4.

11.2 Networks over signed graphs

One of the traditional assumptions on the networks topology relies with the nonnegativity of the edges weights and reflects the fact that the interactions among the nodes of the network are cooperative. However, especially in human interaction networks, such as social networks, antagonism is commonly observed. A tool to model such interactions is offered by the so-called *signed graphs*, introduced in the Fifties by Harary to model disliking, indifference and liking sentiments described by psychologist in social interactions. As we pointed out since the beginning of this work, the problem of steering the nodes of a dynamical network towards a collective behavior, in some way, the general goal of the control of complex networks theory. Departing from the pioneering work of DeGroot in the Seventies [145], substantial research effort has been devoted to unravel the mechanisms leading to the emergence of consensus in networks of simple integrators. The problem has been deeply studied both in continuous and discrete time [146], on undirected or directed graphs, and in presence of delays [11]. Consensus has been also investigated in a leader-following setting, in which one node, the leader, drives a network of linear systems towards a desired value [147]. The cross assumption of all the above works is the collaborative interactions among the nodes of the networks. In [148], Altafini firstly investigated if it would still be possible to achieve a form of agreement even in the presence of antagonistic interactions. He proposed the so-called *bipartite consensus* as a consensus protocol for networks whose graph is signed, that is, the adjacency matrix

can have negative weights (the formal definition will be given in Chapter 13). He gave conditions on the structural properties of the signed network under which: i) all the nodes polarize (asympthotically converge to zero), and ii) the network nodes partition into two sets, one converging to $\bar{x}$, and the other one to $-\bar{x}$. However, achieving consensus is not the only possible control goal in multi-agent systems. Indeed, in applications of networks of autonomous agents, the goal is often to *contain* the agent into a region, for instance to impede that a group of robot or autonomous vehicle enter into hazardous areas [149], to comprise the opinions of voter into a certain range [6], or to avoid the spreading of an epidemic. Motivated by these kinds of phenomena, Ji and coworkers introduced the so-called containment control problem, where multiple leaders have to drive a group of mobile agents within a desired convex polytope [150]. Later works have further analyzed the problem to account for the presence of directed interactions [151], possible switches in the network topology [2, 152], uncertainty [153], and higher-order dynamics [154, 155]. Recently, a first definition of containment control over signed graphs was given in [156]. Specifically, the author says that a network is contained when the states of its nodes converge towards the convex hull spanned by the leaders and by their symmetric trajectories. Assuming continuous-time dynamics, conditions guaranteeing the achievement of full network containment were achieved. Similar results were obtained in [157] for the case of generic linear heterogeneous node dynamics. Similarly to the case of networks with symmetries, provided that a large directed signed networks present structural constraints and that it is unfeasible, or too expensive to inject control signal whenever in the networks. This motivates us to formulate the *partial containment control problem* over signed graphs, that is, a protocol aiming to contained a portion of the network within the convex hull defined by the leaders' state. Moreover, we present an algorithm aiming to maximize the number of nodes asymptotically contained with a limited number of control inputs.

12 Controlling group consensus in networks with symmetries

In this Chapter, we deal with linear networks endowing symmetries. We will show that

1) there exists a group consensus subspace of the state space, that is, the set of all the nodes' states such that the nodes in the same cluster asympthotically converge to the same value, according to Definition 11.1;
2) the group consensus subspace encompasses the controllable subspace.

As we are interested in studying the group consensus manifold we will refer to two partitions of the nodes that are A-invariant[1], *orbital* and *equitable* partitions. Roughly speaking, an orbital partition subdivides the nodes set $\mathcal{V}$ in clusters according to the permutations in the set of all permutations in $\mathrm{aut}(\mathcal{G}(A))$, while the *equitable* partition is more related to dynamics as it groups the nodes in a cluster if their dynamics are affected equally by the nodes outside from other clusters) (more details and formal definitions will be given later). Therefore, we prove points 1) and 2) for both partitions (in Section 12.2 for the orbital partitions and in Section 12.3 for the equitable partitions) and as it can be proved that all the equitable partitions are orbital but not vice-versa, we will present a way to control group consensus in the case of equitable partitions (in Section 12.4).

12.1 Mathematical Preliminaries

Before going into the details of the problem, we list some definitions and preliminaries that will turn useful.

We denote by $\mathcal{G}(\mathcal{V}, \mathcal{E})$ an undirected graph with $\mathcal{V}$, the set of N nodes, and $\mathcal{E} \subseteq \mathcal{V} \times \mathcal{V}$ the set of edges defining the interconnections among the nodes. The symmetric binary matrix $A \in \mathbb{R}^{N \times N}$ is the adjacency matrix of the graph, that is, a matrix whose elements are $A_{ij} = A_{ji} \neq 0$ if $(i, j) \in \mathcal{E}$ and $A_{ij} = A_{ji} = 0$ otherwise. The symmetry properties of $\mathcal{G}$ are defined by the existence of the *authomorphism* as defined in what follows.

[1]Note that as we refer to linear networks A A describes both the network topology, being an adjacency matrix, and the netework dynamics.

Definition 12.1 (Automorphism). *A permutation $\pi(\mathcal{V}) = \widetilde{\mathcal{V}}$ of the nodes set $\mathcal{V}$ is an automorphism of $\mathcal{G}$ if*

1. $\mathcal{V} = \widetilde{\mathcal{V}}$;
2. *if* $(i, j) \in \mathcal{E}$, *then* $(\pi(i), \pi(j)) \in \mathcal{E}$.

The set of all the automorphisms of a graph with adjacency matrix A, with the operation of composition, is the automorphism group which we will denote by $\mathrm{aut}(\mathcal{G}(A))$. Any permutation in $\mathrm{aut}(\mathcal{G}(A))$ is encoded in a permutation matrix P that commutes with A, i.e., such that $PA = AP$. The set of all automorphisms in the group will only permute certain subsets of nodes (the *orbits* or *clusters*) among each other. For any two nodes in the same orbit there exists a permutation that maps them into each other. Therefore,

Definition 12.2 (Orbital partition). *All the permutations in* $\mathrm{aut}(\mathcal{G})$ *define orbital partitions, Π_{or}, of $\mathcal{V}$, into s subsets, the* orbits *or* clusters, $\{C_1, C_2, ...C_s\}$, *such that* $\cup_{i=1}^{s} C_i = \mathcal{V}$, $C_i \cap C_j = \emptyset$ *for* $i \neq j$.

Orbital partitions fall in the general class of the equitable partitions, that is

Definition 12.3 (Equitable partition). *A partition, Π^{eq}, of the nodes set, $\mathcal{V}$, in K clusters $C_1, C_2, \ldots, C_K$ is* equitable *if for all i*

$$\sum_{p \in C_j} A_{lp} = d_{ip} \ \forall l \in C_i. \tag{12.1}$$

An orbital and an equitable partition Π are said *coarsest* if it partitions the nodes through the minimum number of clusters.

Definition 12.4 (Indicator matrix). *To each partition of s clusters, Π, it can be associated a $N \times s$ indicator matrix E^{Π}, such that $E^{\Pi}_{ij} = 1$ if node i belongs to C_j and $E^{\Pi}_{ij} = 0$ otherwise. We will denote by $E^{\Pi_{or}}$ and $E^{\Pi_{eq}}$ the indicator matrix corresponding to the orbital and equitable partition, respectively.*

12.2 Controllability Properties of Networks with orbital partitions

We consider a linear dynamical network described by

$$\dot{\mathbf{x}} = A\mathbf{x} + B\mathbf{u}. \tag{12.2}$$

where $\mathbf{x} \in \mathbb{R}^N$ defines the state space $\mathcal{X}$ and is the vector stacking the states of the N network nodes and $\mathbf{u}$ is the vector stacking the M input signals injected in the network. Consistently, the $N \times N$ symmetric matrix A defines the network topology, while the

$N \times M$ matrix B describes the way in which the M input signals affect the network dynamics. Namely, if the j-th input is injected in the i-th node then $B_{ij} = 1$, while $B_{ij} = 0$ otherwise.

We will show how the presence of symmetries in network (12.2) affects its controllability.

Lemma 12.5. *The subset of automorphisms of $\mathcal{G}(A)$ associated to the set of matrices $\mathcal{P} := \{P_i : P_iA = AP_i \text{ and } P_iB = B\}$ forms a subgroup of* $\text{aut}(\mathcal{G}(A))$.

Proof. For the set $\mathcal{P}$ to be a subgroup, the following four properties must be true:

(i) $P_i(P_jP_k) = (P_iP_j)P_k \ \forall \ (P_i, P_j, P_k) \in \mathcal{P}$;
(ii) $P_i \in \mathcal{P}$ is non singular $\forall \ i$;
(iii) $I \in \mathcal{P}$;
(iv) given any two matrices $P_i \in \mathcal{P}$ and $P_j \in \mathcal{P}$, then $P_iP_j \in \mathcal{P}$.

Proving that the matrices in $\mathcal{P}$ satisfy property (i) and (ii) is trivial as (i) is true for any three square matrices with the same dimensions $(P_i, P_j, P_k) \in \mathcal{P}$ regardless of whether these are, or are not, in $\mathcal{P}$, while (ii) is true as permutation matrices are not singular. Moreover, (iii) holds as $IA = AI = A$, and $IB = B$. Moreover, property (iv) is proved as

$$(P_iP_j)A = P_i(P_jA) = P_i(AP_j) = AP_iP_j = A(P_iP_j)$$

which proves that $P_iP_jA = AP_jP_i$ for all $(P_i, P_j) \in \mathcal{P}$. Then, finally, the proof is completed by noting that, as from our hypotheses $P_jB = P_iB = B$ for all $(P_i, P_j) \in \mathcal{P}$, it follows that $P_iP_jB = P_iB = B$. □

We will denote as $\text{aut}(\mathcal{G}(A, B))$ the group represented by the permutation matrices P such that $PA - AP = 0$ and $PB - B = 0$. Similarly to $\text{aut}(\mathcal{G}(A))$, $\text{aut}(\mathcal{G}(A, B))$ partitions the set of network nodes into orbits or clusters, where an orbit is a subset of symmetric nodes. Hence, we can define the coarsest orbital partition Π_{or} into clusters corresponding to the orbits of the automorphism group $\text{aut}(\mathcal{G}(A, B))$, $C_1, C_2, \ldots, C_K$, such that $\cup_{i=1}^{K} C_i = \mathcal{V}$, and $C_i \cap C_j = 0$ for $i \neq j$. We will rely on the indicator matrix $E^{\Pi_{or}}$ to keep track of the orbit to which each node belongs.

Lemma 12.6. *Each orbit of the coarsest partition Π_{or} induced by $aut(\mathcal{G}(A, B))$ is a subset of an orbit of the coarsest partition induced by $aut(\mathcal{G}(A))$.*

Proof. The thesis follows from the observation that if two (or more) nodes are permuted by a permutation matrix P in $aut(\mathcal{G}(A, B))$ and thus belong to the same orbit, then they also belong to the same orbit of the coarsest orbital partition induced by $aut(\mathcal{G}(A))$, as the same matrix P also belongs to $aut(\mathcal{G}(A))$. □

Theorem 12.7. *If there exists a permutation matrix $P \neq I$ such that $PA - AP = 0$ and $PB - B = 0$, then*

(i) the set of states $\mathcal{X}_{or} := \{x : x_i = x_l \ \forall \, i, l \in C_j, \ \forall j\} \subset \mathcal{X}$, is an invariant

subspace of the matrix A, i.e., $\forall x \in \mathcal{X}_{or}$, $Ax \in \mathcal{X}_{or}$;
(ii) if $x_i = x_l$ *then* $\dot{x}_i = \dot{x}_l$ *for all* $(i,l) \in C_j$ *and for all* j.

Proof. Let us start by showing that if there exists a permutation matrix P such that $PA = AP$ and $PB = B$, then the network state x and the permuted state vector $\mathbf{y} := P\mathbf{x}$ share the same dynamics. Indeed, by left multiplying both sides of Equation (12.2) by P we get

$$P\dot{\mathbf{x}} = PA\mathbf{x} + PB\mathbf{u}.$$

Then, as $PA = AP$ and $PB = B$, we get

$$\dot{\mathbf{y}} = A\mathbf{y} + B\mathbf{u}.$$

Now, as there always exists a permutation matrix $P \in \mathrm{aut}(\mathcal{G}(A,B))$ that maps into each other any two nodes belonging to the same clusters [142], this proves statement (ii), i.e., that nodes in the same clusters share the same dynamics, and thus that if $x_i = x_j$ for all i and j in the same cluster, then also $\dot{x}_i = \dot{x}_j$. Moreover, this also means that the subspace made of all the points of the state-space such that $x_i = x_l$ for all (i,l) in the same cluster and for each of the K clusters is A-invariant (statement (i)). □

Theorem 12.7 establishes the existence of the group consensus subspace $\mathcal{X}_{or}$ for network (12.2). Hence, to tackle consensus control problems, it is useful to perform a transformation that allows us to separate the dynamics along the subspace $\mathcal{X}_{or}$ from that orthogonal to the subspace $\mathcal{X}_{or}$ itself. This task is accomplished by the so called Irreducible Representation (IRR) of the symmetry group through a transformation in a new coordinate system [140]. This is a state transformation $\mathbf{z}_{\mathrm{or}} = T_{\mathrm{or}}\mathbf{x}$ where the transformation matrix

$$T_{\mathrm{or}} = \begin{bmatrix} T^{\parallel} \\ T^{\perp} \end{bmatrix} \in \mathbb{R}^{N\times N}$$

is orthogonal, and the elements of the block $T^{\parallel} \in \mathbb{R}^{K\times N}$ are such that

$$T^{\parallel}_{ij} = \sqrt{|C_i|}^{-1} \tag{12.3}$$

if node j is in cluster i and 0 otherwise. The K rows of the matrix $T^{\parallel}$ are thus a basis of the group consensus subspace $\mathcal{X}_{\mathrm{or}}$. The rows of the matrix $T^{\perp} \in \mathbb{R}^{(N-K)\times N}$, which complete the transformation, are thus a basis of the orthogonal complement to the group consensus subspace. Consistently, we have that the dynamic matrix $\tilde{A} = T_{\mathrm{or}} A T_{\mathrm{or}}^{-1}$ has the following structure:

$$\tilde{A} = T_{\mathrm{or}} A T_{\mathrm{or}}^{T} = \begin{bmatrix} A_{\parallel} & 0 \\ 0 & A_{\perp} \end{bmatrix}. \tag{12.4}$$

From Equation (12.4), we see that the IRR decouples motion along the consensus subspace from that orthogonal to the group consensus subspace. In this new coordinate system, the dynamics of network (12.2) can be rewritten as

$$\dot{\mathbf{z}}_{\mathrm{or}} = \tilde{A}\mathbf{z}_{\mathrm{or}} + \tilde{B}\mathbf{u}, \tag{12.5}$$

and

$$\tilde{B} = T_{\text{or}} B = \begin{bmatrix} B_{\parallel} \\ B_{\perp} \end{bmatrix}.$$

Indeed, the pair $(A_{\parallel}, B_{\parallel})$, which we will denote as the *quotient pair*, determines the controllability properties of the dynamics along the subspace $\mathcal{X}_{\text{or}}$ and thus our ability to control the consensus state, while the pair $(A_{\perp}, B_{\perp})$ determines our ability to stabilize such solution. We are interested in studying the controllability properties of the two pairs $(A_{\parallel}, B_{\parallel})$ and $(A_{\perp}, B_{\perp})$. Before doing so, we will present a few more details on this representation. First of all, let us point out that the block $T_{\parallel}$ of the matrix T is such that $T_{\parallel} = E_{\text{or}}^{\dagger}$, where $E_{\text{or}} \in \mathbb{R}^{N \times K}$ is the indicator matrix corresponding to the coarsest partition Π_{or}. Consistently, the state of the quotient network, the network associated to pair $(A_{\parallel}, B_{\parallel})$, can be computed as

$$\mathbf{z}_{\text{or}}^{\parallel} = E_{\text{or}}^{\dagger} \mathbf{x} \in \mathbb{R}^{K}$$

and thus, we have that $A_{\parallel} = E_{\text{or}}^{\dagger} A E_{\text{or}}$ and $B_{\parallel} = E_{\text{or}}^{\dagger} B$.

Remark 12.8. *Note that the quotient network associated to the coarsest orbital partition does not encompass symmetries, i.e., the only permutation matrix P such that $PA_{\parallel} - A_{\parallel}P = 0$ and $PB_{\parallel} - B_{\parallel} = 0$ is the identity matrix.*

Now, we are ready to give the following theorem.

Theorem 12.9. *If there exists a matrix $P \neq I$ such that $PA = AP$ and $PB = B$, then $\mathcal{X}_{\text{or}}$, the invariant subspace of the matrix A associated to the cluster consensus solution, encompasses the controllable subspace.*

Proof. To prove the statement we must show that if $PB = B$, this subspace encompasses the range of B. Indeed, if $PB = B$, as left-multiplying a vector by the matrix P only permutes the elements associated to nodes of the same cluster, B is such that $b_{il} = b_{jl}$ for all l and for all i, j in the same cluster. Hence, all the columns of B and thus its range, are encompassed in the A-invariant subspace defined by the clusters (see Theorem 12.7). As the controllable subspace is defined as the smallest A-invariant subspace encompassing the range of B, the thesis follows. □

Corollary 12.10. $B_{\perp} = \mathbf{0}_{(N-K)\times M}$.

Proof. The statement is a direct consequence of the statement of Theorem 12.9 and of the definition of $B_{\perp}$. □

12.3 Controllability properties of networks with equitable partitions

In this section we extend the results of section 12.2 to the case in which the network clusters correspond to an equitable partition (see Definition 12.3). Let us now extend the definition of equitable partition to the graph induced by the pair (A, B).

Definition 12.11. *A partition $\tilde{\Pi}_{eq}$ of the node set $\mathcal{V}(\mathcal{G}(A,B))$ of the graph $\mathcal{G}(A,B)$ induced by the pair (A,B) is* equitable *if and only if for all (i,j)*

1) $\sum_{k\in C_j} A_{lk} = d_{ij}\ \forall l \in C_i$;
2) $B_{lp} = d_{ip}\ \forall\, l \in C_i$ *and* $\forall\ p = 1,\dots,M$.

We denote by $\tilde{E}$ the indicator matrix corresponding to $\tilde{\Pi}_{eq}$.

Note that all the orbital partitions of a graph $\mathcal{G}(A,B)$ are equitable but the converse is not true [141, 142]. An example of an equitable partition that is not orbital is shown in Fig as the equitable partition has two clusters C_1 and C_2, with its nodes colored in light blue and green respectively, while the coarsest orbital partition defines three clusters $\{1,2,3,4\}$, $\{5,6,7,8\}$ and $\{9,10\}$. Also, all the clusters of the orbital partition Π_{or} are subsets of the clusters of the equitable partition Π_{eq}. Now, we are ready to give the following theorem.

Theorem 12.12. *Let $\mathcal{G}(A,B)$ be the graph induced by the pair (A,B) and $\tilde{\Pi}_{eq}$ be an equitable partition of the nodes of $\mathcal{G}(A,B)$ with indicator matrix $\tilde{E}$. Then,*

a) $\tilde{\Pi}_{eq}$ is equitable if and only if the column space of $\tilde{E}$ is $A-$invariant;
b) the column space of $\tilde{E}$ encompasses the controllable subspace.

Proof. In proving a) we start from the definition of $A-$invariance, that is, the column space of $\tilde{E}$ is $A-$invariant if and only if there exists a matrix Q such that $A\tilde{E} = \tilde{E}Q$ [158]. Then, we show that if $\tilde{\Pi}_{eq}$ is equitable, then $Q = (\tilde{E}^T\tilde{E})^{-1}E^TAE$. To do so, we need to prove that

$$A\tilde{E} = \tilde{E}(\tilde{E}^T\tilde{E})^{-1}E^TAE$$

which can be easily done by left multiplying both terms of this expression by $\tilde{E}^T$, yielding

$$\tilde{E}^TA\tilde{E} = \tilde{E}^T\tilde{E}(\tilde{E}^T\tilde{E})^{-1}\tilde{E}^TA\tilde{E}$$

which implies that $\tilde{E}^TA\tilde{E} = \tilde{E}^TA\tilde{E}$ thus proving statement a). To prove b) note that, as $B_{lp} = d_{ip}\ \forall\, l \in C_i$ and $\forall\ p = 1,\dots,M$ the range of B is encompassed in the $A-$invariant subspace generated by the columns of $\tilde{E}$ and as the controllable subspace is defined as the smallest $A-$invariant subspace encompassing the range of B, b) is proved. □

Definition 12.13. *The coarsest equitable partition φ_{eq} of the graph $\mathcal{G}(A, B)$ is the equitable partition of the graph $\mathcal{G}(A, B)$ with the minimum number K of clusters. We denote by E_φ the corresponding indicator matrix.*

Let us write the transformation matrix as done in Section 12.2:

$$T_{\text{eq}} = \begin{bmatrix} E_\varphi^\dagger \\ T_\perp \end{bmatrix} \tag{12.6}$$

with the rows of $E_\varphi^\dagger = span\left\{E_\varphi^{(1)}, E_\varphi^{(2)}, \ldots, E_\varphi^{(K)}\right\}$ where $E_\varphi^{(i)}$ is the $i-$th column of E_φ, and $T_\perp$ is an $(N-K)\times N$ matrix whose rows span the orthogonal complement to the column space of E. Then, we can give the following two Corollaries to Theorem 12.12:

Corollary 12.14. *Let $\mathcal{G}(A, B)$ be a graph, and φ_{eq} be its coarsest equitable partition. Let T_{eq} be the $N \times N$ matrix of Equation (12.6). Then, through the change of variable $\mathbf{z}_{\text{eq}} = T_{\text{eq}}\mathbf{x} \in \mathbb{R}^N$ the transformed network dynamics is*

$$\dot{\mathbf{z}}_{\text{eq}} = \hat{A}\mathbf{z}_{\text{eq}} + \hat{B}\mathbf{u}$$

where the matrices

$$\hat{A} = \begin{bmatrix} A_\parallel & 0 \\ 0 & A_\perp \end{bmatrix}, \; \hat{B} = \begin{bmatrix} B_\parallel \\ 0 \end{bmatrix}, \tag{12.7}$$

with the dimensions of each block being defined by that of the matrix $A_\parallel := E_\varphi^\dagger A E_\varphi \in \mathbb{R}^{K\times K}$. Moreover, if the pair $(A_\parallel, B_\parallel)$ is controllable, then the transformation T_{eq} is a controllability transformation.

Proof. Note that, as by definition of the matrix T_{eq} in Equation (12.6), $A_\parallel$ is the quotient network, and thus the first K state variables capture the dynamics along the column space of E_φ. Hence, from Theorem 12.12 a), which states that the column space of E_φ is A-invariant, we can prove the existence of the 0 block in $\hat{A}$. Moreover statement b) of Theorem 12.12 implies the existence of the 0 block in $\hat{B}$, as the dynamics orthogonal to the column space of E_φ are uncontrollable. □

12.4 Controlling group consensus

In Sections 12.2 and 12.3, we have established some controllability limitations of networks with symmetries and equitable partitions. Here, we show how to operate within these limitations so to control group consensus.

Corollary 12.15. *Consider a graph $\mathcal{G}(A, B)$ with coarsest equitable partition φ_{eq}. If the pair $(A_\parallel, B_\parallel)$ is controllable, then for any cost function $J(\mathbf{u}(t))$ the optimal*

control problem

$$\min_{\mathbf{u}} \int_0^{t_f} J(\mathbf{u}(t))\mathrm{d}t \tag{12.8a}$$

$$s.t.$$

$$\dot{\mathbf{x}} = A\mathbf{x} + B\mathbf{u} \tag{12.8b}$$

$$\mathbf{x}(0) = \mathbf{0} \tag{12.8c}$$

$$\mathbf{x}(t_f) = \mathbf{x}_f \tag{12.8d}$$

admits solution $\mathbf{u}(t)^* := argmin \int_0^{t_f} J(\mathbf{u}(t))\mathrm{d}t$ *if and only if* $x_{f,i} = z^{\parallel}_{f,l}$ *for all* $i \in C_l$ *and for all* l*. Moreover, if* $x_{f,i} = z^{\parallel}_{f,l}$*, then* $\mathbf{u}^* = \mathbf{u}^{**}$*, where* $\mathbf{u}^{**}$ *is the solution of the following optimal control problem*

$$\min_{\mathbf{u}} \int_0^{t_f} J(\mathbf{u}(t))\mathrm{d}t \tag{12.9a}$$

$$s.t.$$

$$\dot{\mathbf{z}}^{\parallel}_{\mathrm{eq}} = A_{\parallel}\mathbf{z}^{\parallel}_{\mathrm{eq}} + B_{\parallel}\mathbf{u} \tag{12.9b}$$

$$\mathbf{z}^{\parallel}_{\mathrm{eq}}(0) = 0 \tag{12.9c}$$

$$\mathbf{z}^{\parallel}_{\mathrm{eq}}(t_f) = \mathrm{z}^{\parallel}_f . \tag{12.9d}$$

Proof. From Corollary (12.14), if $\exists\, i, l$ such that $x_{f,i} \neq z_{f,l}$ then $\mathbf{x}_f$ is not reachable, and thus problem (12.8) is not feasible. On the other hand, if $x_{f,i} = z_{f,l}$ for all $i \in C_l$ and for all l, then $x_f \in \mathcal{X}_{or}$, from Theorem 12.9 and from the hypotheses, the controllable subspace coincides with $\mathcal{X}_{or}$. Then, reaching $\mathbf{z}^{\parallel} = \mathbf{z}^{\parallel}_f$ implies reaching the point $\mathbf{x}_f$. Hence, to prove our thesis, we are left with showing that $\mathbf{u}^* = \mathbf{u}^{**}$. We will do so by showing that problems (12.8) and (12.9) share the same decision variables, cost function, and constraints. Indeed, the decision variables are the same by definition, as well as the cost function as input signals are not affected by equivalent transformations. Finally, to prove that problems (12.8) and (12.9) share the same constraints, let us show that by left multiplying both sides of equations (12.8b)-(12.8d), we obtain eqs. (12.9b)-(12.9d) together with a set of equations that are always verified independently of u. Indeed this is trivially true for Equation (12.8b), as $\mathbf{x}(0) = \mathbf{0}$ and $\mathbf{z}^{\parallel}_{\mathrm{eq}}(0) = \mathbf{0}$. Moreover, if $x_{f,i} = z_{f,l}$, and from the definition of T_{eq} in (12.6), then

$$T_{\mathrm{eq}}\mathbf{x}_f = \begin{bmatrix} \mathbf{z}^{\parallel}_f \\ 0 \end{bmatrix}$$

which implies that $\mathbf{z}^{\perp}_f = \mathbf{0}$. This is ensured independently of $\mathbf{u}$ as $\mathbf{z}^{\perp}(0) = \mathbf{0}$ and as from Theorem 12.12 we know that $\mathbf{z}^{\perp}$ are the state variables of the non-controllable subsystem of the pair (A, B). Finally, from Equation (12.7) we know that left-multiplying Equation

(12.8a) by T_{eq} yields the set of equations

$$\dot{\mathbf{z}}^{\parallel} = A_{\parallel}\mathbf{z}^{\parallel} + B_{\parallel}\mathbf{u} \tag{12.10a}$$

$$\dot{\mathbf{z}}^{\perp} = A_{\perp}\mathbf{z}^{\perp}. \tag{12.10b}$$

As $\mathbf{z}^{\perp}(0) = \mathbf{0}$, from Equation (12.10b) we have that $\mathbf{z}^{\perp}(t) = \mathbf{0}$ for all t, and thus Equation (12.10a), which coincides with Equation (12.9b), captures completely the dynamics in Equation (12.8b) independently of $\mathbf{u}$. Hence, problem (12.8) and the reduced order problem in (12.9) share the same decision variables, cost function, and constraints which implies that $\mathbf{u}^{*} = \mathbf{u}^{**}$. □

Remark 12.16. *Note that as orbital partitions are also equitable, Corollary 12.15 also holds for networks with symmetries.*

Remark 12.17. *Corollary 12.15 provides an approach to control the consensus solution. Note however that this solution is not stabilizable neither in the case of symmetries nor in that of equitable partitions, as the dynamics orthogonal to the group consensus subspace are uncontrollable (see Theorems 12.9 and 12.12). However, in both cases, the transformations in eqs. (12.3) and (12.6) allow to study the stability of the group consensus solution by computing the eigenvalues of the block $A_{\perp}$ of the matrices $\tilde{A}$ in Equation (12.4) and $\hat{A}$ in Equation (12.7) respectively. Note that the block $A_{\perp}$ of the matrix $\tilde{A}$ of the irreducibile representation in Equation (12.4) is itself block-diagonal, with each block representing the dynamics orthogonal to the consensus subspace of single or intertwined clusters [140]. Hence, in the case of symmetries, analysis of the eigenvalues of each one of the diagonal subblocks of $A_{\perp}$ in Equation (12.4) provides information about which clusters will asymptotically reach consensus (and which ones will not).*

Remark 12.18. *Note that Corollary 12.15 provides an approach to design a a possible control input to steer the network towards a desired group consensus value. A viable alternative is to solve*

$$\min_{\mathbf{u}} \int_{0}^{t_f} J(\mathbf{u}(t))\mathrm{d}t \tag{12.11a}$$

$$s.t.$$

$$\dot{\mathbf{x}} = A\mathbf{x} + B\mathbf{u} \tag{12.11b}$$

$$\mathbf{y} = E_{\varphi}^{T}\mathbf{x} \tag{12.11c}$$

$$\mathbf{x}(0) = \mathbf{0} \tag{12.11d}$$

$$\mathbf{y}(t_f) = \mathbf{y}_f\,. \tag{12.11e}$$

with E_φ being the indicator matrix of an equitable partition $C_1, C_2, \dots C_K$ of the network nodes, and

$$\frac{y_i}{|C_i|}$$

being the consensus value for all the nodes of the cluster C_i.

12.5 Numerical example

In this section we will show the powerful of Corollary 12.15, highlighting the chance offered by networks with symmetries in dimensionality reduction. We consider the $N = 10$ nodes network in Figure 12.1, with an equitable partition φ_{eq} that partitions the network nodes in $K = 2$ clusters, $C_1 \cup C_2 = \mathcal{V}$ and $C_1 = \{1, 2, 3, 4\}$ and $C_2 = \mathcal{V} \setminus C_1$ and then not completely controllable. The corresponding indicator matrix is

$$E_\varphi^T = \begin{bmatrix} 1 & 1 & 1 & 1 & 0 & 0 & 0 & 0 & 0 & 0 \\ 0 & 0 & 0 & 0 & 1 & 1 & 1 & 1 & 1 & 1 \end{bmatrix}. \tag{12.12}$$

Consistently with Corollary 12.14, performing the state transformation $\mathbf{z}_{\text{eq}} = T_{\text{eq}}\mathbf{x}$, with the matrix T_{eq} selected according to Equation (12.6) we obtain that $B_\perp = 0$. Moreover, we have that

$$A_\parallel = \begin{bmatrix} -10 & 3 \\ 2 & -8 \end{bmatrix}, B_\parallel = \begin{bmatrix} 1 \\ 0 \end{bmatrix}, \tag{12.13}$$

and the reader may easily check that the pair $(A_\parallel, B_\parallel)$ is controllable. Hence, we can exploit the results in Section 12.4 to control group consensus. Indeed, to steer the network towards the group consensus state $[\mathbf{1}_{1\times 4}\ \mathbf{2}_{1\times 6}]^T$ by spending the minimum control energy, from Corollary 12.15, instead of solving

$$\begin{aligned} &\min_{\mathbf{u}} \frac{1}{2}\int_0^1 \mathbf{u}(t)^T\mathbf{u}(t)\mathrm{d}t \\ &s.t. \\ &\dot{\mathbf{x}} = A\mathbf{x} + B\mathbf{u} \\ &\mathbf{x}(0) = \mathbf{0}_{10\times 1} \\ &\mathbf{x}(1) = [\mathbf{1}_{1\times 4}\ \mathbf{2}_{1\times 6}]^T \end{aligned} \tag{12.14}$$

we can solve

$$\begin{aligned} &\min_{\mathbf{u}} \frac{1}{2}\int_0^1 \mathbf{u}^T(t)\mathbf{u}(t)\mathrm{d}t \\ &s.t. \\ &\dot{\mathbf{z}}_{\text{eq}}^{\parallel} = A_\parallel \mathbf{z}_{\text{eq}}^{\parallel} + B_\parallel \mathbf{u} \\ &\mathbf{z}_{\text{eq}}^{\parallel}(0) = \mathbf{0}_{2\times 1} \\ &\mathbf{z}_{\text{eq}}^{\parallel}(1) = [1\ 2]^T \end{aligned} \tag{12.15}$$

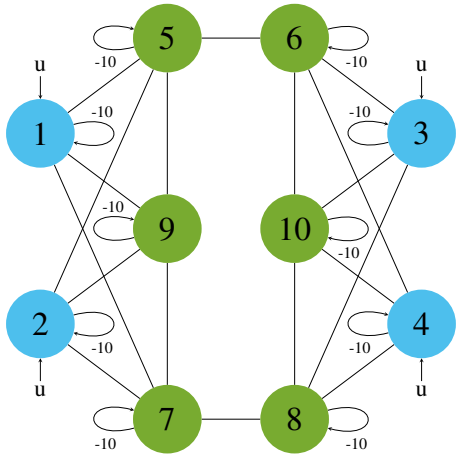

$$A = \begin{bmatrix} -10 & 0 & 0 & 0 & 1 & 1 & 1 & 0 & 0 & 0 \\ 0 & -10 & 0 & 0 & 1 & 1 & 1 & 0 & 0 & 0 \\ 0 & 0 & -10 & 0 & 0 & 0 & 0 & 1 & 1 & 1 \\ 0 & 0 & 0 & -10 & 0 & 0 & 0 & 1 & 1 & 1 \\ 1 & 1 & 0 & 0 & -10 & 1 & 0 & 1 & 0 & 0 \\ 1 & 1 & 0 & 0 & 1 & -10 & 1 & 0 & 0 & 0 \\ 1 & 1 & 0 & 0 & 0 & 1 & -10 & 0 & 0 & 1 \\ 0 & 0 & 1 & 1 & 1 & 0 & 0 & -10 & 1 & 0 \\ 0 & 0 & 1 & 1 & 0 & 0 & 0 & 1 & -10 & 1 \\ 0 & 0 & 1 & 1 & 0 & 0 & 1 & 0 & 1 & -10 \end{bmatrix}$$

$$B = \begin{bmatrix} 1 & 1 & 1 & 1 & 0 & 0 & 0 & 0 & 0 & 0 \end{bmatrix}^T$$

Figure 12.1: A simple 10 node network, with edge weights all equal to one, and self-loop weights all equal to -10 that serve to stabilize the network and so make the minimum control energy problem meaningful. The coarsest equitable partition of the network shown in the figure has two clusters C_1 and C_2, with colored in light blue and green respectively.

where $\mathbf{z}_{\text{eq}}^{\parallel} \in \mathbb{R}^2$ is the state variable of the quotient network associated to pair $(A_{\parallel}, B_{\parallel})$. The solution of problem (12.15) is

$$\mathbf{u}^{**}(t) = B_{\parallel}^T \mathrm{e}^{A_{\parallel}(1-t)} W^{-1} \mathbf{z}_{eq}^{\parallel}. \tag{12.16}$$

where

$$W = \int_0^1 \mathrm{e}^{A_{\parallel}(1-t)} B_{\parallel} B_{\parallel}^T \mathrm{e}^{A_{\parallel}^T(1-t)} \mathrm{d}t$$

is the reachability gramian of the quotient network. For Corollary 12.15 we can compute paper and pen the optimal control input (12.16) of a 2×2 dynamical network instead of the original 10-dimensional one. Indeed, diagonalizing $A_{\parallel}^T = V_T \Lambda V_T^{-1}$, where V_T is the matrix containing the right eigenvectors and Λ is the diagonal matrix containing the eigenvalues of $A_{\parallel}^T$, we obtain

$$\begin{aligned} \mathbf{u}^{**}(t) =& B_{\parallel}^T \mathrm{e}^{A_{\parallel}^T(1-t)} W^{-1} \mathbf{z}_{\text{eq}}^{\parallel}(1) \\ =& B_{\parallel}^T V_T^{-1} \mathrm{e}^{\Lambda(1-t)} V_T W^{-1} \mathbf{z}_{\text{eq}}^{\parallel}(1) \\ \approx& -1058 \mathrm{e}^{(9+\sqrt{7})(t-1)} + 806 \mathrm{e}^{(9-\sqrt{7})(t-1)} \end{aligned} \tag{12.17}$$

that is, the optimal control input is a linear combination of the two eigenmodes corresponding to the two clusters of the partition φ_{eq} of $\mathcal{G}(A, B)$. Thus $\mathbf{u}^{**}$ can be used to control the original network whose graph is depicted in Figure 12.1. Note that the optimal control input (12.17), that is shown in Figure 12.2b is able to steer nodes in C_1 to 1 and nodes in C_2 to 2 at $t_f = 1$, as shown in Figure 12.2a.

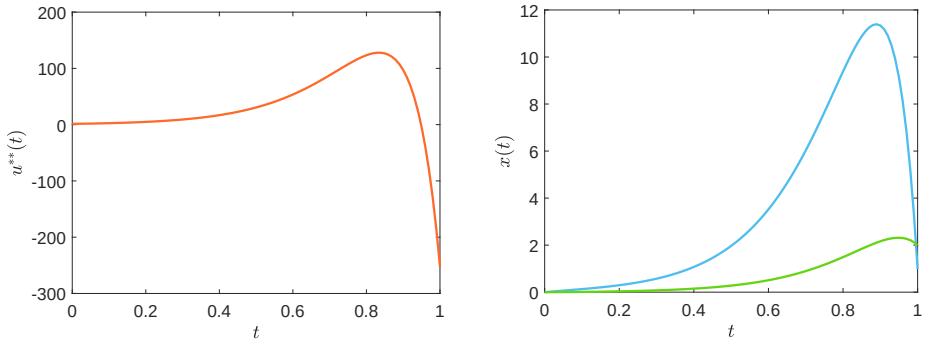

(a) (b)

Figure 12.2: In (a) the state trajectories of the original network when forced by the optimal control input $\mathbf{u}^{**}$ of (12.17) depicted in (b). In light blue the trajectories of nodes in cluster C_1 and in green those of nodes in cluster C_2.

12.6 Discussion

Motivated by the observation that symmetries induce loss of controllability and the emergence of group consensus, in this work we studied the controllability properties of networks endowed of symmetries. We found that controllability is lost in directions orthogonal to the group consensus subspace, but we can still control the consensus state either if the network initial condition belongs to the group consensus subspace, or if the subsystem of the dynamics orthogonal to this subspace is asymptotically stable. Moreover, we showed that when the network controllable subspace coincides with the group consensus subspace, we can control consensus by designing control strategies on a lower-dimensional network, the quotient network associated to the original one, thus reducing the computational burden, something that turns useful when the networks to be controlled are large. We demonstrated our theoretical analysis through a representative numerical example.

13 Partial Containment control over signed networks

In this Chapter, we propose a new control protocol, the *partial containment control* over signed networks (Section 13.2), especially useful either when the network is large or when we do not aim to achieve the complete containment control. To do so, we reformulate the graph condensations introduced in section 13.1.3, to make them suitable for signed graphs. On the basis of these condensations, we will derive sufficient conditions to contain the larger number of nodes of our network, that is, the strongly connected components (SCCs) (Section 13.3). Finally, employing the convergence analysis results, we design a suboptimal algorithm to efficiently deploy the control input in the network (Section 13.4).

13.1 Mathematical Preliminaries

13.1.1 Signed graphs

A weighted directed signed graph $\mathcal{G}$ consists of a weighted digraph $\mathcal{U} = \{\mathcal{V}, \mathcal{E}\}$ and a partial mapping $\sigma : \mathcal{E} \to \{+, -\}$ [159]. An edge $(i, j) \in \mathcal{E}$ is called positive if $\sigma(i, j) = \{+\}$, while it is called negative otherwise. We associate to $\mathcal{G}$ a weighted adjacency matrix A, whose ij-th element a_{ij} is positive if $(i, j) \in \mathcal{E} \wedge \sigma(i, j) = \{+\}$, negative if $(i, j) \in \mathcal{E} \wedge \sigma(i, j) = \{-\}$, and zero otherwise.

Throughout the thesis, we shall consider signed graphs fulfilling the following assumption.

Assumption 13.1. $|a_{ii}| > 0$ *and* $\sum_{j=1}^{n} |a_{ij}| = 1$, *for all* $i = 1, \ldots, n$.

Definition 13.2. *A directed signed graph $\mathcal{G}$ is structurally balanced if there exists a bipartition $\{\mathcal{V}^1, \mathcal{V}^2\}$ of $\mathcal{V}$, such that $a_{ij} \geq 0$, for all i and $j \in \mathcal{V}^\theta$ and $a_{ij} \leq 0$ for all $(i \in \mathcal{V}^\theta, j \in \mathcal{V} \setminus \mathcal{V}^\theta)$, for all $\theta \in \{1, 2\}$. $\mathcal{G}$ is unbalanced otherwise.*

Notice that every unsigned graph is structurally balanced with $\mathcal{V}^1 = \mathcal{V}$ and $\mathcal{V}^2 = \emptyset$. Following [160] and [161], we define the *enlarged graph* associated to $\mathcal{G}$ as follows:

Definition 13.3. *The enlarged graph $\widetilde{\mathcal{G}} = \{\widetilde{\mathcal{V}}, \widetilde{\mathcal{E}}\}$ associated to $\mathcal{G}$ (see for instance Figure 13.1) is a (unsigned) directed graph of $2n$ nodes ($\widetilde{\mathcal{V}} = \{1, \dots, n, 1^-, \dots, n^-\}$) and all positive edges related to that of $\mathcal{G}$ through the adjacency matrix $\widetilde{A}$, whose elements are*

$$\begin{aligned} \tilde{a}_{ij} = \tilde{a}_{i+N,j+N} &= \max(0, a_{ij}) \geq 0, \\ \tilde{a}_{i+N,j} = \tilde{a}_{i,j+N} &= \max(0, -a_{ij}) \geq 0, \end{aligned}$$

for $i, j = 1, \dots, N$.

13.1.2 Some useful lemmata

Lemma 13.4. *[162]Let us consider a reducible matrix in normal form:*

$$M = \begin{bmatrix} M_1 & 0 & 0 & 0 \\ \vdots & \ddots & \ddots & \vdots \\ 0 & \cdots & M_q & 0 \\ R_1 & \cdots & R_q & S \end{bmatrix},$$

where M_j, $j = 1, \dots, q$, are semi-convergent irreducible matrices and S is a convergent matrix [163]. We then have

$$\lim_{k \to +\infty} M^k = \begin{bmatrix} M_1^\infty & 0 & 0 & 0 \\ \vdots & \ddots & \ddots & \vdots \\ 0 & \cdots & M_q^\infty & 0 \\ \cdots & R_j^* & \cdots & 0 \end{bmatrix},$$

where $M_j^\infty = \lim_{k \to +\infty} M_j^k$ and $R_j^* = (I - S)^{-1} R_j M_j^\infty$. Furthermore, if $\lambda = 1$ is an eigenvalue of M_j, then $M_j^\infty = \psi_j \xi_j^T$, where ξ_j and ψ_j are the left and right eigenvectors associated to $\lambda = 1$, respectively, scaled so that $\xi_j^T \psi_j = 1$.

Lemma 13.5. *[160] Given a strongly connected signed graph $\mathcal{G}$ and its associated enlarged graph $\widetilde{\mathcal{G}}$, $\mathcal{G}$ is structurally balanced if and only if $\widetilde{\mathcal{G}}$ is disconnected and composed of two strongly connected components.*

Lemma 13.6. *[160] Given a strongly connected signed graph $\mathcal{G}$ and its associated enlarged graph $\widetilde{\mathcal{G}}$, $\mathcal{G}$ is structurally unbalanced if and only if $\widetilde{\mathcal{G}}$ is strongly connected.*

13.1.3 Graph condensations

In this subsection we give some useful notations regarding graph condensations. A condensation of a graph $\mathcal{G}$ is a new directed graph whose nodes represent the strongly connected components of $\mathcal{G}$.

Definition 13.7. *Given any pair of vertex sets $\{\mathcal{V}, \mathcal{V}'\}$, with $|\mathcal{V}| \geq |\mathcal{V}'|$, any (single-valued) function $f : \mathcal{V} \to \mathcal{V}'$ is called a* condensing function. *Moreover,*

$$\mathcal{V}_i := \{t \in \mathcal{V} : f(t) = i\}, \quad i \in \mathcal{V}'.$$

Definition 13.8. *Let us consider a graph $\mathcal{G} = (\mathcal{V}, \mathcal{E})$, a vertex set $\mathcal{V}'$, a condensing function $f : \mathcal{V} \to \mathcal{V}'$, and the edge set $\mathcal{E}' = \{(i \in \mathcal{V}', j \in \mathcal{V}'), i \neq j | \exists (t, u) \in \mathcal{E} | f(t) = i, f(u) = j\}$. The graph $\mathcal{G}' = \{\mathcal{V}', \mathcal{E}'\}$ is the condensation of $\mathcal{G}$ induced by f.*

Definition 13.9. *The classic condensation $\mathcal{G}^c$ of a graph $\mathcal{G}$ is the condensation of $\mathcal{G}$ induced by the condensing function f^c condenses into the same node of $\mathcal{V}^c$, all the nodes of $\mathcal{V}$ that belong to the same SCC of $\mathcal{G}$.*

Now, we introduce a novel condensation of a graph $\mathcal{G}$, denoted as the *signed condensation* $\mathcal{G}^s$ of $\mathcal{G}$:

Definition 13.10. *The signed condensation $\mathcal{G}^s$ of a graph $\mathcal{G}$ is the condensation of $\mathcal{G}$ induced by the condensing function f^s that condenses in the same node of $\mathcal{V}^s$ all the nodes of $\mathcal{V}$ belonging to the same SCC of $\widetilde{\mathcal{G}}$.*

Notice that if $\mathcal{G}$ is unsigned, then $\mathcal{G}^c = \mathcal{G}^s$. The correspondences between the diverse condensations are illustrated in Figure 13.1. Moreover, we observe that the signed condensation $\mathcal{G}^s$ is a directed acyclic graph. From now on, we call directed acyclic condensation every condensation that is a directed acyclic graph (DAG). We can now give the following definition.

Definition 13.11. *Let us consider a directed acyclic condensation $\mathcal{G}^d = (\mathcal{V}^d, \mathcal{E}^d)$ of a graph $\mathcal{G} = (\mathcal{V}, \mathcal{E})$ induced by a condensing function f^d. Node $i \in \mathcal{V}^d$ belongs to level 1 if $\nexists j : (j, i) \in \mathcal{E}^d$. Furthemore, a node $i \in \mathcal{V}^d$ belongs to the $l(>1)$-th level of $\mathcal{V}^d$ if*

$$\forall (j, i) \in \mathcal{E}^d; \; j \in \text{level } p < l.$$

Moreover, the total number of levels is denoted by ℓ_d and the number of nodes of $\mathcal{G}^d$ in a given level l is n_l^d.

Given a directed acyclic condensation $\mathcal{G}^d$ of $\mathcal{G}$, we associate to each node in $\mathcal{V}^d$ a pair of indexes (a, b): the first will indicate the level the node belongs to and the second its

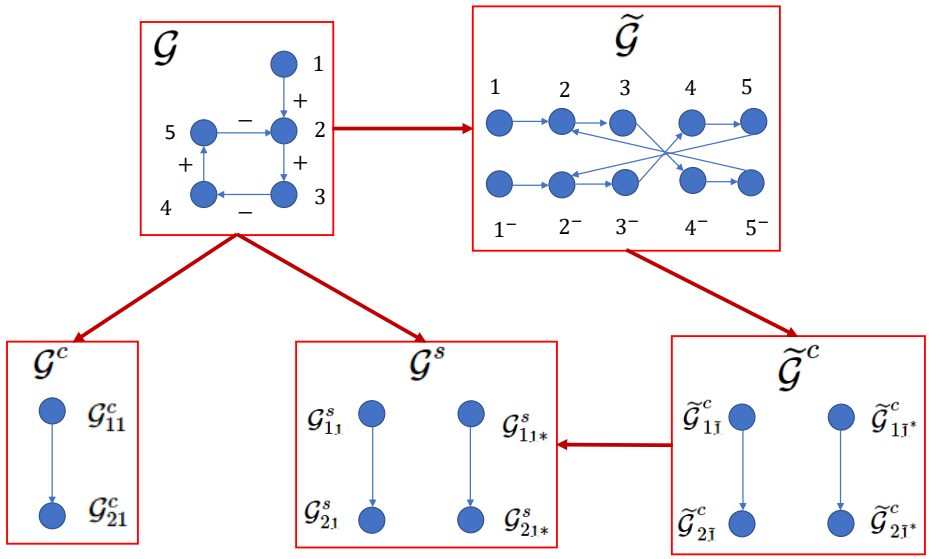

Figure 13.1: The correspondences between the various condensations and their decomposition in levels are illustrated with reference to a sample signed graph $\mathcal{G}$.

(random) ranking in that level, see Figure 13.1. Notice that, by definition, all the leaders belong to level 1. Accordingly, we can define a function g^d that associates to each (a, b) the corresponding node of $\mathcal{V}^d$. Now, we can partition (and sort) the set of nodes of $\mathcal{V}$ as

$$\mathcal{V} = \{\mathcal{V}^d_{11}, \dots, \mathcal{V}^d_{1n^d_1}, \dots, \mathcal{V}^d_{\ell_d n^d_\ell}\}, \tag{13.1}$$

where

$$\mathcal{V}^d_{ij} := \{t \in \mathcal{V} : f^d(t) = g^d(i, j)\}. \tag{13.2}$$

Moreover, we denote $\mathcal{G}^d_{ij} \subseteq \mathcal{G}$ the subgraph induced by $\mathcal{V}^d_{ij}$. Consequently, we indicate by $\mathcal{G}^c_{ij}$ a strongly connected component (SCC) of $\mathcal{G}$, for all $i = 1, \dots, \ell_c$, $j = 1, \dots, n^c_i$, and that $\mathcal{G}^c_{11}, \dots, \mathcal{G}^c_{1h}, \dots, \mathcal{G}_{1n^c_1}$ are its $n^c_1 \geq 1$ aperiodic root strongly connected components (RSCCs). Notice that the number of levels of $\mathcal{G}^c$, $\widetilde{\mathcal{G}}^c$ and $\mathcal{G}^s$ is the same, that is, $\ell_c = \tilde{\ell}_c = \ell_s := \ell$. Moreover, for all $l = 1, \dots, \ell$, $n^c_l \leq n^s_l \leq \tilde{n}^c_l$. Moreover, any SCC of $\mathcal{G}$ can be classified as of

1. *type 1* if it has no negative weights;
2. *type 2* if it has at least one negative weight and is structurally balanced;
3. *type 3* if it has at least one negative weight and is structurally unbalanced.

Remark 13.12. *For all $h = 1, \dots, n_l$, $l = 1, \dots, \ell$, we associate to the h-th node of the l-th level of $\mathcal{G}^c$*

- *the* $\mathfrak{h}$*-th* ($\tilde{\mathfrak{h}}$*-th) and the* $\mathfrak{h}^*$*-th* ($\tilde{\mathfrak{h}}^*$*-th) nodes of the* l*-th level of* $\mathcal{G}^s$ ($\widetilde{\mathcal{G}}^c$) *such that* $\mathcal{V}^c_{lh} = \mathcal{V}^s_{l\mathfrak{h}} \cup \mathcal{V}^s_{l\mathfrak{h}^*} \subset \widetilde{\mathcal{V}}^c_{l\tilde{\mathfrak{h}}} \cup \widetilde{\mathcal{V}}^c_{l\tilde{\mathfrak{h}}^*}$, *if* $\mathcal{G}^c_{lh}$ *is of type 1 or type 2;*
- *the* $\mathfrak{h}$*-th* ($\tilde{\mathfrak{h}}$*-th) node of the* l*-th level of* $\mathcal{G}^s$ *such that* $\mathcal{V}^c_{lh} = \mathcal{V}^s_{l\mathfrak{h}} \subseteq \widetilde{\mathcal{V}}^c_{l\tilde{\mathfrak{h}}}$, *if* $\mathcal{G}^c_{lh}$ *is of type 3.*

Moreover, we associate to the $\tilde{\mathfrak{h}}$*-th node of the* l*-th level of* $\widetilde{\mathcal{G}}^c$ *the* h*-th node of the* l*-th level of* $\mathcal{G}^c$ *such that*

$$\widetilde{\mathcal{V}}^c_{l\tilde{\mathfrak{h}}} \cap \mathcal{V}^c_{lh} \neq \emptyset.$$

These associations between the nodes of the condensations are clearly illustrated in Figure 13.1.

13.2 Problem formulation

Let us consider a signed graph $\mathcal{G}$ with n nodes, and let $x_i \in \mathbb{R}$ be the state of the i-th node, and $\mathcal{N}_i = \{j \in \mathcal{V} : (j,i) \in \mathcal{E}\}$ is the set of neighbors of i, for all $i = 1, \dots, n$. Then, let us denote by $\mathcal{C} \subset \mathcal{V}$ the set of *m leaders* (sometimes also denoted pinners [121, 128, 164], depending on the context), that is, nodes that have no incoming links. The dynamics over this signed graph are described by

$$x_i(k+1) = x_i(k) + \sum_{j=1}^{N} a_{ij} \left(x_j(k) - \text{sign}(a_{ij}) x_i(k) \right), \tag{13.3}$$

for all $i = 1, \dots, n$, or, equivalently,

$$x(k+1) = Ax(k),$$

where $x = [x_1, \dots, x_n]^T$ is the vector of the nodes' states.

Here, we focus on the case in which

$$|a_{ij}| = \begin{cases} \frac{1}{|\mathcal{N}_i|} & \text{if } j \in \mathcal{N}_i, \\ 0 & \text{otherwise,} \end{cases}$$

but the results given in the following can be easily extended to alternative rules for computing a_{ij} that are consistent with Assumption 13.1. Notice that, assuming $a_{ii} > 0$ for all $i \in \mathcal{C}$, $x_i(k+1) = x_i(k) = x_i(0)$ for all $i \in \mathcal{C}$. From [156], we give the following definition of containment in signed graphs.

Definition 13.13. *A node* $i \in \mathcal{V} - \mathcal{C}$ *is asymptotically signed contained when*

$$\limsup_{k \to +\infty} |x_i(k)| \leq \max_{j \in \mathcal{C}} |x_j(0)|, \tag{13.4}$$

Definition 13.14. *Network* (13.3) *is q-partially signed contained if there exist a subset* $\mathcal{Q} \subseteq \mathcal{V} \setminus C$ *of cardinality* q *such that all the nodes in* $\mathcal{Q}$ *are asymptotically contained. If* $q = n - m$*, then network* (13.3) *is signed contained.*

Let us denote by $\mathcal{L}$ the set of nodes directly controlled by the leaders, that is,

$$\mathcal{L} = \left\{ i \in \mathcal{V} \mid \exists\, a_{ji} > 0, j \in C \right\}.$$

Then, we can define $\mathcal{K}(\mathcal{L}) := \{i \in \mathcal{V} \mid \text{eq. (13.4) holds}\}$, as the set of asymptotically contained nodes. For a given cardinality, say d, of the set $\mathcal{L}$, the partial containment control problem consists in finding optimal selection $\mathcal{L}^*(d)$ that maximizes the number of contained nodes, that is,

$$\begin{aligned} \mathcal{L}^*(d) &= \arg\max_{\mathcal{L}} |\mathcal{K}(\mathcal{L})| \\ \text{s.t.} \quad & |\mathcal{L}| = d. \end{aligned} \tag{13.5}$$

We observe that the numerical solution of this problem for $d > 1$, although conceptually simple, would require to test for a number of alternative selections of the pinned nodes that is in the order of $n!$. An extensive search of the optimal solution is therefore computationally prohibitive even for relatively small networks. In what follows, we propose a computationally efficient heuristic approach to find a suboptimal solution of problem (13.5).

13.3 Convergence analysis

Before giving our main results, we give some relevant notation. Specifically, for the h-th SCC of the l-th level, we introduce the stack vector x_{lh} of the states $\{x_i\}_{i \in \mathcal{V}^c_{lh}}$, and the vector

$$y_{lh}(k) := \left[x_{lh}(k)^T, -x_{lh}(k)^T \right]^T. \tag{13.6}$$

If $\mathcal{G}^c_{lh}$ is of type 2, y_{hl} can be viewed as the vector containing all the states of the nodes in $\widetilde{\mathcal{V}}^c_{l\tilde{\mathfrak{h}}} \cup \widetilde{\mathcal{V}}^c_{l\tilde{\mathfrak{h}}^*}$. From Lemma 13.5, $\widetilde{\mathcal{G}}_{lh}$ is composed by two disconnected SCCs. Therefore, we can find a permutation matrix T_{lh} such that, defining $z_{lh}(k) = T_{lh} y_{lh}(k) = [z_{l\tilde{\mathfrak{h}}}(k)^T z_{l\tilde{\mathfrak{h}}^*}(k)^T]^T$, we can write

$$z_{lh}(k+1) = \begin{bmatrix} Z_{l\tilde{\mathfrak{h}}} & 0 \\ 0 & Z_{l\tilde{\mathfrak{h}}^*} \end{bmatrix} z_{lh}(k), \tag{13.7}$$

where $Z_{l\tilde{\mathfrak{h}}}$ and $Z_{l\tilde{\mathfrak{h}}^*}$ are the submatrices extracted from $\widetilde{A}$ associated to the nodes in $\widetilde{\mathcal{V}}^c_{l\tilde{\mathfrak{h}}}$ and in $\widetilde{\mathcal{V}}^c_{l\tilde{\mathfrak{h}}^*}$. In what follows, for any node h of level l in $\mathcal{G}^c$ corresponding to a type 1 SCC of $\mathcal{G}$, we indicate with ξ_{lh} the left eigenvector associated to the unique eigenvalue $\lambda = 1$ of block A_{lh} of matrix A in Equation (13.3), while, given a type 2 SCC $\mathcal{G}^c_{lh}$, we denote $\widetilde{\xi}_{l\tilde{\mathfrak{h}}}$ ($\widetilde{\xi}_{l\tilde{\mathfrak{h}}^*}$) the left eigenvector associated to the unique eigenvalue $\lambda = 1$ of $Z_{l\tilde{\mathfrak{h}}}$ ($Z_{l\tilde{\mathfrak{h}}^*}$).

By exploiting the condensations introduced in Section 13.1.3, here we explore the network level by level, to finally provide an algorithm that computes the steady-state configuration of any SCC in the graph. Let us start by characterizing the asymptotic behaviors of the nodes in the RSCCs (i.e. in the level 1 of $\mathcal{G}^c$).

Theorem 13.15. *For all* $h = 1, \dots, n_1^c$,

- *if* $\mathcal{G}_{1h}^c$ *is of* type 1, *then*

$$\lim_{k\to+\infty} x_i(k) = \xi_{1h}^T x_{1h}(0), \qquad \forall i \in \mathcal{V}_{1h}^c \tag{13.8}$$

- *if* $\mathcal{G}_{1h}^c$ *is of* type 2, *the SCC polarizes and*

$$\begin{aligned} \lim_{k\to+\infty} x_i(k) &= \widetilde{\xi}_{1\tilde{\mathfrak{h}}}^T z_{1\tilde{\mathfrak{h}}}(0) \qquad && \forall i \in \mathcal{V}_{1\tilde{\mathfrak{h}}}^s \\ \lim_{k\to+\infty} x_i(k) &= -\widetilde{\xi}_{1\tilde{\mathfrak{h}}^*}^T z_{1\tilde{\mathfrak{h}}^*}(0) \qquad && \forall i \in \mathcal{V}_{1\tilde{\mathfrak{h}}^*}^s \end{aligned} \tag{13.9}$$

- *if* $\mathcal{G}_{1h}^c$ *is of* type 3, *then*

$$\lim_{k\to+\infty} x_{1h}(k) = 0. \tag{13.10}$$

Proof. Sorting the network nodes according to (13.1) and setting $d = c$, we can rewrite matrix A as

$$\begin{bmatrix} A_{11} & 0 & 0 & 0 \\ \vdots & \ddots & \ddots & \vdots \\ 0 & \cdots & A_{1n_1^c} & 0 \\ R_1 & \cdots & R_{n_1^c} & Q \end{bmatrix} \tag{13.11}$$

From (13.11), we can then write

$$x_{1h}(k+1) = A_{1h} x_{1h}(k), \qquad h = 1, \dots, n_1^c.$$

We distinguish three cases:

1. $\mathcal{G}_{1h}^c$ *is of type 1.* In this case, the classical results on discrete-time consensus hold [11], and we can write

$$\lim_{k\to+\infty} x_{1h}(k) = \xi_{1h}^T x_{1h}(0) \mathbf{1}_{|\mathcal{V}_{1h}^c|},$$

   which is equivalent to (13.8).
2. $\mathcal{G}_{1h}^c$ *is of type 2.* From (13.7), and being $Z_{1\tilde{\mathfrak{h}}}$ and $Z_{1\tilde{\mathfrak{h}}^*}$ irreducible and row stochastic, we can conclude that

$$\lim_{k\to+\infty} x_i(k) = \begin{cases} \widetilde{\xi}_{1\tilde{\mathfrak{h}}}^T z_{1\tilde{\mathfrak{h}}}(0) & \forall i \in \mathcal{V}_{1\tilde{\mathfrak{h}}}^s, \\ \widetilde{\xi}_{1\tilde{\mathfrak{h}}^*}^T z_{1\tilde{\mathfrak{h}}^*}(0) & \forall i \in \mathcal{V}_{1\tilde{\mathfrak{h}}^*}^s. \end{cases} \tag{13.12}$$

   From (13.6), we have $\widetilde{\xi}_{1\tilde{\mathfrak{h}}}^T z_{1\tilde{\mathfrak{h}}}(0) = -\widetilde{\xi}_{1\tilde{\mathfrak{h}}^*}^T z_{1\tilde{\mathfrak{h}}^*}(0)$, which, together with (13.12), implies (13.9).

3. $\mathcal{G}^c_{1h}$ *is of type 3.* In this case, from Lemma 13.6, the corresponding graph $\widetilde{\mathcal{G}}_{1\tilde{\mathfrak{h}}}$ is strongly connected, and then all the elements of y_{1h} must converge to a common value, say c_{1h}. However, since the vector y_{1h} contains both x_{1h} and $-x_{1h}$, then we have $c_{1h} = 0$.

□

Next, we define the upstream and the downstream of a node of a DAG.

Definition 13.16. *For each node i of a directed acyclic graph, its upstream (downstream) is the set of nodes, including i itself, from which i is reachable (which i can reach) through a directed path. Moreover, we denote with $\Upsilon^{\mathcal{G}^d}_{lh}$ the upstream of the node lh of $\mathcal{G}^d$.*

For any node lh of $\mathcal{G}^c$, $\delta_i(lh)$ is the number of nodes of the i-th level of $\mathcal{G}^c$ that are in the upstream of lh, for $i = 1, \dots, l-1$. Furthermore, we define the set $\mathcal{J}_i(lh) := \{j_1, \dots, j_{\delta_i}\}$ as the set of nodes of level i that are in the upstream of node lh, $i = 1, \dots, l-1$. Set $\mathcal{J}_i(lh)$ can be partitioned as follows:

$$\mathcal{J}_i(lh) = \{\mathcal{J}_{i1}(lh), \mathcal{J}_{i2}(lh), \mathcal{J}_{i3}(lh)\},$$

where $\mathcal{J}_{it}(lh) = \left\{\alpha \in \mathcal{J}_{it}(lh) \mid \mathcal{G}^c_{i\alpha} \text{ is type } t\right\}$, $t = 1, 2, 3$.

We now give an algorithmic procedure to compute the steady-state values of the states of the nodes belonging to a generic SCC of $\mathcal{G}$.

Theorem 13.17. *For all $l = 2, \dots, \ell$, $h = 1, \dots, n^c_l$, the steady-state values $\bar{x}_{lh}$ of the nodes in $\mathcal{G}^c_{lh}$ can be computed through the following algorithm*

$$\begin{aligned}
\bar{x}_{1p} &= \begin{cases} \begin{bmatrix} +\widetilde{\xi}^T_{1\tilde{\mathfrak{p}}} z_{1\tilde{\mathfrak{p}}}(0)\mathbf{1}_{|\mathcal{V}^s_{1\tilde{\mathfrak{p}}}|} \\ -\widetilde{\xi}^T_{1\tilde{\mathfrak{p}}} z_{1\tilde{\mathfrak{p}}^*}(0)\mathbf{1}_{|\mathcal{V}^s_{1\tilde{\mathfrak{p}}^*}|} \end{bmatrix} & \text{if } \mathcal{G}^c_{1p} \text{ is of type 1} \\ \xi^T_{1p} x_{1p}(0)\mathbf{1}_{|\mathcal{V}^c_{1p}|} & \text{if } \mathcal{G}^c_{1p} \text{ is of type 2} \\ 0 & \text{if } \mathcal{G}^c_{1p} \text{ is of type 3} \end{cases}, \\
&\forall p \in \mathcal{J}_1(hl), \\
\bar{x}_{sp} &= \left(I - A_{sp}\right)^{-1} \sum_{\lambda=1}^{s-1} \sum_{i \in \mathcal{J}_\lambda(sp)} A_{sp,\lambda i} \bar{x}_{\lambda i}, \\
&\forall s = 2, \dots, l, p \in \mathcal{J}_s(hl).
\end{aligned} \tag{13.13}$$

Proof. The algorithm initialization is a direct application of Theorem 13.15. Now, let us assume that, at step $s \in \{2, \dots, l\}$ we can compute all the steady-state values $\bar{x}_{\lambda i}$, for all $\lambda = 1, \dots, s-1$, $i \in \mathcal{J}_\lambda(sp)$, $p \in \mathcal{J}_s(hl)$. Then, as A_{sp} is sub-stochastic, from Lemma 13.4 we can compute $\bar{x}_{sp}$ according to (13.13), for all $p \in \mathcal{J}_s(hl)$. As this assumption holds for $s = 2$ (we can compute all the steady-state values in level 1 according to Theorem 13.15), algorithm (13.13) follows by induction. □

Corollary 13.18. *If* $\cup_{h=1}^{n_1^c} \mathcal{V}_{1h} = C$*, then network* (13.3) *is signed contained.*

Proof. The thesis directly follows from Theorems 13.17. □

The above corollary means that the network is signed contained if the leaders set C is connected to each of the f SCCs of the graph of the followers, that is, the subgraph $\mathcal{F}$ induced by the node set $\mathcal{V} - C$. This implies that, to guarantee signed containment, the number of outgoing edges d from the leaders has to be equal or higher than f. The following corollary gives sufficient conditions guaranteeing asymptotic containment of a given SCC of $\mathcal{G}$.

Corollary 13.19. *For all* l=2, . . . , ℓ, h=1, . . . , n_c^l*, the* h*-th SCC of the* l*-th level of* $\mathcal{G}$ *is signed contained if* $\cup_{k \in \Upsilon_{lh}^{\mathcal{G}^c}} \mathcal{V}_{1k} \subseteq C$.

Proof. The dynamics of the nodes in any SCC of the network are decoupled by those of the nodes that are not in its upstream. Then, the thesis follows from Theorem 13.17. □

In other words, this means that if the RSCCs of the upstream of the considered SCC are (a subset of) the network leaders, then the SCC is contained.

13.4 An algorithm for control design

Given a network topology $\mathcal{G}$, the nodes that will be asymptotically signed contained may be more than those of the SCCs fulfilling the assumption of Corollary 13.19. However, this will depend on the initial conditions of the RSCCs of $\mathcal{G}$ that are not the network leaders. Therefore, if one aims at finding the optimal solution for problem (13.5), then the knowledge of the initial conditions of all the followers would be necessary for the leaders. In absence of this information, a suboptimal solution maximizing the number of nodes that are *guaranteed* to be signed contained can be found. Specifically, rather then solving problem (13.5), we will focus on finding the optimal solution of the following problem:

$$\begin{aligned} \hat{\mathcal{L}}(d) = \arg\max_{\mathcal{L}} & |\phi(\mathcal{L})| \\ \text{s.t.} & \\ |\mathcal{L}| = d, & \end{aligned} \tag{13.14}$$

where $\phi(\mathcal{L})$ is the subset of nodes of $\mathcal{G}$ belonging to SCCs fulfilling the assumptions of Corollary 13.19. Contrary to problem (13.5), the solution of this problem does not require a full exploration of the feasible solutions, and can be translated into an integer linear program (ILP). The steps of the algorithm can be adapted from [17] as follows.

Consider the condensation $\mathcal{F}^c$ of the subgraph $\mathcal{F}$ of the followers. The algorithm solving problem (13.14) consists of the following steps:

(a) build a new graph $\overline{\mathcal{G}} = \{\overline{\mathcal{V}}, \overline{\mathcal{E}}\}$ as follows:

- add to $\overline{\mathcal{V}}$ the set of roots r_i of $\mathcal{F}^c$ and all the non-roots γ_i of $\mathcal{F}^c$ that are in the downstream of no more than d roots r_i;
- for all pairs $\gamma_i, r_j \in \overline{\mathcal{V}}$, add an edge (γ_i, r_j) to $\overline{\mathcal{E}}$, with associated binary variable y_{ij}, if in $\mathcal{F}^c$, γ_i is in the downstream of r_j;
- add an additional node, π, representing the leader set $\mathcal{C}$, and connect it to all the r_j in $\overline{\mathcal{V}}$ by adding a set of edges (r_j, π) to $\overline{\mathcal{E}}$, with associated binary variable $y_{j\pi}$;

(b) associate to all edges of the graph $\bar{\mathcal{G}}$ the following weights:

- $w_{ij} = |\gamma_i|, \forall i$, that is, all edges entering the i-th node γ_i have a weight equal to the number of nodes in the SCC γ_i;
- $w_{j\pi} = |r_j|, \forall j$, that is, all edges entering the j-th root r_j have a weight equal to the number of nodes in the SCC r_j;

(c) solve the following ILP:

$$\max_{y} \sum_i \sum_j w_{ij} y_{ij} + \sum_j w_{j\pi} y_{j\pi} \tag{13.15}$$

s.t.

$$\sum_j y_{j\pi} = d \tag{13.16}$$

$$\sum_i y_{ij} \leq k_j^{\text{out}} y_{j\pi} \qquad \forall j \tag{13.17}$$

$$k_i^{\text{in}} \sum_j y_{ij} \leq \sum_{j | \exists y_{ij}} y_{j\pi} \qquad \forall i \tag{13.18}$$

$$y_{ij}, y_{j\pi} \in \{0, 1\} \qquad \forall i, j \tag{13.19}$$

where k_i^{in} and k_i^{out} are the in- and out-degree of the $i-th$ node of graph $\overline{\mathcal{G}}$, respectively.

Let us briefly illustrate the procedure outlined above. We first create a new graph $\overline{\mathcal{G}}$, whose nodes are either RSCC of the subgraph of the followers, or SCCs in the downstream of such RSCCs. Each node representing a RSCC is connected to the SCCs in its downstream. Notice that we do not include any node representing a SCC that has more than d RSCCs in its upstream, and thus cannot be guaranteed to be contained according to Corollary 13.19. Then, we add an extra node π to $\overline{\mathcal{G}}$ representing the set of leaders, and we connect it to all nodes r_i representing the RSCCs. Finally, we associate to each edge in $\overline{\mathcal{G}}$ a weight equal to the number of nodes in the (R)SCC it points to. The solution of the ILP in (13.15)-(13.18) is then equivalent to determine the RSCCs that have to be directly controlled, together with the corresponding SCCs that are guaranteed to be contained. Namely, SCC γ_i is contained for all possible initial conditions if there exists a j such that $y_{ij} = 1$, and RSCC r_j will be directly controlled if $y_{j\pi} = 1$. Accordingly, the objective function to be maximized in (13.15) represents the total number of nodes that we can guarantee to contain according to Corollary 13.19. The constraint (13.16) guarantees that the directly controlled nodes are d, while (13.17) that all the contained nodes are in the downstream of (some of) the leaders. Finally, Equation (13.18) imposes that the nodes of

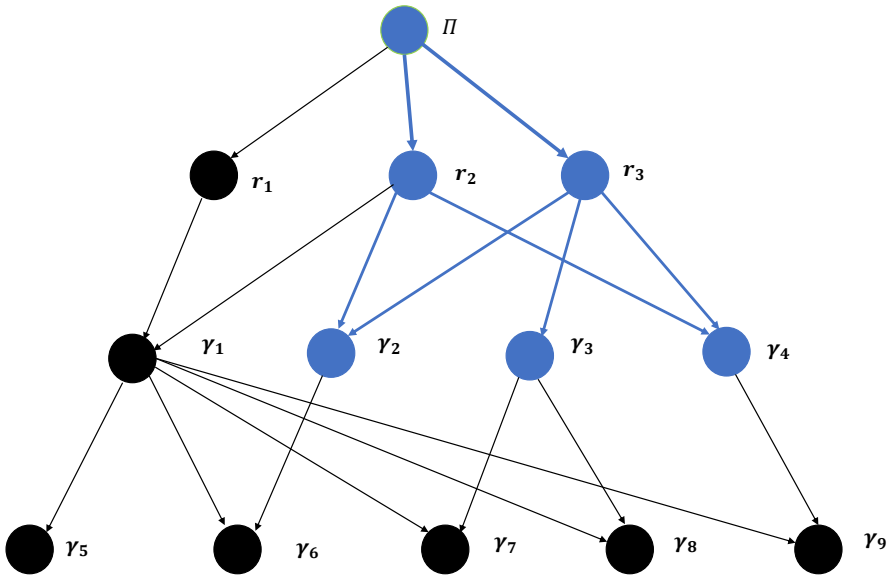

Figure 13.2: Graph $\bar{\mathcal{G}}$ associated to the signed graph $\mathcal{G}$ in the numerical example. The (R)SCCs of $\mathcal{G}$ that are guaranteed to be asymptotically contained are depicted in blue, while the remaining (R)SCCs are in black.

an SCC are contained only if a node in each of the RSCCs in their upstream is directly controlled by one of the leaders.

Remark 13.20. *Notice that our algorithm only determines which RSCCs of $\mathcal{F}$ have to be connected to the set of leaders. Indeed, the selection of the specific node of each RSCC, and the leader connected to it, is indifferent to the objective function of problem (13.14). Therefore, this selection will be performed randomly in the numerical example that follows. Clearly, the selection may indeed impact on both the convergence rate and on the width of the convex hull in which the followers are asymptotically contained. However, the investigation of these aspects goes beyond the scope of the present work.*

Numerical example

We consider a signed graph $\mathcal{G}$ of $N = 1500$ nodes distributed over 4 levels and 15 SCCs, whose dynamics follow equation (13.3). We assume that only $d = 2$ nodes can be directly controlled by the 3 leaders of the network. Following the steps of the algorithm, we first build the graph $\bar{\mathcal{G}}$, which is depicted in Figure 13.2. Then, we solve the ILP (13.15)-(13.18) and find that the leaders should directly control the RSCCs denoted by r_2

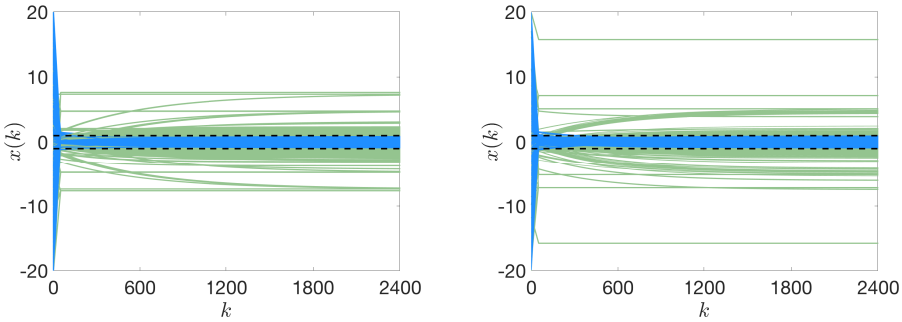

Figure 13.3: Two simulations of the network dynamics with leader states $x_C = [-1, 0.5, 1]^T$. The two simulations differ for the initial conditions of the followers, which are randomly selected from a uniform distribution in $[-10; 10]$. The dotted black lines delimit the region where the leader aim at containing the followers, whose trajectories are in blue if they belong to SCCs fulfilling the assumptions of Corollary 13.19, while they are in green otherwise. In the top panel, the total number of asymptotically contained nodes is 516, while they are 843 in the bottom panel.

and r_3 in Figure 13.2 to maximize $|\phi|$, that is, the number of followers that are contained regardless of the initial conditions of the network. The optimum value of the objective function of problem (13.14) is $|\phi(\hat{\mathcal{L}}(2))| = 508$. To validate our results, we simulated the system with the same leaders' states ($[-1, 0.5, 1]^T$) and two different sets of initial conditions, randomly selected from a uniform distribution in $[-20; 20]$. In both cases, the nodes in $\phi(\hat{\mathcal{L}}(2))$ (depicted in blue in Figure 13.3) are asymptotically contained. Then, depending on the specific selection of the initial conditions, further nodes of the network might be asymptotically contained, as in the two simulations $|\mathcal{K}(\hat{\mathcal{L}}(2))|$ is equal to 516 and 843, respectively, see Figure 13.3.

13.5 Discussion

We tackled the containment control problem in a multi-agent discrete-time system where the interactions can be both cooperative and antagonistic. In particular, we focused on the case in which the containment of the entire network is prohibited by constraints on the number of control inputs the leaders can exert on the follower. The partial containment control problem was then defined as searching for the optimal deployment of the available control inputs so as to maximize the number of contained nodes. A preliminary graphical study, based on two alternative condensations of the original graph, allowed the derivation of the conditions guaranteeing the containment of the atomic element of a directed network, that is, a strongly connected component. Leveraging the convergence analyses, an algorithm for maximizing the number of followers we can

guarantee to contain was built. Our solution strategy was translated into an integer linear program, and its effectiveness was demonstrated on a testbed examples. Future work will extend this analysis to alternative scenarios in which, for instance, the leaders may not cooperate and have contrasting goals.

14 Conclusions

In this thesis we gave a picture of how to deal with complex dynamical networks whose topologies change in time. Indeed, we relaxed the typical assumption on the invariance of the network structures and we named the class of networks with changing topology as *evolving networks*. Specifically, following the footsteps of complex networks scientists, we investigated if and when the extra information on the structure of the network can be fruitfully used for control purposes. For instance, recent results [29] suggested that exploiting temporality, that is, the variability of the network topology over time, could reduce control energy requirements without increasing the number of signals required to control the network. However, this result has been achieved under the unrealistic assumption of a complete knowledge of the future network evolution. Therefore, in Part I, we addressed the challenging problem of controlling a temporal network (i.e., an element of the evolving networks class) in a more realistic scenario, that is, when we can only have a probabilistic, description of the variability of the network. By using stochastic programming, we reformulated the minimum control energy problem of what we called a *stochastic temporal networks*. By assuming to know deterministically only the current topology of the network we aim to control, we stated the problem of finding the optimal waypoints, that is, the intermediate points on the optimal trajectory between the (fixed) initial and final (desired) network states. As a result, we showed the control energy be a quadratic function of the initial and final network states. To quantify if the network temporality, when it comes hand in hand with uncertainty (as in our more realistic scenario), could actually improve our ability of controlling complex dynamical networks, we performed numerical simulations both on real and synthetic data. We showed that the temporality is not a panacea for reducing the energy required for network control, however, it can still be leveraged to obtain substantial energy savings provided that the time-scale of the network matches its temporality.

Part II was instead devoted to consider the case in which the topology does not commute between a set of predefined graphs, but dynamically coevolves with the network nodes. We referred to this class of networks as *coevolving networks*. First, we focused on a model of socio-economic phenomena to illustrate how this novel framework is instrumental in domains of applications in which it is essential to consider the inertia associated to interconnections topology changes. Specifically, we presented a model of artificial financial markets where the investors are not perfectly rational and can be affected by the cognitive bias, which has an impact on their mutual relations. We showed

how coevolving networks are able to simultaneously model the dynamical evolution of the relations among the financial agents and the effect on the overall market dynamics in terms of some global observables, such as the distribution of the agents' wealth. After showing the relevance of coevolution for modeling, we then turned our attention on the possible implications for network control. Therefore, we provided two instances that illustrated how the edge dynamics can be tailored to foster the achievement of collective behavior. In particular, we showed how edge evolution can be tuned to optimally solve the pinning controllability problem over coevolving networks.

The thesis then concludes with Part III, where we focused on additional aspects of the network structure, other than its temporality or coevolution, that might challenge our ability to control the network. Specifically, we discussed the case of symmetries in the network structure, and that of signed network topology modeling the presence of antagonistic interactions. In a network endowed with symmetries, we gave conditions under which it is possible to achieve group consensus and offered a control design alternative to set a desired value for the group consensus. To cope with the presence of antagonistic interactions, we then modeled a network on a signed graph, and provided an algorithmic solution for maximizing the nodes contained within a desired convex hull while keeping limited the number of control inputs.

Bibliography

[1] Z. Chen, J. Wu, Y. Xia, and X. Zhang, "Robustness of interdependent power grids and communication networks: A complex network perspective," *IEEE Transactions on Circuits and Systems II: Express Briefs*, vol. 65, no. 1, pp. 115–119, 2017.

[2] P. DeLellis, A. DiMeglio, F. Garofalo, and F. Lo Iudice, "The evolving cobweb of relations among partially rational investors," *PloS one*, vol. 12, no. 2, 2017.

[3] P. DeLellis, A. Di Meglio, and F. Lo Iudice, "Overconfident agents and evolving financial networks," *Nonlinear Dynamics*, vol. 92, no. 1, pp. 33–40, 2018.

[4] D. Delpini, S. Battiston, G. Caldarelli, and M. Riccaboni, "Portfolio diversification, differentiation and the robustness of holdings networks," *Applied Network Science*, vol. 5, no. 1, pp. 1–20, 2020.

[5] R. Pastor-Satorras, C. Castellano, P. Van Mieghem, and A. Vespignani, "Epidemic processes in complex networks," *Reviews of modern physics*, vol. 87, no. 3, p. 925, 2015.

[6] P. DeLellis, A. DiMeglio, F. Garofalo, and F. Lo Iudice., "Steering opinion dynamics via containment control," *Computational social networks*, vol. 4, no. 1, p. 12, 2017.

[7] P. Jia, N. E. Friedkin, and F. Bullo, "Opinion dynamics and social power evolution over reducible influence networks," *SIAM Journal on Control and Optimization*, vol. 55, no. 2, pp. 1280–1301, 2017.

[8] S. Pei, F. Morone, and H. A. Makse, *Theories for Influencer Identification in Complex Networks*, pp. 125–148. Cham: Springer International Publishing, 2018.

[9] D. J. Watts and S. H. Strogatz, "Collective dynamics of 'small-world'networks," *nature*, vol. 393, no. 6684, p. 440, 1998.

[10] A.-L. Barabási, "Scale-free networks: a decade and beyond," *science*, vol. 325, no. 5939, pp. 412–413, 2009.

[11] J. A. F. R. Olfati-Saber and R. M. Murray, "Consensus and cooperation in networked multi-agent systems," *Proceedings of the IEEE*, vol. 95, no. 1, pp. 215–233, 2007.

[12] A. Arenas, A. Díaz-Guilera, J. Kurths, Y. Moreno, and C. Zhou, "Synchronization in complex networks," *Physics reports*, vol. 469, no. 3, pp. 93–153, 2008.

[13] Y.-Y. Liu, J.-J. Slotine, and A.-L. Barabási, "Controllability of complex networks," *nature*, vol. 473, no. 7346, pp. 167–173, 2011.

[14] J. Sun and A. Motter, "Controllability transition and nonlocality in network control," *Physical review letters*, vol. 110, no. 20, p. 208701, 2013.

[15] G. Yan, Y.-C. L. J. Ren, C.-H. Lai, and B. Li, "Controlling complex networks: How much energy is needed?," *Physical review letters*, vol. 108, no. 21, p. 218703, 2012.

[16] J. Gao, Y.-Y. Liu, R. M. D'Souza, and A.-L. Barabási, "Target control of complex networks," *Nature Communications*, vol. 5, p. 5415, 2014.

[17] P. DeLellis, F. Garofalo, and F. Lo Iudice, "The partial pinning control strategy for large complex networks," *Automatica*, vol. 89, pp. 111–116, 2018.

[18] A. S. I. Klickstein and F. Sorrentino, "Energy scaling of targeted optimal control of complex networks," *Nature communications*, vol. 8, no. 1, pp. 1–10, 2017.

[19] P. Holme and J. Saramäki, "Temporal networks," *Physics reports*, vol. 519, no. 3, pp. 97–125, 2012.

[20] T. Gross and B. Blasius, "Adaptive coevolutionary networks: a review," *Journal of the Royal Society Interface*, vol. 5, no. 20, pp. 259–271, 2008.

[21] A. Réka and A.-L. Barabási, "Statistical mechanics of complex networks," *Review of Modern Physics*, vol. 74, no. 1, pp. 47–97, 2002.

[22] B. Kozma and A. Barrat, "Consensus formation on coevolving networks: groups' formation and structure," *Journal of Physics A: Mathematical and Theoretical*, vol. 41, p. 224020, 2008.

[23] G. Iniguez, J. Kertész, K. Kaski, and R. A. Barrio, "Opinion and community formation in coevolving networks," *Physical Review E*, vol. 80, no. 6, p. 066119, 2009.

[24] S. D. Yi, S. K. Baek, C.-P. Zhu, and B. J. Kim, "Phase transtion in coevolving network of conformist and contrarian voters," *Phisical Review E*, vol. 81, no. 012806, pp. 1–5, 2013.

[25] D. S. Bassett, N. F. Wymbs, M. A. Porter, P. J. Mucha, J. M. Carlson, and S. T. Grafton, "Dynamic reconfiguration of human brain networks during learning," *Proceedings of the National Academy of Sciences*, vol. 108, no. 18, pp. 7641–7646, 2011.

[26] B. J. Kinne and J. B. Bunte, "Guns or money? defense co-operation and bilateral lending as coevolving networks," *British Journal of Political Science*, pp. 1–22, 2018.

[27] R. Gallotti and M. Barthelemy, "The multilayer temporal network of public transport in great britain," *Scientific Data*, vol. 2, no. 1, pp. 1–8, 2015.

[28] L. B. Shaw and I. B. Schwartz, "Fluctuating epidemics on adaptive networks," *Physical Review E*, vol. 77, no. 6, pp. 066101–1–10, 2008.

[29] A. Li, S. Cornelius, Y.-Y. Liu, L. Wang, and A.-L. Barabási, "The fundamental advantages of temporal networks," *Science*, vol. 358, no. 6366, pp. 1042–1046, 2017.

[30] B. D. MacArthur, R. J. Sanchez-Garcia, and J. W. Anderson, "Symmetry in complex networks," *Discrete Applied Mathematics*, vol. 156, no. 18, pp. 3525–3531, 2008.

[31] A. Chapman and M. Mesbahi, "State controllability, output controllability and stabilizability of networks: A symmetry perspective," in *2015 54th IEEE Conference on Decision and Control (CDC)*, pp. 4776–4781, IEEE, 2015.

[32] A. Chapman and M. Mesbahi, "On symmetry and controllability of multi-agent systems," in *53rd IEEE Conference on Decision and Control*, pp. 625–630, IEEE, 2014.

[33] A. Di Meglio, F. Lo Iudice, F. Della Rossa, and F. Sorrentino, "Controlling the consensus state in the networks with symmetries." arXiv:2005.11667v1, May 2020.

[34] P. DeLellis, A. DiMeglio, F. Garofalo, and F. Lo Iudice, "Partial containment control over signed graphs," in *2019 18th European Control Conference (ECC)*, pp. 596–601, IEEE, 2019.

[35] G. Yan, G. Tsekenis, B. Barzel, J.-J. Slotine, Y.-Y. Liu, and A.-L. Barabási, "Spectrum of controlling and observing complex networks," *Nature Physics*, vol. 11, no. 9, pp. 779–786, 2015.

[36] Z. Yuan, C. Zhao, Z. Di, W.-X. Wang, and Y.-C. Lai, "Exact controllability of complex networks," *Nature Communications*, vol. 4, p. 2447, 2013.

[37] F. M. Callier and C. A. Desoer, *Linear system theory*. Springer Science & Business Media, 2012.

[38] P. J. Antsaklis and A. N. Michel, *Linear systems*. Springer Science & Business Media, 2006.

[39] F. Pasqualetti, S. Zampieri, and F. Bullo, "Controllability metrics, limitations and algorithms for complex networks," *IEEE Transactions on Control of Network Systems*, vol. 1, no. 1, pp. 40–52, 2014.

[40] T. Spyropoulos, K. Psounis, and C. S. Raghavendra, "Spray and wait: an efficient routing scheme for intermittently connected mobile networks," in *Proceedings of the 2005 ACM SIGCOMM workshop on Delay-tolerant networking*, pp. 252–259, 2005.

[41] J.-P. Onnela, A. Chakraborti, K. Kaski, J. Kert'esz, and A. Kanto, "Dynamics of market correlations: Taxonomy and portfolio analysis," *Physical Review E*, vol. 68, no. 056110, pp. 1–12, 2003.

[42] R. Bellman, "Dynamic programming," *Science*, vol. 153, no. 3731, pp. 34–37, 1966.

[43] P. DeLellis, A. Di Meglio, F.Garofalo, and F. Lo Iudice., "The inherent uncertainty of temporal networks: a true challenge for control." To appear in Scientific Reports.

[44] J. Wang, X. Peng, M. Li, and Y. Pan, "Construction and application of dynamic protein interaction network based on time course gene expression data," *Proteomics*, vol. 13, no. 2, pp. 301–312, 2013.

[45] R. M. May, *Stability and Complexity in Model Ecosystems*. Princeton, NJ, USA: Princeton University Press, 1973.

[46] W. Gawronski and J.-N. Juang, "Model reduction in limited time and frequency intervals," *International Journal of System Science*, vol. 21, no. 2, pp. 349–376, 1990.

[47] E. A. Lee and D. G. Messerschmitt, *Digital communication*. Springer Science & Business Media, 2012.

[48] D. Brockmann and D. Helbing, "The hidden geometry of complex, network-driven contagion phenomena," *Science*, vol. 342, no. 6164, pp. 1337–1342, 2013.

[49] "https://www.ncbi.nlm.nih.gov/geo/query/acc.cgi?acc=gse4987."

[50] D. Šiljak, "Dynamic graphs," *Nonlinear Analysis: Hybrid Systems*, vol. 2, no. 2, pp. 544–567, 2008.

[51] P. DeLellis, M. Di Bernardo, T. E. Gorochowski, and G. Russo, "Synchronization and control of complex networks via contraction, adaptation and evolution," *IEEE Circuits and Systems Magazine*, vol. 10, no. 3, pp. 64–82, 2010.

[52] T. E. Gorochowski, M. di Bernardo, and C. Grierson, "Evolving dynamical networks: a formalism for describing complex systems," *Complexity*, vol. 17, no. 3, pp. 18–25, 2012.

[53] A. Di Meglio, F. Garofalo, and P. De Lellis, "Controlling network systems towards an equilibrium: a minimum energy adaptive pinning strategy." 2020.

[54] P. DeLellis and A. Di Meglio and M. di Bernardo, "Decetralized gain adaptation for optimal pinning controllability of complex networks," *IEEE Control Systems Letters*, vol. 4, no. 1, pp. 253–258, 2019.

[55] W. Arthur, "Complexity and the economy," *Science*, vol. 284, no. 5411, pp. 107–109, 1999.

[56] P. M. Garber, "Famous first bubbles," *Journal of Economic perspectives*, vol. 4, no. 2, pp. 35–54, 1990.

[57] P. Temin and H.-J. Voth, "Riding the south sea bubble," *The American Economic Review*, vol. 94, no. 5, pp. 1654–1668, 2004.

[58] N. Barberis and R. Thaler, "A survey of behavioral finance," *Handbook of the Economics of Finance*, vol. 1, pp. 1053–1128, 2003.

[59] R. J. Shiller, "From efficient markets theory to behavioral finance," *Journal of Economic Perspectives*, vol. 17, no. 1, pp. 83–104, 2003.

[60] T. J. Brennan and A. W. Lo, "An evolutionary model of bounded rationality and intelligence," *PLoS One*, vol. 7, no. 11, p. e50310, 2012.

[61] H. A. Simon, *Models of bounded rationality: Empirically grounded economic reason*, vol. 3. MIT press, 1997.

[62] A. Tversky and D. Kahneman, "Judgment under uncertainty: Heuristics and biases," *Science*, vol. 185, no. 4157, pp. 1124–1131, 1974.

[63] D. Kahneman and A. Tversky, "Prospect theory: An analysis of decision under risk," *Econometrica: Journal of the Econometric Society*, vol. 47, no. 2, pp. 263–291, 1979.

[64] K. Daniel and D. Hirshleifer, "Overconfident investors, predictable returns, and excessive trading," *The Journal of Economic Perspectives*, vol. 29, no. 4, pp. 61–87, 2015.

[65] T. Odean, "Do investors trade too much?," *Available at SSRN 94143*, 1998.

[66] D. Kahneman and M. W. Riepe, "Aspects of investor psychology," *The Journal of Portfolio Management*, vol. 24, no. 4, pp. 52–65, 1998.

[67] J.-H. Cho and A. Swami, "Dynamics of uncertain opinions in social networks," in *2014 IEEE Military Communications Conference*, pp. 1627–1632, IEEE, 2014.

[68] C. H. Hommes, "Financial markets as nonlinear adaptive evolutionary systems," *Quantitative Finance*, vol. 1, no. 1, pp. 149–167, 2001.

[69] C. Castellano, S. Fortunato, and V. Loreto, "Statistical physics of social dynamics," *Reviews of Modern Physics*, vol. 81, no. 2, p. 591, 2009.

[70] J. Voit, *The statistical mechanics of financial markets*. Springer Science & Business Media, 2005.

[71] B. Tóth, Y. Lempérière, C. Deremble, J. de Lataillade, J. Kockelkoren, and J.-P. Bouchaud, "Anomalous price impact and the critical nature of liquidity in financial markets," *Physical Review X*, vol. 1, no. 021006, pp. 1–11, 2011.

[72] H. E. Stanley, V. Afanasyev, L. Amaral, S. V. Buldyrev, A. L. Goldberger, S. Havlin, H. Leschhorn, P. Maass, R. N. Mantegna, C. K. Peng, P. A. Prince, M. A. Salinger, M. H. R. Stanley, and G. M. Viswanathan, "Anomalous fluctuations in the dynamics of complex systems: from dna and physiology to econophysics," *Physica A: Statistical Mechanics and its Applications*, vol. 224, no. 1, pp. 302–321, 1996.

[73] E. Bonabeau, "Agent-based modeling: Methods and techniques for simulating human systems," *Proceedings of the National Academy of Sciences*, vol. 99, no. suppl 3, pp. 7280–7287, 2002.

[74] N. Gilbert, *Agent-based models*. Sage, 2008.

[75] M. Galbiati and K. Soramäki, "An agent-based model of payment systems," *Journal of Economic Dynamics and Control*, vol. 35, no. 6, pp. 859–875, 2011.

[76] L. Tesfatsion, "Agent-based computational economics: modeling economies as complex adaptive systems," *Information Sciences*, vol. 149, no. 4, pp. 262–268, 2003.

[77] A. Chakraborti, I. M. Toke, M. Patriarca, and F. Abergel, "Econophysics review: Ii agent-based models," *Quantitative Finance*, vol. 11, no. 7, pp. 1013–1041, 2011.

[78] H. M. Singer, I. Singer, and H. J. Herrmann, "Agent-based model for friendship in social networks," *Physical Review E*, vol. 80, no. 2, p. 026113, 2009.

[79] F. Schweitzer and B. Tilch, "Self-assembling of networks in an agent-based model," *Physical Review E*, vol. 66, no. 2, p. 026113, 2002.

[80] E. Samanidou, E. Zschischang, D. Stauffer, and T. Lux, "Agent-based models of financial markets," *Reports on Progress in Physics*, vol. 70, no. 3, p. 409, 2007.

[81] T. Lux and M. Marchesi, "Scaling and criticality in a stochastic multi-agent model of a financial market," *Nature*, vol. 397, no. 6719, pp. 498–500, 1999.

[82] M. Raberto, S. Cincotti, S. M. Focardi, and M. Marchesi, "Agent-based simulation of a financial market," *Physica A: Statistical Mechanics and its Applications*, vol. 299, no. 1, pp. 319–327, 2001.

[83] B. LeBaron, "Agent-based computational finance," *Handbook of Computational Economics*, vol. 2, pp. 1187–1233, 2006.

[84] R. G. Palmer, W. B. Arthur, J. H. Holland, B. LeBaron, and P. Tayler, "Artificial economic life: a simple model of a stockmarket," *Physica D*, vol. 75, no. 1, pp. 264–274, 1994.

[85] S. Pincus and R. E. Kalman, "Irregularity, volatility, risk, and financial market time series," *Proceedings of the National Academy of Sciences*, vol. 101, no. 38, pp. 13709–13714, 2004.

[86] L. Muchnik, S. Aral, and S. J. Taylor, "Social influence bias:a randomized experiment," *Science*, vol. 341, no. 6146, pp. 647–651, 2013.

[87] G. Bonanno, G. Caldarelli, F. Lillo, S. Miccichè, N. Vandewalle, and R. N. Mantegna, "Networks of equities in financial markets," *The European Physical Journal B*, vol. 38, no. 2, pp. 363–371, 2004.

[88] V. M. Eguiluz and M. G. Zimmermann, "Transmission of information and herd behavior: an application to financial markets," *Physical Review Letters*, vol. 85, no. 26, p. 5659, 2000.

[89] S. Boccaletti, V. Latora, Y. Moreno, M. Chavez, and D.-U. Hwang, "Complex networks: Structure and dynamics," *Physics reports*, vol. 424, no. 4-5, pp. 175–308, 2006.

[90] R. A. Bentley, P. Ormerod, and M. Batty, "Evolving social influence in large populations," *Behavioral Ecology and Sociobiology*, vol. 65, no. 3, pp. 537–546, 2010.

[91] M. G. Zimmermann and V. M. Eguíluz, "Cooperation, social networks, and the emergence of leadership in a prisoner's dilemma with adaptive local interactions," *Physical Review E*, vol. 72, no. 5, p. 056118, 2005.

[92] F. Fu, C. Hauert, M. A. Nowak, and L. Wang, "Reputation-based partner choice promotes cooperation in social networks," *Physical Review E*, vol. 78, no. 2, p. 026117, 2008.

[93] G. Bianconi and A. Barabási, "Competition and multiscaling in evolving networks," *Europhysics Letters*, vol. 54, no. 4, p. 436, 2001.

[94] P. DeLellis, M. di Bernardo, F. Garofalo, and M. Porfiri, "Evolution of complex networks via edge snapping," *IEEE Transactions on Circuits and Systems I: Regular Papers*, vol. 57, no. 8, pp. 2132–2143, 2010.

[95] D. Hirshleifer and S. Hong Teoh, "Herd behaviour and cascading in capital markets: A review and synthesis," *European Financial Management*, vol. 9, no. 1, pp. 25–66, 2003.

[96] R. I. M. Dunbar, "Neocortex size as a constraint on group size in primates," *Journal of Human Evolution*, vol. 22, no. 6, pp. 469–493, 1992.

[97] M. T. Rivera, S. B. Soderstrom, and B. Uzzi, "Dynamics of dyads in social networks: Assortative, relational, and proximity mechanisms," *Annual Review of Sociology*, vol. 36, pp. 91–115, 2010.

[98] G. Miritello, R. Lara, M. Cebrian, and E. Moro, "Limited communication capacity unveils strategies for human interaction," *Scientific Reports*, vol. 3, no. 1950, pp. 1–7, 2013.

[99] J. Saramäki and E. Moro, "From seconds to months: an overview of multi-scale dynamics of mobile telephone calls," *The European Physical Journal B*, vol. 88, no. 6, pp. 1–10, 2015.

[100] P. Holme and F. Liljeros, "Birth and death of links control disease spreading in empirical contact networks," *Scientific Reports*, vol. 4, p. 4999, 2014.

[101] R. A. Bentley, C. C. S. Caiado, and P. Ormerod, "Effects of memory on spatial heterogeneity in neutrally transmitted culture," *Evolution and Human Behavior*, vol. 35, no. 4, pp. 257–263, 2014.

[102] R. Cont and J. Bouchaud, "Herd behavior and aggregate fluctuations in financial markets," *Macroeconomic Dynamics*, vol. 4, no. 02, pp. 170–196, 2000.

[103] P. DeLellis, F. Garofalo, F. Lo Iudice, and E. Napoletano, "Wealth distribution across communities of adaptive financial agents," *New Journal of Physics*, vol. 17, no. 8, p. 083003, 2015.

[104] P. Erdos and A. Rényi, "On the evolution of random graphs," *Publ. Math. Inst. Hung. Acad. Sci*, vol. 5, no. 1, pp. 17–60, 1960.

[105] E. Estrada, "Network robustness to targeted attacks. the interplay of expansibility and degree distribution," *The European Physical Journal B*, vol. 52, no. 4, pp. 563–574, 2006.

[106] M. Hanke, J. Huber, M. Kirchler, and M. Sutter, "The economic consequences of a Tobin tax - An experimental analysis," *Journal of Economic Behavior & Organization*, vol. 74, no. 1, pp. 58–71, 2010.

[107] R. E. Hall, A. Rabushka, and J. Krepelka, *The flat tax*, vol. 423. Wiley Online Library, 1995.

[108] C. Gini, "Measurement of inequality of incomes," *The Economic Journal*, vol. 31, no. 121, pp. 124–126, 1921.

[109] M. Glaser, M. Nöth, and Weber, "Behavioral finance," in *Blackwell handbook of judgment & decision making* (D. J. Koehler and N. Harvey, eds.), pp. 527–546, Oxford, UK: Blackwell, 2004.

[110] M. Chinazzi, G. Fagiolo, J. A. Reyes, and S. Schiavo, "Post-mortem examination of the international financial network," *Journal of Economic Dynamics and Control*, vol. 37, no. 8, pp. 1692–1713, 2013.

[111] G. Fagiolo, "Clustering in complex directed networks," *Physical Review E*, vol. 76, no. 026107, pp. 1–8, 2007.

[112] J. He, Q.-G. Wang, P. Cheng, J. Chen, and Y. Sun, "Multi-period mean-variance portfolio optimization with high-order coupled asset dynamics," *IEEE Transactions on Automatic Control*, vol. 60, no. 5, 2015.

[113] H. Uchida and R. Nakagawa, "Herd behavior in the japanese loan market: Evidence from bank panel data," *Journal of Financial Intermediation*, vol. 16, no. 4, pp. 555–583, 2007.

[114] P. DeLellis, M. di Bernardo, and M. Porfiri, "Pinning control of complex networks via edge snapping," *Chaos: An Interdisciplinary Journal of Nonlinear Science*, vol. 21, no. 3, p. 033119, 2011.

[115] W. Yu, P. DeLellis, G. Chen, M. di Bernardo, and J. Kurths, "Distributed adaptive control of synchronization in complex networks," *IEEE Transactions on Automatic Control*, vol. 57, no. 8, pp. 2153–2158, 2012.

[116] Y. Tang, Z. Wang, H. Gao, H. Qiao, and J. Kurths, "On controllability of neuronal networks with constraints on the average of control gains," *IEEE Transactions on Cybernetics*, vol. 44, no. 12, pp. 2670–2681, 2014.

[117] L. Farina and S. Rinaldi, *Positive linear systems: theory and applications*, vol. 50. John Wiley & Sons, 2011.

[118] S. Sastry, *Nonlinear systems: analysis, stability, and control*, vol. 10. Springer Science & Business Media, 2013.

[119] W. Cao, J. Zhang, and W. Ren, "Leader–follower consensus of linear multi-agent systems with unknown external disturbances," *Systems & Control Letters*, vol. 82, pp. 64–70, 2015.

[120] Z. Li, Z. Duan, and L. Huang, "Leader-follower consensus of multi-agent systems," in *2009 American control conference*, pp. 3256–3261, IEEE, 2009.

[121] X. Li, X. Wang, and G. Chen, "Pinning a complex dynamical network to its equilibrium," *IEEE Transactions on Circuits and Systems I: Regular Papers*, vol. 51, no. 10, pp. 2074–2087, 2004.

[122] J. Zhou, J.-a. J. Lu, and J. Lü, "Pinning adaptive synchronization of a general complex dynamical network," *Automatica*, vol. 44, no. 4, pp. 996–1003, 2008.

[123] F. Chen, Z. Chen, L. Xiang, Z. Liu, and Z. Yuan, "Reaching a consensus via pinning control," *Automatica*, vol. 45, no. 5, pp. 1215–1220, 2009.

[124] F. Sorrentino, M. di Bernardo, F. Garofalo, and G. Chen, "Controllability of complex networks via pinning," *Physical Review E*, vol. 75, no. 4, p. 046103, 2007.

[125] T. Chen, X. Liu, and W. Lu, "Pinning complex networks by a single controller," *IEEE Transactions on Circuits and Systems I: Regular Papers*, vol. 54, no. 6, pp. 1317–1326, 2007.

[126] W. Yu, G. Chen, and J. Lü, "On pinning synchronization of complex dynamical networks," *Automatica*, vol. 45, no. 2, pp. 429–435, 2009.

[127] P. DeLellis, M. di Bernardo, and M. Porfiri, "Pinning control of complex networks via edge snapping," *Chaos: An Interdisciplinary Journal of Nonlinear Science*, vol. 21, no. 3, p. 033119, 2011.

[128] M. Porfiri and M. di Bernardo, "Criteria for global pinning-controllability of complex networks," *Automatica*, vol. 44, no. 12, pp. 3100–3106, 2008.

[129] M. Jalili, O. A. Sichani, and X. Yu, "Optimal pinning controllability of complex networks: Dependence on network structure," *Physical Review E*, vol. 91, no. 1, p. 012803, 2015.

[130] L. Kempton, G. Herrmann, and M. di Bernardo, "Self-organization of weighted networks for optimal synchronizability," *IEEE Transactions on Control of Network Systems*, vol. 5, no. 4, pp. 1541–1550, 2017.

[131] L. Kempton, G. Herrmann, and M. di Bernardo, "Adaptive weight selection for optimal consensus performance," in *2014 IEEE 53rd Annual Conference on Decision and Control (CDC)*, pp. 2234–2239, 2014.

[132] L. Kempton, G. Herrmann, and M. di Bernardo, "Distributed optimisation and control of graph laplacian eigenvalues for robust consensus via an adaptive multilayer strategy," *International Journal of Robust and Nonlinear Control*, vol. 27, no. 9, pp. 1499–1525, 2017.

[133] L. N. Trefethen and D. Bau, *Numerical linear algebra*, vol. 50. Philadelphia, PA, USA: Siam, 1997.

[134] I. C. Ipsen and B. Nadler, "Refined perturbation bounds for eigenvalues of hermitian and non-hermitian matrices," *SIAM Journal on Matrix Analysis and Applications*, vol. 31, no. 1, pp. 40–53, 2009.

[135] P. Yang, R. A. Freeman, G. J. Gordon, K. Lynch, S. S. Srinivasa, and R. Sukthankar, "Decentralized estimation and control of graph connectivity for mobile sensor networks," *Automatica*, vol. 46, no. 2, pp. 390–396, 2010.

[136] R. A. Freeman, P. Yang, and K. M. Lynch, "Stability and convergence properties of dynamic average consensus estimators," in *2006 45th IEEE Conference on Decision and Control*, pp. 338–343, 2006.

[137] J. Von Neumann and O. Morgenstern, *Theory of Games and Economic Behavior (60th Anniversary Commemorative Edition)*. Princeton University Press, 2007.

[138] B. Clair, "The biggest numbers in the universe," Apr. 2001.

[139] C. D. Godsil, "Compact graphs and equitable partitions," *Linear Algebra and its Applications*, vol. 255, no. 1-3, pp. 259–266, 1997.

[140] L. Pecora, F. Sorrentino, A. Hagerstrom, T. E. Murphy, and R. Roy, "Cluster synchronization and isolated desynchronization in complex networks with symmetries," *Nature communications*, vol. 5, no. 1, pp. 1–8, 2014.

[141] F. Sorrentino, L. M. Pecora, A. M. Hagerstrom, T. E. Murphy, and R. Roy, "Complete characterization of the stability of cluster synchronization in complex dynamical networks," *Science advances*, vol. 2, no. 4, p. e1501737, 2016.

[142] I. Klickstein, L. Pecora, and F. Sorrentino, "Symmetry induced group consensus," *Chaos: An Interdisciplinary Journal of Nonlinear Science*, vol. 29, no. 7, p. 073101, 2019.

[143] K. A. Blaha, K. Huang, F. Della Rossa, L. Pecora, M. Hossein-Zadeh, and F. Sorrentino, "Cluster synchronization in multilayer networks: A fully analog experiment with l c oscillators with physically dissimilar coupling," *Physical review letters*, vol. 122, no. 1, p. 014101, 2019.

[144] M. Mesbahi and F. Y. Hadaegh, "Formation flying control of multiple spacecraft via graphs, matrix inequalities, and switching," *Journal of Guidance, Control, and Dynamics*, vol. 24, no. 2, pp. 369–377, 2001.

[145] M. H. DeGroot, "Reaching a consensus," *Journal of the American Statistical Association*, vol. 69, no. 345, pp. 118–121, 1974.

[146] R. Olfati-Saber and R. M. Murray, "Consensus problems in networks of agents with switching topology and time-delays," *IEEE Transactions on automatic control*, vol. 49, no. 9, pp. 1520–1533, 2004.

[147] W. Ni and D. Cheng, "Leader-following consensus of multi-agent systems under fixed and switching topologies," *Systems & Control Letters*, vol. 59, no. 3-4, pp. 209–217, 2010.

[148] C. Altafini, "Consensus problems on networks with antagonistic interactions," *IEEE Transactions on Automatic Control*, vol. 58, no. 4, pp. 935–946, 2013.

[149] H. Haghshenas, M. A. Badamchizadeh, and M. Baradarannia, "Containment control of heterogeneous linear multi-agent systems," *Automatica*, vol. 54, no. 4, p. 2, 2015.

[150] M. Ji, G. Ferrari-Trecate, M. Egerstedt, and A. Buffa, "Containment control in mobile networks," *IEEE Transactions on Automatic Control*, vol. 53, no. 8, pp. 1972–1975, 2008.

[151] Y. Cao and W. Ren, "Containment control with multiple stationary or dynamic leaders under a directed interaction graph," in *Decision and Control, 2009 held jointly with the 2009 28th Chinese Control Conference. CDC/CCC 2009. Proceedings of the 48th IEEE Conference on*, pp. 3014–3019, IEEE, 2009.

[152] Y. Cao, W. Ren, and M. Egerstedt, "Distributed containment control with multiple stationary or dynamic leaders in fixed and switching directed networks," *Automatica*, vol. 48, no. 8, pp. 1586–1597, 2012.

[153] Z. Peng, D. Wang, Y. Shi, H. Wang, and W. Wang, "Containment control of networked autonomous underwater vehicles with model uncertainty and ocean disturbances guided by multiple leaders," *Information Sciences*, vol. 316, pp. 163–179, 2015.

[154] Y. Cao, D. Stuart, W. Ren, and Z. Meng, "Distributed containment control for multiple autonomous vehicles with double-integrator dynamics: algorithms and experiments," *IEEE Transactions on Control Systems Technology*, vol. 19, no. 4, pp. 929–938, 2011.

[155] H. Liu, G. Xie, and L. Wang, "Necessary and sufficient conditions for containment control of networked multi-agent systems," *Automatica*, vol. 48, no. 7, pp. 1415–1422, 2012.

[156] D. Meng, "Bipartite containment tracking of signed networks," *Automatica*, vol. 79, pp. 282–289, 2017.

[157] S. Zuo, Y. Song, F. L. Lewis, and A. Davoudi, "Bipartite output containment of general linear heterogeneous multi-agent systems on signed digraphs," *IET Control Theory & Applications*, vol. 12, no. 9, pp. 1180–1188, 2018.

[158] C. Godsil and G. Royle, *Algebraic graph theory*, vol. 207. Springer Science & Business Media, 2013.

[159] T. Zaslasvsky, "Signed graphs," *Discrete Applied Mathematics*, vol. 4, no. 1, pp. 47–74, 1982.

[160] W. Xiauo, M. Cao, and K. H. Johansson, "Structural balance and opinion separation in trust–mistrust social networks," *IEEE Transactions on Control of Network Systems*, vol. 3, no. 1, pp. 46–56, 2016.

[161] J. M. Hendrickx, "A lifting approach to models of opinion dynamics with antagonisms," in *Decision and Control (CDC), 2014 IEEE 53rd Annual Conference on*, pp. 2118–2123, IEEE, 2014.

[162] F. Gantmacher, "The theory of matrices," *Volume I*, pp. 95–103, 1964.

[163] R. A. Horn and C. R. Johnson, *Matrix analysis*. Cambridge university press, 2012.

[164] Y.-Y. Liu and A.-L. Barabási, "Control principles of complex systems," *Reviews of Modern Physics*, vol. 88, no. 3, p. 035006, 2016.